National Library of Canada

Acquisitions and Bibliographic Services Branch

395 Wellington Street
Ottawa, Ontario
K1A 0N4

Bibliothèque nationale du Canada

Direction des acquisitions et des services bibliographiques

395, rue Wellington
Ottawa (Ontario)
K1A 0N4

Your file Votre référence

Our file Notre référence

NOTICE

The quality of this microform is heavily dependent upon the quality of the original thesis submitted for microfilming. Every effort has been made to ensure the highest quality of reproduction possible.

If pages are missing, contact the university which granted the degree.

Some pages may have indistinct print especially if the original pages were typed with a poor typewriter ribbon or if the university sent us an inferior photocopy.

AVIS

La qualité de cette microforme dépend grandement de la qualité de la thèse soumise au microfilmage. Nous avons tout fait pour assurer une qualité supérieure de reproduction.

S'il manque des pages, veuillez communiquer avec l'université qui a conféré le grade.

La qualité d'impression de certaines pages peut laisser à désirer, surtout si les pages originales ont été dactylographiées à l'aide d'un ruban usé ou si l'université nous a fait parvenir une photocopie de qualité inférieure.

Canada

INVESTIGATIONS OF IONIC AND NEUTRAL SPECIES IN THE GAS PHASE BY TANDEM MASS SPECTROMETRY

By Hongwen Chen

A Thesis
Presented to the University of Ottawa
in fulfilment of the
thesis requirement for the degree of
Master in Science
in
the Department of Chemistry

University of Ottawa

ISBN 0-315-85821-4

Canada

UNIVERSITÉ D'OTTAWA
UNIVERSITY OF OTTAWA

To

My Parents

Abstract

A major application of tandem mass spectrometry is the study of gas-phase ion chemistry. Gas-phase ion chemistry involving ion thermochemistry and ion dissociation characteristics, is one of the foundations of analytical chemistry.

A signal (peak) in a mass spectrum is only identified by its mass-to-charge ratio (m/z) and may represent several isomeric ions. Isomeric species having the same element composition can be distinguished by tandem mass spectrometry. An investigation of isomeric $[C,H_3,N,O]^{+\bullet}$ ions provides such an example, where four isomeric ions ($[H_2NC(H)O]^{+\bullet}$, $[H_2NCOH]^{+\bullet}$, $[H_3CNO]^{+\bullet}$ and $[H_2CNOH]^{+\bullet}$) and their neutral counterparts were identified by a combination of experimental results and a resent high level *ab initio* molecular orbital theory calculation.

Many elusive neutral species of great interest have been accessed by a tandem mass spectrometric technique, neutralization-reionization mass spectrometry (NRMS), which was developed in the last decade. In this thesis, three oxides of carbon, O=C=C=O, C=C=O and O=C=C=C=O, which have been the object of many studies by experimentalists and theoreticians for almost a century, were first observed as stable neutral species in the gas phase by NRMS.

In the gas phase, structures of isomeric species having unique behaviours, such as the two cis and trans isomeric 2-buten-dicarboxylic acids, maleic and fumaric acids, can be defined by full investigations of their molecular ions and major fragment ions. The investigations which involved studies of ion thermochemistry and ion dissociation characteristics as well as the use of isotopically labelled compounds provide more information than an early work which used only conventional mass spectrometric techniques.

Table of Contents

Tables

Figures

Chapter 1 Introduction

Tandem mass spectrometry has entered its third decade of application to basic studies of gas phase ion chemistry and its second decade of use in the area of complex mixture analysis, while the era of mass spectrometry started a century ago. The bases of mass spectrometry are the production of ions from neutral compounds and the examination of the subsequent decomposition of these ions. A Tandem mass spectrometer consists of two or more analyzers (magnetic, electrostatic and quadrupole etc.) in which an ion of interest can be selected and then its structure may be analysized. In mass spectrometric terms, structure is defined as the arrangement of atoms only and their connectivity, i.e. how they are bound together in the ion, and not to the bond lengths and angles between atoms.

A mass spectrum contains only peaks of certain mass-to-charge ratios (m/z) and gives no direct information on ion structures. However, on the basis of the indirect evidence of ion thermochemistry and experiments which yield ion dissociation characteristics, combined with the results of high level *ab initio* molecular orbital theory calculations, one can often confidently assign structures to ionic and neutral species produced in a mass spectrometer. The experimentally obtained heats of formation can reflect the stability and dissociation pathways of the ion. These values may be compared with experimental values from similar systems or with those calculated theoretically. The observed decomposition products, structure characteristic fragments of the precursor ion, may be considered on their own merits, or by comparison with the fragmentation pattern of other, reference, precursor ions. In either case, the analysis of

isotopically labelled derivatives can also serve to underline the proposed structure.

The focus of this thesis will be on the generation and structure elucidation of gas-phase isomeric ionic and neutral species and the production of elusive neutral species. Proposed structures have been assigned based on the available thermochemical data, both experimental and theoretical, and the characteristic dissociation pathways observed, for the ions and their isotopomers. Experimental results are detailed in chapters 4, 5 and 6. Chapters 2 and 3 provide a brief review of history and instrumentation as well as description of basic principles and experimental techniques of tandem mass spectrometry.

Chapter 2 provides a brief historical view of tandem mass spectrometry and a detailed description of the mass spectrometers used in this thesis.

Chapter 3 introduces the theory of unimolecular reactions in the gas phase and its application to mass spectrometry. Different types of reactions used in tandem mass spectrometry are discussed on both their chemical and physical basis. The experimental methodology for observation of these reactions and their applications to thermochemical and dissociation characteristic studies are given.

Chapter 4 describes the $[C,H_3,N,O]^{+\bullet}$ isomeric system. Four unique isomeric ionic species are identified. Assignment of their structures has been made on the basis of their metastable ion dissociation (MI), collisional activation (CA) and charge-stripping (CS) mass spectra and high level *ab initio* molecular orbital theory calculations. The neutral counterparts of these ions were also found to be stable neutral species in the gas phase. The experimental and theoretical results are in good agreement.

In chapter 5 an investigation of three elusive molecules, OC_2O, OC_3O and C_2O is presented. Their neutralization-reionization (NR) mass spectra provide evidence of their existence as stable oxides of carbon in the gas phase other than CO and CO_2. This result also proves the related conclusions of previous theoretical calculations which predicted the existence of these species as stable neutral.

Chapter 6 reexamines maleic and fumaric acids and their major fragment ions. The recent work, which combines the use of isotopically labelled derivatives, thermochemical and dissociation characteristic experiments by tandem mass spectrometry, provides more information than an earlier work from this laboratory, reported in 1969.

Chapter 2 History and Basic Instrumentation

2.1 History of Tandem Mass Spectrometry

The development of mass spectrometry can be traced back to 1886, when E. Goldstein[1] discovered positively charged electrical particles. Goldstein used discharge tubes containing perforated cathodes to observed a slightly divergent discharge behind the holes in the cathodes, called "kanalstrahlen" or anode rays. Later, W. Wien [2] showed that the rays of Goldstein were deflected by a magnetic field and then established that these rays carried a positive electrical charge.

Much of the credit for the development of mass spectrometry in the early days has to be given to J.J. Thomson, [3a] the father of mass spectrometry. He built several mass spectrometers including the first tandem instrument consisting of two magnets in series, with the field of one magnet oriented perpendicularly to the other. [3b] In Thomson's days, the pressure within the mass spectrometers were high by today's standards, and numerous ion/molecule interactions took place as a result. Therefore, Thomson not only studied the singly and multiply charged positive ions and negative ions generated in the "ion source", but also identified the nature of some ion/molecule processes, such as charge stripping (section 3.4.4), charge exchange and charge inversion, and observed metastable (section 3.4.2) and collisional activation processes.(section 3.4.3)

For several decades following Thomson's pioneering work in mass spectrometry, much effort went into the attainment of a better vacuum to prevent the "problem" that produced the

extra peaks in Thomson's mass spectra. During this time, F.W. Aston [4] and A.J. Dempster [5] were among the leading practitioners of mass spectrometry, using the technique to determine the relative masses of the isotopes of many atomic elements.

The next major development leading to the technique of tandem mass spectrometry occurred in 1945 when J.A. Hipple and E.U. Condon [6] observed and explained the presence of metastable ions in a mass spectrum. This is the beginning of the required fundamental studies on the use of metastable ions as a source of chemical and physical information.

In the early 1960's, the first tandem mass spectrometry experiments were performed in which instruments were used in unconventional modes to study the metastable decompositions of ions. The first development [7] was the introduction of the accelerating-voltage scan on sector instruments. The next development [8,9] was the discovery of the enhancement of magnitude and quantity of peaks in a "metastable ion" mass spectrum upon introduction of a collision gas into a localized region of the mass spectrometer.

At the time of the initial experiments using collision gas, the focus of the studies was very narrow, and directed primarily towards exploration of physical aspects of the phenomenon. It was in the 1970's, marked by the publication of the book *Metastable Ions* [10], that tandem mass spectrometry entered its modern era, a period in which instruments would be designed expressly for tandem mass spectrometry experiments. The next mile-stone of the modern tandem mass spectrometry is the development of the Neutralization-Reionization technique [11,12] which extended the use of mass spectrometry to study the gaseous ions' neutral counterparts whose structures have not been known.

2.2 Basic Tandem Mass Spectrometry Instrumentation

The primary purpose of a mass spectrometer is to measure the mass-to-charge ratio, m/z, of ions, thus providing a means to identify them. The mass-to-charge ratio of ions can be measured by determining an ion's physical properties, e.g. determination of momentum (by a magnetic analyzer) and energy (by an electrostatic analyzer) of ions are the most popular methods. The principles of this kind of method will be described by the example of the Vacuum Generators Analytical ZAB-2F mass spectrometer which is the major instrument used in this thesis. Two other mass spectrometers involved in this thesis will be also described briefly.

There are many other methods of ion separation that have been used in mass spectrometry. Some important methods are: Time-of-Flight (TOF) [13,14] which measures velocities of ions; Ion Cyclotron Resonance (ICR) [15,16] which measures cyclotron frequencies of ions in a magnetic field; Quadrupole and Ion Trap [17,18] which use the mass selective instabilities of ion trajectories in an oscillating electric field.

2.2.1 Principles of Magnetic-Electrostatic Sector Mass Spectrometers

In a magnetic-electrostatic sector mass spectrometer, the sample to be analyzed is generally introduced into an ion source in which ions characteristic of the sample molecules are produced, usually by electron impact. By the action of electric and magnetic fields, these ions

are sorted according to their mass-to-charge ratios and a plot of the relative abundances of the ions against these ratios constitutes the mass spectrum. *Figure 2-1* is the schematic diagram of the modified VG ZAB-2F double focusing mass spectrometer of reversed geometry.

2.2.1.1 The Ion Source

The arrangement of the electron ionization (EI) ion source is shown in *Figure* 2-2. Sample molecules can be introduced into the ion source via different inlet systems: The septum-injection inlet system is used for volatile liquids. In such an inlet system, volatile liquids are vaporized in the heated reservoir and the vapor diffuses into the source through a capillary leak. The Granville-Phillips (GP) inlet system consists of a variable leak and a pin hole leak. It is used for gases and volatile solids and liquids which have relatively high vapor pressures at room temperature. Nonvolatile samples (mainly solids) are introduced by a probe inlet system where samples are placed into a glass ampule fixed to a probe tip which is inserted directly into the source housing. Finally, gaseous samples may be introduced directly into the ion source via gas lines connected to the ion source block. Electrons are produced from a filament made of tungsten which at a high temperature will emit free electrons. The emitted electrons are attracted to a trap (anode) situated on the opposite side of the ion source from the filament. As a result, the electrons are forced through the central space of the ion source in travelling 15 to 20 mm from the filament to the trap. A pair of small magnets generate a weak magnetic field that causes the electrons to follow a helical path of small diameter, therefore increasing the probability of

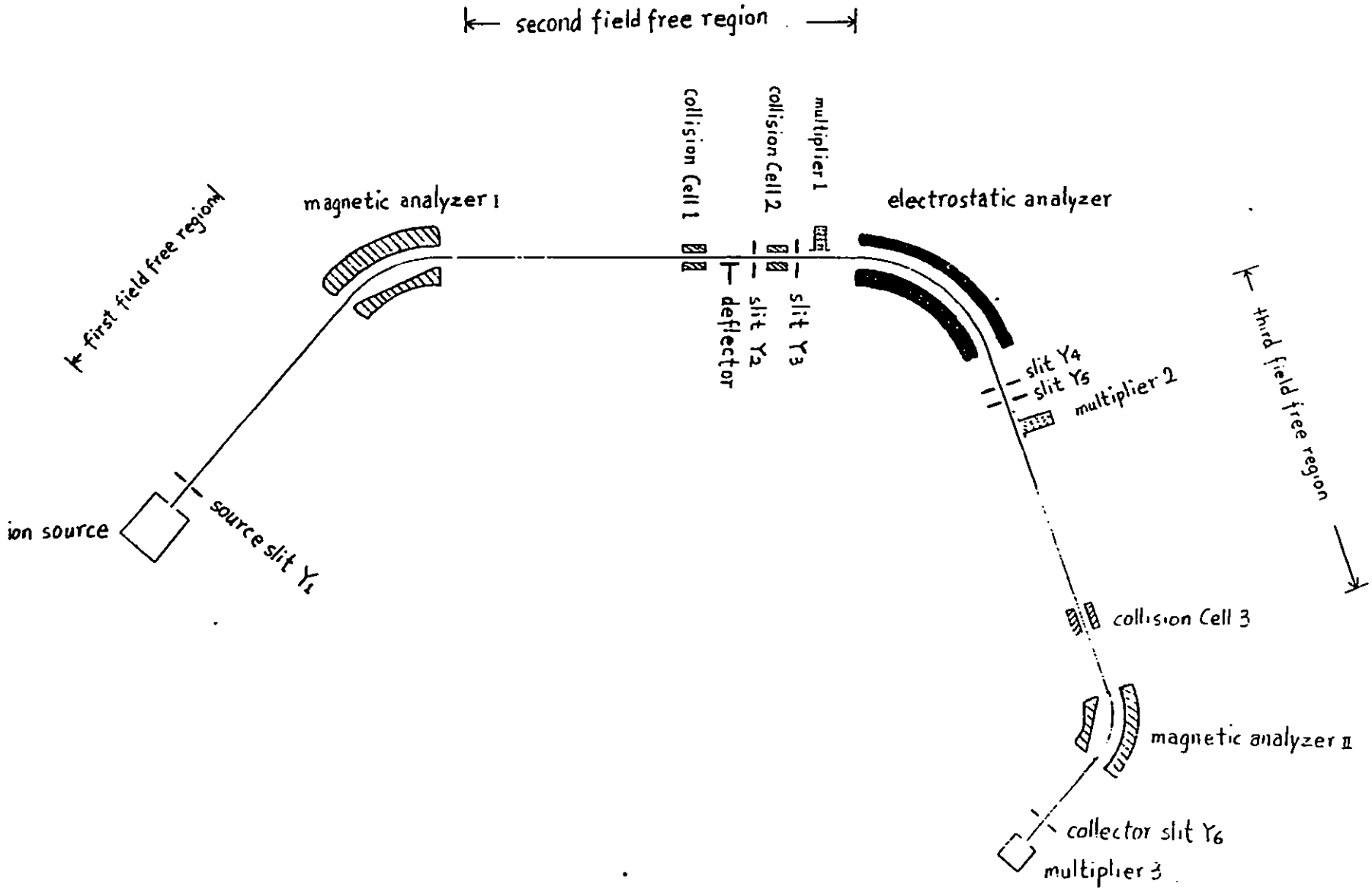

Figure 2-1 Schematic diagram of the modified Vacuum Generators ZAB-2F mass spectrometer.

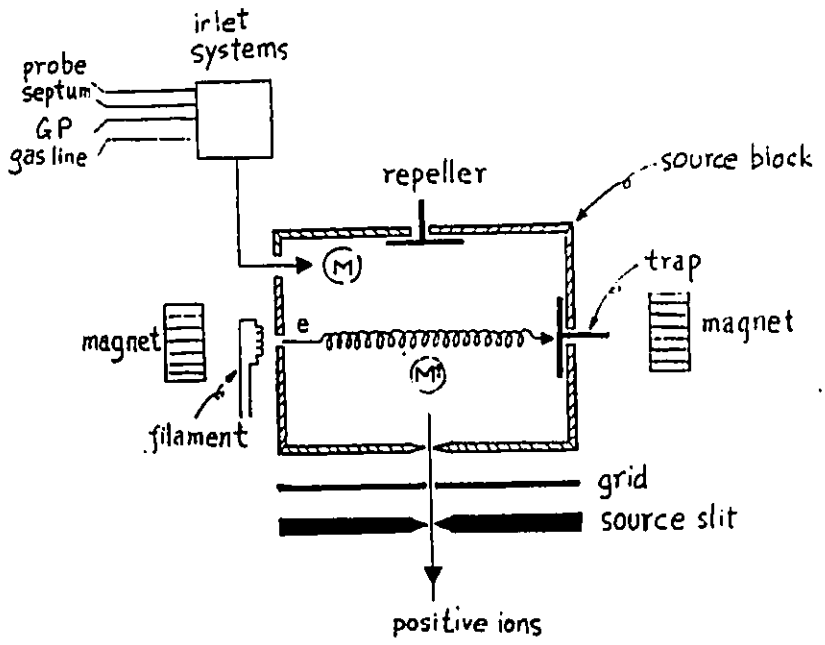

Figure 2-2 Schematic diagram of the ion source of the VG ZAB-2F mass spectrometer.

interaction with sample molecules. The result of the interaction between the sample molecules and the electron beam is that the sample molecules lose an outer shell electron and become radical cations:

$$M_1 + e \rightarrow M_1^{+\bullet} + 2e$$

The ionization time is very short (10^{-16} sec) compared to vibrational periods ($>10^{-14}$ sec). Electron ionization can be considered mainly to be a vertical process in the Franck-Condon sense (section 3.3.2). By changing the potential between the filament and the trap, the energy of the electron beam can be varied. Most reference mass spectra are obtained and reported at 70 eV electron

energy. This amount of energy is much larger than the ionization energy (IE) of molecules (ca 10 eV for most organic compounds). The excess energy will contribute to the internal energy of the sample molecule radical cations. The radical cations, $M_1^{+\cdot}$, with a sufficient amount of internal energy may fragment into fragment ions, M_2^+ and neutral radicals, $M_3^\cdot$:

$$M_1^{+\cdot} \rightarrow M_2^+ + M_3^\cdot$$

By the use of an electron monochromator or precise control of the potential between the filament and the trap to vary the electron energy, one can measure the Ionization Energy (IE) of neutral molecules and the Appearance Energy (AE) of the fragment ions (section 3.3).

Between the repeller plate and the source block there is a weak electric field that is used to draw out the positive ions to the acceleration zone, between the source block and the grid. A large potential gradient (several kilovolts), the acceleration voltage, V, is put between the source block and the grid. The translational energy, E_{tr}, acquired by the ions in their drop through the acceleration zone is:

$$E_{tr} = mv^2/2 = zV \qquad (2\text{-}1)$$

where m is the mass of an ion, v is the velocity of an ion and z is the charge of an ion.

Thus, all the ions carrying the same number of charges leave the ion source with the same translational energy regardless of their mass.

2.2.1.2 The Magnetic Analyzer

After the first field free region (see *Figure 2-1*) there is a magnetic analyzer. The magnetic analyzer disperses ions according to their momentum-to-charge ratios. Ions which pass through a magnetic field, B, perpendicular to their motion, will travel in a circular path in a plane. The motion of the ion is described by:

$$mv^2/r = zvB \tag{2-2}$$

where m, v and z are as defined previously, B is the magnetic field strength and r is the radius of deflection.

If this equation is rearranged, the relation between momentum-to-charge ratios of ions, mv/z, and B can be seen as:

$$mv/z = Br \tag{2-3}$$

Thus ions of different mass, but having the same translational energy, emanating from the same point, follow different trajectories through a stationary magnetic field. At a given magnetic field strength, ions of only one mass-to-charge ratio will follow a trajectory along the central circular path (with radius r_B) of the magnetic analyzer. The mass-to-charge ratio of ions following this trajectory is determined by equation:

$$m/z = B^2r_B^2/2V \tag{2-4}$$

(This equation is obtained by substituting the expression for the ion velocity from equation (2-1) into equation (2-3). The SI units for m, z, B, r, and V are kilogram, coulomb, tesla, meter and volt respectively.)

The mass-to-charge ratio of the ions focused along this trajectory is thus a function of the magnetic field strength, B, and accelerating voltage, V. Therefore, by use of the electron multiplier 1 and scanning the magnetic field B, while the accelerating voltage is (usually) fixed at 8 keV, the normal EI mass spectrum of the ions travelling along the trajectory can be obtained.

2.2.1.3 The Electrostatic Analyzer (ESA)

An energy analyzer, the electrostatic analyzer, is located after the second field free region (see *Figure 2-1*). The electrostatic analyzer disperses ions according to their translational energy-to-charge ratios. The equation of motion of an ion in an electric field is:

$$mv^2/r = zE \qquad (2\text{-}5)$$

where E is the electric field strength (in volt/meter) and other parameters are as previously defined.

In the electrostatic analyzer, ions with the same translational energy-to-mass ratio will be focused on the trajectory along the central circular path with radius r_E. Thus, equation (2-5) can be rearranged to give:

$$mv^2/z = Er_E \qquad (2\text{-}6)$$

The translational energy-to-charge ratio of an ion is therefore a function of electric field strength. With the electron multiplier 2, by scanning the magnetic field B while the electric field E and accelerating voltage are usually fixed at 8 keV, a normal EI mass spectrum with energy resolution can be acquired.

2.2.1.4 The Third Sector

Recently, another magnetic analyzer was added to the ZAB-2F instrument and is located after the electrostatic analyzer (see *Figure 2-1*). This magnetic analyzer functions similarly to the other magetic analyzer. The use of this magnetic analyzer makes it possible to study the reactions taking place in the third field free region, which is the flight tube between the electrostatic analyzer and the second magnetic analyzer.

2.2.1.5 The Electron Multiplier

The detectors used in the ZAB-2F mass spectrometer are electron multipliers. *Figure 2-3* schematically shows such a multiplier. The principle upon which this type of multiplier functions is relatively simple. Fast positive ions strike upon the metal surface of a cathode and cause the emission of a number of secondary electrons. These electrons are then accelerated and allowed to impinge upon another electrode (dynode), causing additional electron emission. Again and

again this process is repeated, using up to 16 stages (dynodes), until finally all of the electrons are collected on the anode. In this way, a large electron current with a multiplication factor of 10^6 to 10^7 can be obtained for each positive ion collected at the cathode.

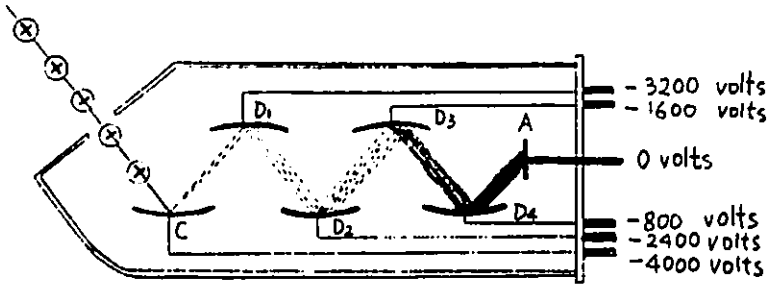

Figure 2-3 *Schematic diagram of an electron multiplier. Positive ions fall on the cathode, C, and cause emission of secondary electrons; D_1 to D_4 are dynodes separated by 800 V each; A is the anode for collection of the electrons.*

For detecting positive ions, the operation of the electron multiplier usually involves a rather large negative potential on the cathode, with the anode held at or near ground potential. For detecting negative ions, a large positive potential is put on the anode while the cathode is kept at or near ground potential. This kind of multiplier has high sensitivity and rapid response; but because the amplification of the multiplier in vacuum and in the presence of various gases changes with time and sample, it does not give an absolute ion current and abundance measurement. Alternatively, a Faraday cup detector can be used to measure absolute ion currents and abundances. A Faraday cup detector is a metal cup equipped with a pair of magnets. When fast ions impact the inside surface of the cup, electrons will be emitted and prevented from escaping by the magnets, and the resulting electric current change on the surface can be detected.

2.2.2 The GEC-AEI MS-902S Mass Spectrometer

The MS-902S is a forward geometry mass spectrometer, that is the electrostatic analyzer precedes the magnetic analyzer (*Figure 2-4*). The principle of obtaining a mass spectrum by this instrument is simular to that of the ZAB-2F mass spectrometer. The MS-902S does not have the septum inlet system but does have three inlet systems: probe, GP and gas inlet. Due to the precise design and construction of the ion source the MS-902S provides better control of the energy of the electron beam. Therefore, it is used in ion thermodynamic experiments, such as appearance energy (AE) measurements of metastably generated ions produced in the first field free region. (section 3.3.7.2)

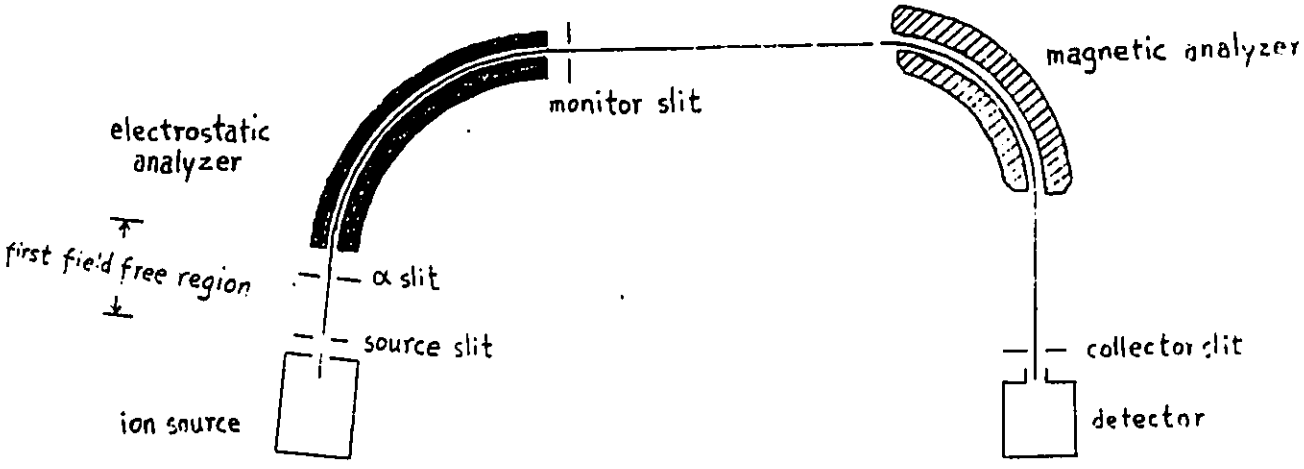

Figure 2-4 Schematic diagram of the GEC-AEI MS-902S mass spectrometer.

2.2.3 The Electron Energy Selector Mass Spectrometer

The electron energy selector mass spectrometer is not a tandem instrument. It consists of a two-stage double-hemispherical electron energy selector, electron monochromator, and a quadrupole mass analyzer (*Figure 2-5*). It was designed and built by F.P. Lossing and co-workers[19]. This type of instrument has been successfully used in a number of laboratories for the accurate measurement of adiabatic ionization energies (IE) and appearance energies (AE).

In this mass spectrometer, an electron beam is generated by an electron gun and then focused through two pairs of hemispherical electrodes and a collimator. Sample molecules are ionized by the energy selected electron beam in the ion source and analyzed by a quadrupole mass analyzer. The electron monochromator can produce a nearly monoenergetic electron beam over an energy range from 5 to 30 eV. With a calibrant, like H_2O, and a computer data processing system, the adiabatic AE and IE values may be obtained with an accuracy of ± 0.05 eV.

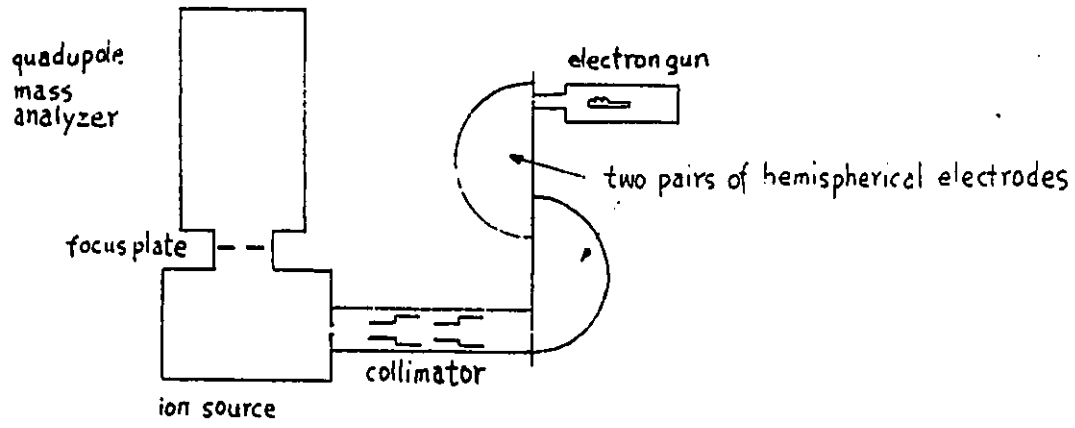

Figure 2-5 Schematic diagram of the electron selector mass spectrometer.

Chapter 3 Reactions and Experimental Techniques

3.1 Introduction

Tandem mass spectrometry has played a particularly important role in assigning structures to ions in the gas phase. Studies performed using tandem instruments (specifically, double focusing mass spectrometers of reversed geometry, such as ZAB-2F) have been successful in obtaining fundamental chemical information from gas-phase ions. Two chief experimental methods are ion thermochemistry and ion dissociation characteristic experiments. As well as experimental studies of gas-phase ion chemistry, the theory of unimolecular reactions of isolated (gas-phase) ions has been also developed.

In this chapter, the theory of unimolecular reactions will be described briefly. The nature of gas-phase ion reactions and the experimental methods used to study them will be discussed in detail.

3.2 Basic Concepts

3.2.1 The Theory of Unimolecular Reactions

The theory of unimolecular reactions has been referred to as both quasi-equilibrium theory

(QET) [20] and the RRKM version of statistical theory (after Rice, Ramsberger, Kassel and Marcus)[21]. Mass spectrometry is a useful tool in testing the assumptions of the theory because gas-phase ion reactions can take place in collision-free conditions (isolated reactants and products), and the ionic species can be selected and identified with high specificity. In general, the theory has been successful in rationalizating conventional electron impact ionization (Normal EI) mass spectra of simple polyatomic molecules and has therefore been adopted as a useful statistical theory of mass spectrometry. For the purpose of this thesis, the four basic assumptions of the theory are as follows:

(1) The time required for dissociation of a polyatomic ion is long compared to the time required for its formation and excitation.

(2) The rate of dissociation of an ion is slower than the rate of redistribution of internal energy among all the internal degrees of freedom.

(3) Ions achieve a condition of internal energy equilibrium in which energy is distributed over all internal degrees of freedom with equal probability.

(4) The observed dissociation products result from a series of competing and consecutive reactions.

Central to the theory is the internal energy-dependent rate constant, $k(\varepsilon)$, that characterizes each possible dissociation reaction. For illustrative purposes, the simplified form of the rate constant equation is given by:

$$k(\varepsilon) = \nu[(\varepsilon - \varepsilon_o)/\varepsilon]^{s-1} \qquad (3\text{-}1)$$

where ε is the internal energy of the ion, ε_o is the critical energy, which is the minimum energy required for the reaction, s is the effective number of oscillators in the ion, and ν is the frequency factor.

This equation is illustrated by *Figure 3-1*:

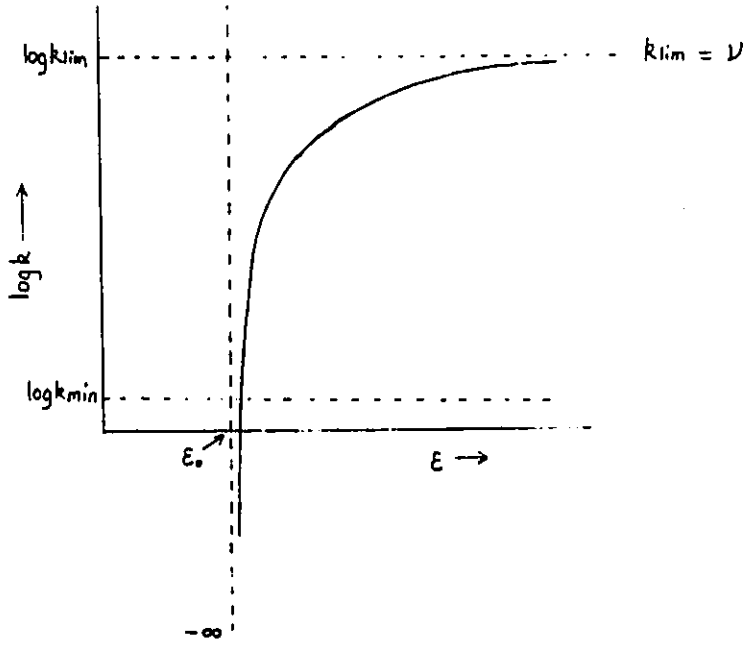

Figure 3-1 *Relationship between the rate constant for unimolecular dissociation, k, and the internal energy of a positively charged ion, ε. k_{lim} is the upper limit of k and k_{min} is the minimum value for k.*

In the following sections of this chapter, some phenomena of the unimolecular reactions taking place in the ion source and the field free regions of the instruments will be explained based on the four assumptions of the theory and the rate constant equation.

3.2.2 Metastable Ions

Ions in a mass spectrometer are classified as stable, unstable, or metastable. Stable ions are those that are formed within the ion source and travel from the ion source to the collector without decomposition. Unstable ions are those that are formed with sufficient internal energy such that they decompose before leaving the ion source. Metastable ions are those that are sufficiently stable to leave the ion source without fragmenting, but decompose before reaching the collector. *Figure 3-2* shows the interrelationship among the ion abundance, internal energy and reaction rate constant of ions formed in an ion source.

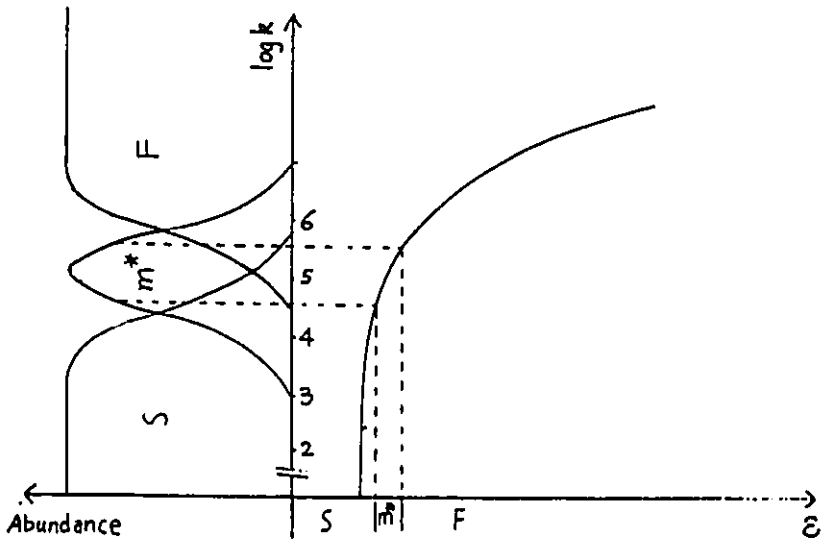

Figure 3-2 *Interrelationship among abundance, internal energy and rate constants of stable (S), metastable (m^*) and fragment (F) ions formed in an ion source.*

From these curves, one can notice that metastable ions only occur over a narrow range of internal energies and reaction rate constants, typically between 10^4 to 10^6 sec^{-1}.

Since the reaction rate constant is related to the time scale of the experiment, the observation of reactions of stable, unstable and metastable ions depends on instrumental parameters, such as source residence time and flight time of the ions. An early study [22] on appearance energy (AE) measurements using the MS-902S and the electron energy selector mass spectrometers showed that the lower observation limits of reaction rate constants were about 10^4 sec^{-1} for the metastable reactions taking place in the first field region of the MS-902S and about 10^3 sec^{-1} for the reactions taking place in the ion source of the electron energy selector mass spectrometer. For the ZAB-2F instrument [23] the detailed time-scale of events is illustrated by *Figure 3-3.*

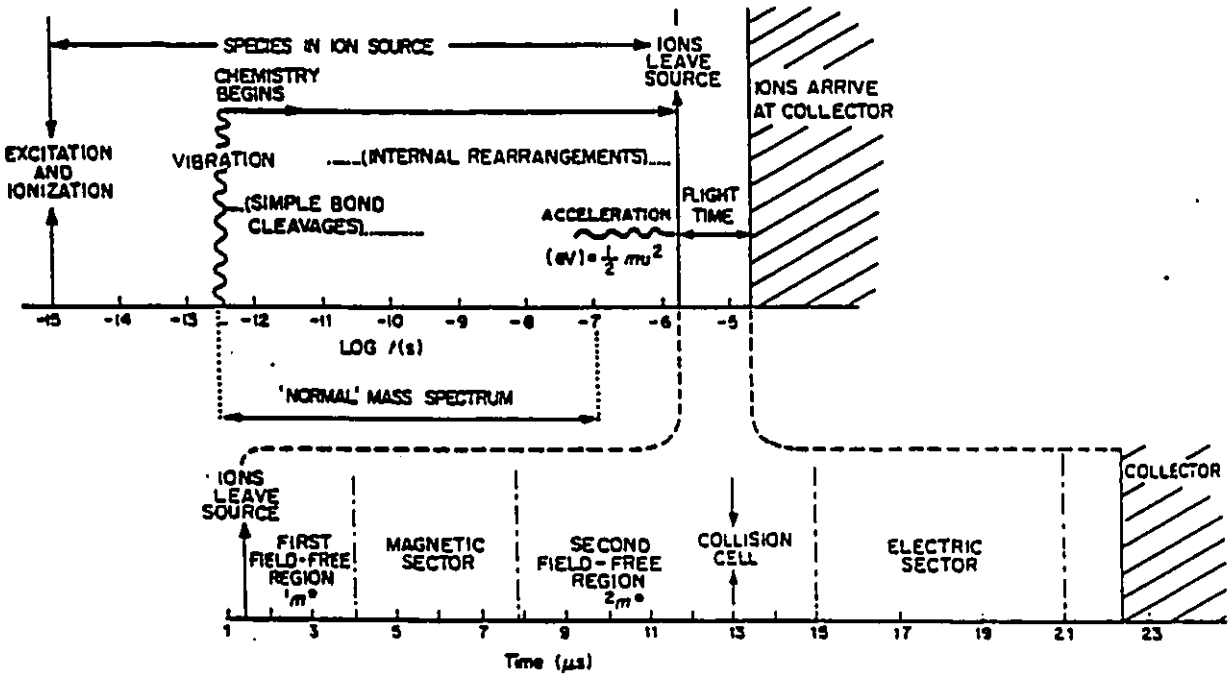

Figure 3-3 Time-scale of events for the ZAB-2F mass spectrometer (acceleration voltage 8kV, ion m/z 100). Reproduced from Ref. 23.

3.2.3 Isomerization

Within the ion source ions are generated with a wide range of internal energies. They are not limited to dissociation but may rearrange to various isomeric structures. These isomerization reactions can make the interpretation of mass spectra complicated and therefore some understanding of the relationship between dissociation and isomerization reactions is necessary.

Figure 3-4 shows that an ion having a structure $[ABC]^{+\bullet}$ needs critical energy ε_0^{AB} for dissociation to $[AB]^+ + \dot{C}$ and ε_0^i for rearrangement to its isomer $[ACB]^{+\bullet}$. The isomer $[ACB]^{+\bullet}$ has its independent dissociation channel to $[AC]^+ + B^\bullet$ with critical energy ε_0^{AC}.

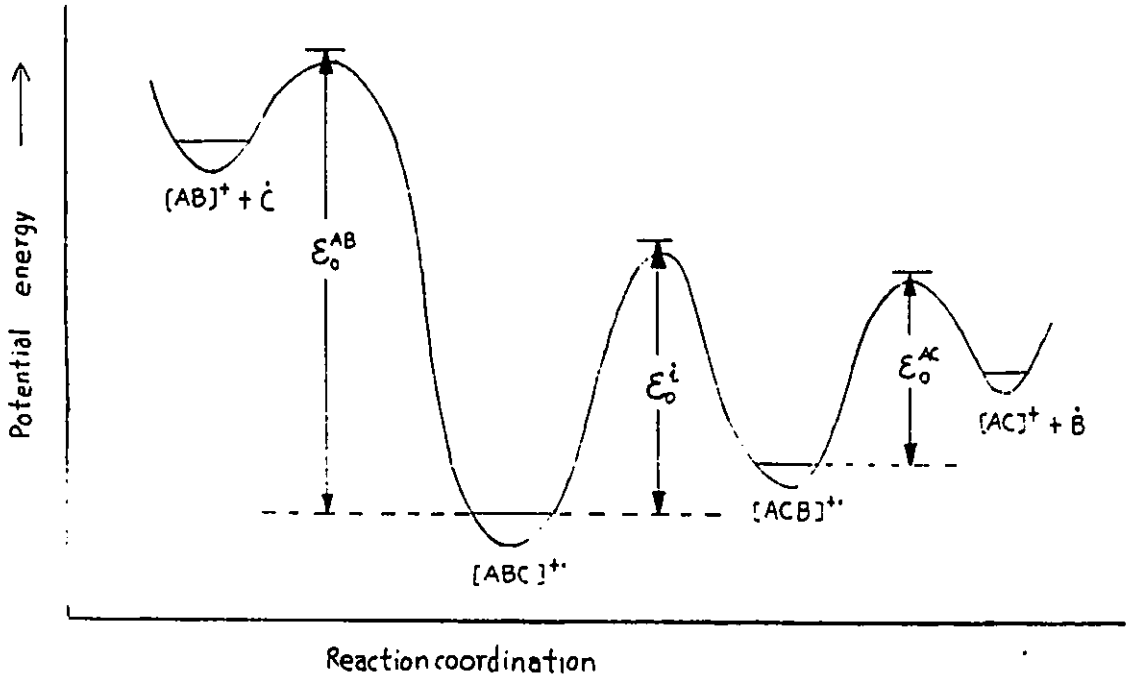

Figure 3-4 *Schematic potential energy diagram illustrating the possibility of isomerization between ions $[ABC]^{+\bullet}$ and $[ACB]^{+\bullet}$, versus their dissociation to $[AB]^+ + \dot{C}$ and $[AC]^+ + B^\bullet$.*

On the time scale for the processes taking place within the ion source, both dissociation and isomerization reactions will take place at internal energies much higher than the critical energies. Therefore, normal electron impact ionization (EI) mass spectra (section 2.2.1.2 and 2.2.1.3), which record information of reactions within the ion source, yield less structural information of isomers than metastable ion (MI) mass spectra (section 3.4.2).

On the metastable time scale, only a narrow range of internal energies, close above the critical energies, is available, so the competition of dissociation and isomerization reactions depends on the rate constants of the reactions. Three typical situations may be found:

(1) If $\varepsilon_i \gg \varepsilon_0^{AB}$ and ε_0^{AC}, the isomerization reaction does not occur. MI mass spectra will give structural information for each of the isomers.

(2) If $\varepsilon_i \ll \varepsilon_0^{AB}$ and ε_0^{AC} are in the same order of magnitude, isomerization between $[ABC]^{+\bullet}$ and $[ACB]^{+\bullet}$ will prohibit the structural elucidation of $[ABC]^{+\bullet}$ and $[ACB]^{+\bullet}$, since $[ABC]^{+\bullet}$ and $[ACB]^{+\bullet}$ can interconvert before they independently fragment. As a result, the MI mass spectrum of $[ABC]^{+\bullet}$ will be the same as that of $[ACB]^{+\bullet}$.

(3) If $\varepsilon_0^{AB} \gg \varepsilon_i$ and ε_0^{AC}, $[ABC]^{+\bullet}$ will not dissociate to $[AB]^+ + \dot{C}$ but rearrange to $[ACB]^{+\bullet}$ prior to fragmenting to $[AC]^+ + B^\bullet$. In this case $[ACB]^{+\bullet}$ is the reacting configuration [24] of $[ABC]^{+\bullet}$, the structure which leads directly to the activation complex without further rearrangement. MI mass spectrum of $[ABC]^{+\bullet}$ will be very close to that of $[ACB]^{+\bullet}$. Further investigation involving other experiments, such as collisional activation (CA) (section 3.4.3) is needed to distinguish the isomers.

3.3 Ion Thermochemistry

3.3.1 Introduction

Ion thermochemistry studies the heats of formation of ions and neutrals which in turn may permit identification of structures of the ions and the neutrals. The experiments include the measurements of ionization energies (IE) of neutral molecules and appearance energies (AE) of dissociation reactions of ions. The data (heats of formation) obtained in these experiments are essential to firmly establish the structures of ionic and neutral species. This is especially true when a whole system of isomeric species is involved. The heat of formation of a species may be considered to be specific. Hence, the structure of the species may be revealed by its heat of formation.

3.3.2 Ionization Energy and Appearance Energy

The minimum energy required to remove an electron from the highest occupied orbital of a molecule is called the first ionization energy (IE). In the production of molecular ions by electron impact ionization

$$M_i + e \rightarrow M_i^{+\bullet} + 2e$$

ionization is said to occur by a vertical or Franck-Condon type of process [25] in which inter-nuclear distances remain fixed at the appropriate values for the neutral molecule because the

ionization time is much shorter than the vibrational periods. Therefore the minimum energy necessary to produce molecular ions by electron impact is usually the vertical ionization energy (IE_v) and may be greater than the minimum energy necessary to produce molecular ions in their ground states (the adiabatic ionization energy, IE_{ad}).

If a fragment ion M_2^+ is formed from $M_1^{+\cdot}$ by the reaction,

$$M_1^{+\cdot} \rightarrow M_2^+ + M_3^{\cdot}$$

according to the quasi-equilibrium theory, the appearance energy of M_2^+, $AE(M_2^+)$, is a measure of the adiabatic ionization energy of M_1, $IE_{ad}(M_1)$, plus the critical energy, ε_0 and nonfixed kinetic shift, $\varepsilon^{\ddagger}$, of the reaction. This situation is illustrated in *Figure 3-5*.

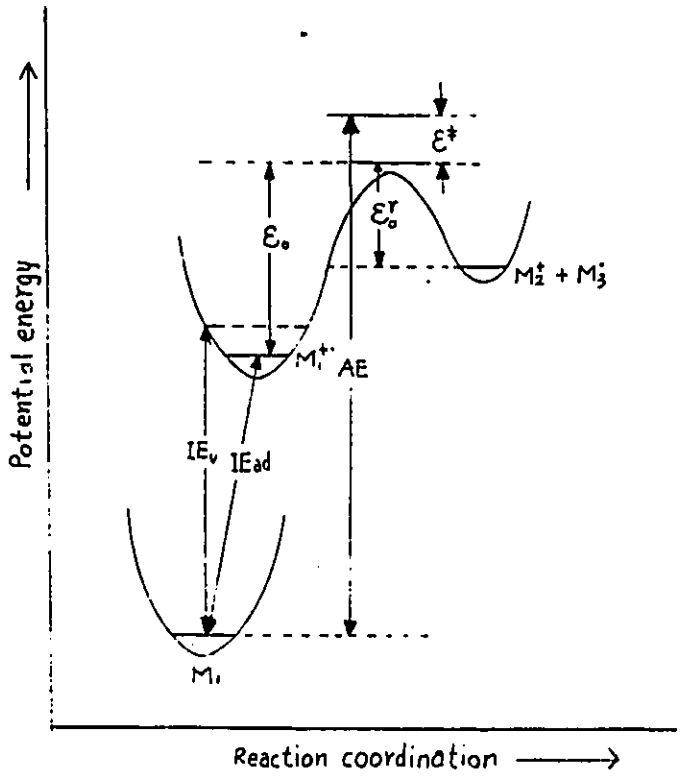

Figure 3-5 *Schematic potential energy diagram illustrating the determination of heats of formation of gaseous ions.*

The heat of formation of the molecular ion, $M_1^{+\bullet}$, is given by:

$$\Delta H_f^\bullet(M_1^{+\bullet}) = IE(M_1) + \Delta H_f^\bullet(M_1) \qquad (3\text{-}2)$$

And the heat of formation of the fragment ion, M_2^+, is expressed by:

$$\Delta H_f^\bullet(M_2^+) = AE(M_2^+) + \Delta H_f^\bullet(M_1) - \Delta H_f^\bullet(M_3^\bullet) \qquad (3\text{-}3)$$

The measured value for $\Delta H_f^\bullet(M_2^+)$ will be close to the true value if the fragmentation of $M_1^{+\bullet}$ has no significant kinetic shift and the reverse reaction

$$M_2^+ + M_3^\bullet \rightarrow M_1^{+\bullet}$$

has no energy barrier. (The problem of kinetic shift and energy barrier of reverse reaction will be discussed in next section.)

With the measured $IE(M_1)$ and $AE(M_2^+)$, one still needs to know $\Delta H_f^\bullet(M_1)$ and $\Delta H_f^\bullet(M_3^\bullet)$ in order to use equations (3-2) and (3-3) to calculate $\Delta H_f^\bullet(M_1^{+\bullet})$ and $\Delta H_f^\bullet(M_2^+)$. The heats of formation of neutral and ionic species are available in the literature. [26,27] If $\Delta H_f^\bullet(M_1)$ and $\Delta H_f^\bullet(M_3^\bullet)$ can not be found in the literature, they may be estimated by Benson's additivity scheme. [28]

Alternatively, in equation (3-3), if $\Delta H_f^\bullet(M_2^+)$ is known, the equation can be used to calculate $\Delta H_f^\bullet(M_3^\bullet)$. $\Delta H_f^\bullet(M_2^+)$ can be found in the literature [26] or can be estimated by a scheme produced by Holmes, Fingas and Lossing. [29]

3.3.3 Kinetic Shift and Reverse Activation Energy

In order to observe fragment ions, M_2^+, in the normal EI mass spectrum, these ions must be formed within the ion source block. Typically an ion spends about 10^{-6} second in this region before acceleration and an appreciable number of M_2^+ ions must be formed in this time interval to ensure their observation. Hence, from the rate constant equation (3-1), some excess energy, $\varepsilon^\ddagger = (\varepsilon - \varepsilon_\circ)$, is necessary for the observation of M_2^+ on this time-scale. This excess energy is termed the kinetic shift. [30] The relative kinetic shift, $(\varepsilon - \varepsilon_\circ)/\varepsilon$, is given by rearranging equation (3-1) to:

$$(\varepsilon - \varepsilon_\circ)/\varepsilon = (k/\nu)^{1/(s-1)} \qquad (3\text{-}4)$$

The absolute kinetic shift $\varepsilon^\ddagger$ is dependent upon the time-scale for the observation of the reaction and the shape of the log k versus ε curve. *Figures 3-6* and *3-7* show how the kinetic shift is affected by these factors.

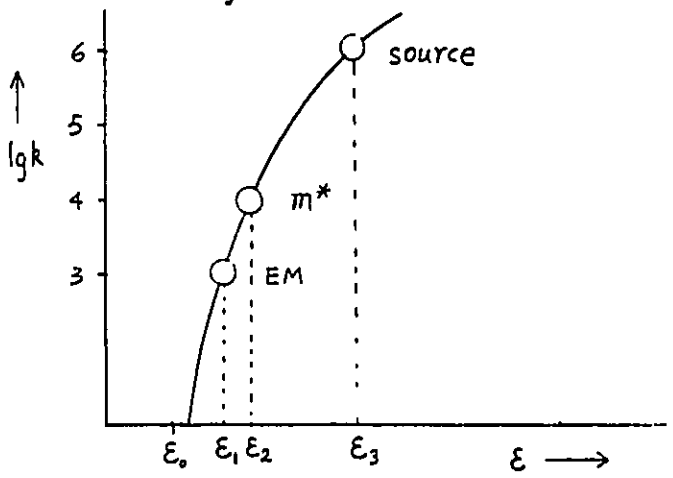

Figure 3-6

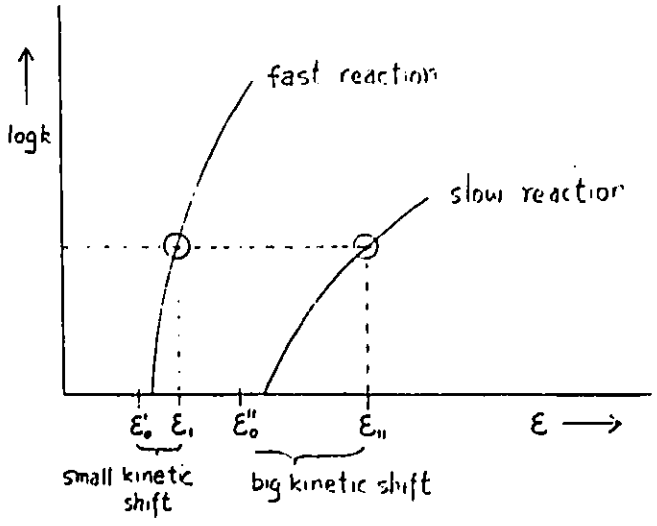

Figure 3-7

Figure 3-6 *logk versus ε curve illustrating the relationship between kinetic shift and experimental time frame, EM - the electron selector mass spectrometer, m* and source - first field free region and ion source of the MS-902S mass spectrometer. Reproduced from Ref.22.*

Figure 3-7 *logk versus ε curves illustrating relationship between kinetic shift and reaction rate.*

From these two figures, one can conclude that

(a) A unimolecular reaction will have a significant kinetic shift when its rate constant rises slowly with increase in internal energy, and as a result, the measured appearance energy will lead to an upper limit for the heat of formation of the fragment ion.

(b) The absence of a metastable peak for a reaction indicates that the reaction is fast and the measured appearance energy may lead to a value close to the true value of the heat of formation of the fragment ion.

(c) The error introduced into the heat of formation of the fragment ion by the kinetic shift can be reduced by measuring the appearance energy of the reaction in the metastable time-frame or at a longer source residence time.

The absence of a corresponding metastable peak does not guarantee that a true value of the heat of formation of the fragment ion is obtained. The error in the heat of formation of the fragment ion caused by the reverse activation energy, ε_r, is obvious (*Figure 3-5*). Generally speaking, most direct bond cleavage reactions have only small or no reverse activation energy and rearrangement reactions may proceed with substantial reverse activation energy. [31]

Both the kinetic shift and reverse activation energy of a unimolecular reaction can be evaluated by the study of the peak shape of the metastable peak generated by the reaction. (section 3.4.2.1)

3.3.4 Competitive Shift

When an ion has more than one dissociation channel, the measurement of the appearance energy may be further complicated if these dissociation reactions have log k(ε) versus ε curves which intersect. One typical example is the competition between rearrangement (r) and direct bond cleavage (c) reactions (*Figure 3-8*). Rearrangement reactions usually have lower critical energies and smaller frequency factors than direct bond cleavage reactions. Therefore, near its threshold, a rearrangement reaction needs much more excess internal energy (ε-ε$_o$) in order to compete with the faster direct bond cleavage reaction, and the observed AE of the rearrangement reaction will be erroneously high as a result.

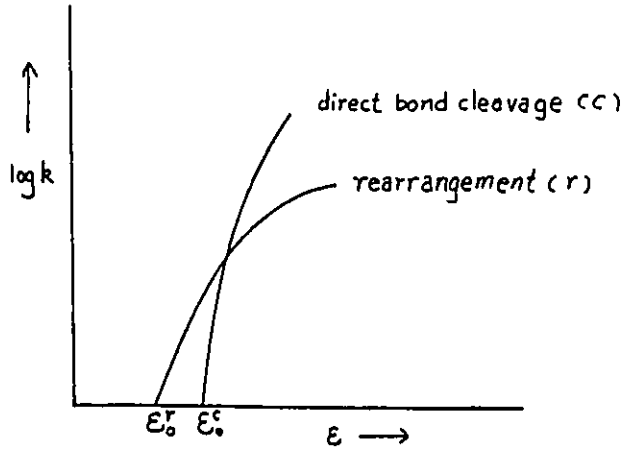

Figure 3-8 *logk versus ε curves for competing reactions involving rearrangement, (r), and direct bond cleavage, (c).*

3.3.5 The Problem Caused by Collisional Activation

With all the problems described above, the IE and AE measurements will yield values of the heat of formation of the fragment ion which are greater than the true value. On the other hand, the problem caused by collisional activation (CA) (section 3.4.3) will lower the apparent value for the heat of formation of the fragment ion. This is because ions can get extra internal energy by converting some of their translational energy into internal energy during collisions. But collisional activation will affect the measurements only when the ion source pressure is too high or the reaction has a large collision cross-section. In practice this problem can be identified by comparing the intensities of the signal under study at different source pressures. If the ratio of the signal intensity/ion source pressure increases when the ion source pressure is increased, there will be a problem due to collisional activation.

3.3.6 Isomeric Species

In ionization energy and appearance energy measurements the abundance of a signal corresponding to a certain m/z value is recorded at different electron energies near the reaction threshold. But the m/z value may possibly corresponds to not only one species. In the situation when several species are generated, the measured AE will correspond to the thermodynamically most stable isomer in the mixture. This problem may be avoided by measuring appearance energies of metastably generated ions whose generation may be more specific (section 3.3.7.2).

3.3.7 IE and AE Experimental Determinations

3.3.7.1 The Method

The method used in this thesis for determining ionization energies and appearance energies is to compare the ionization efficiency curve of a sample ion (with an unknown IE or AE) with the ionization efficiency curve of a calibrant. The calibrant is needed to calibrate the electron energy scale because the electron beam is not usually homogeneous in energy, but rather has an energy distribution due to the thermionic emission of electrons from the hot filament.

In the IE or AE measurements with the MS-902S instrument, ionization efficiency curves (*Figure 3-9*) of both sample ion and calibrant ion are obtained under identical instrumental conditions. The ion abundance (peak height) scale of either the sample ion or the calibrant ion is arbitrarily adjusted to make the ionization efficiency curves parallel. Then, the electron energy (in electron volts) differences, ΔV, at various values of peak height, h, are determined from the bottom parts of the curves. Finally, a plot of ΔV versus h, *Figure 3-10*, is prepared, and the curve is linearly extrapolated to $h = 0$. The value of ΔV at $h = 0$, ΔV_0, is taken as the difference between the appearance energies of the calibrant ion and the sample ion under study. This method, proposed by Warren [32], has been used by a number of workers and was found to be reasonably satisfactory. An accuracy of $\pm$ 0.1 eV can be achieved for this type of experiment.

For the electron energy selector mass spectrometer, ionization energies and appearance energies are measured by a similar method. The electron energy scale is first calibrated by a calibrant, usually H_2O, and the obtained data is stored in a computer data processing system.

Then the ionization efficiency curve of the sample ion is constructed in the calibrated electron energy scale. The electron energy at the onset of the curve corresponds to the ionization energy or appearance energy of the sample ion.

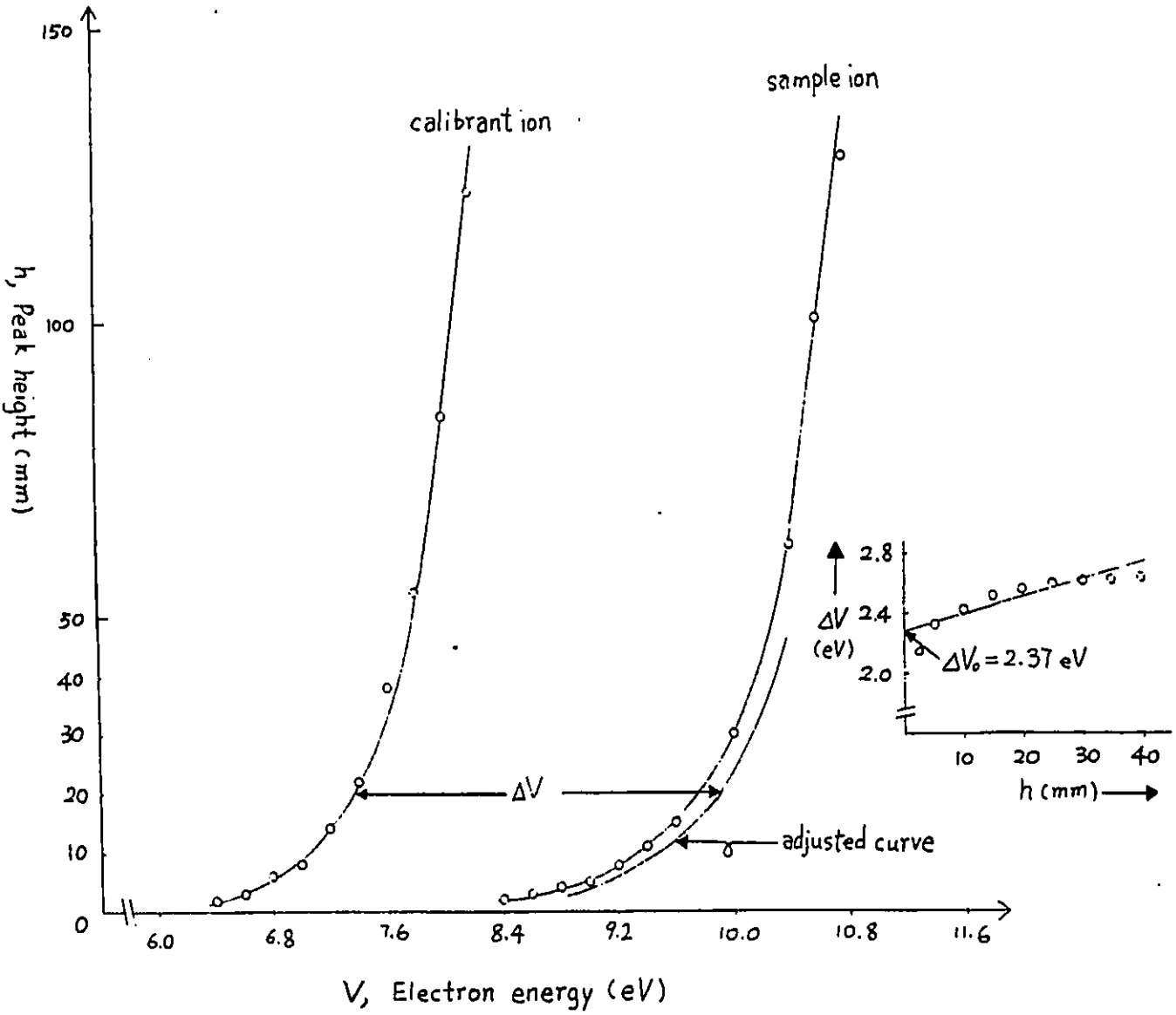

Figure 3-9 *Ionization efficiency curves of the sample ion ($[C_4H_2DO_3]^+$ from fumaric acid-carboxyl-d_2, DOOCCH=CHCOOD) and the calibrant ion, benzene molecular ion.*

Figure 3-10 (inset) *ΔV versus h curve for measuring ΔV.. See text for details.*

3.3.7.2 AE Measurement for Metastably Generated Ions

Reactions of metastable ions take place at lower internal energies than those taking place in the ion source. Hence, the measured appearance energies for the metastably generated ions will be more reliable because the kinetic shift in the metastable time frame will be smaller. Furthermore, ions formed in metastable reactions may be identified by their dissociation characteristics and are less likely to have multiple-structures. [33]

This type of experiment can be done in the first field free region (see *Figure 2-4*) on the MS-902S instrument. For a metastable ion $M_1^{+\bullet}$ dissociating

$$M_1^{+\bullet} \xrightarrow{\bullet} M_2^{+} + M_3^{\bullet}$$

in this region, the electrostatic sector voltage, E, and ion accelerating voltage, V, are both reduced from their normal beam-transmitting values in the ratio m_2/m_1. The fragment ion, M_2^+ is then selected by adjustment of the magnetic field strength, B. Both sample ion, M_2^+, and a calibrant ion will be measured to obtain the ionization efficiency curves. The calibrant ion is usually $H_3CH_2C\text{-}O\text{-}^+CH_2$ generated from metastable diethyl ether molecular ion. [34]

$$H_3CH_2C\text{-}O\text{-}CH_2CH_3 \rightarrow [H_3CH_2C\text{-}O\text{-}CH_2CH_3]^{+\bullet} \xrightarrow{\bullet} H_3CH_2C\text{-}O\text{-}^+CH_2 + \dot{C}H_3$$

AE = 10.26 eV

3.3.8 Applications

Measurements of IE of neutral molecules and AE of fragment ions for ion dissociation reactions provide heats of formation of ionic and neutral species. Knowledge of these heats of formation may permit identification of structures of ions and neutrals as well as reaction processes.

Identical heats of formation for a measured "unknown" species and a known species imply that they may have the same structure. But before any firm conclusion can be made, the reaction pathway by which the new species is formed should be developed by a combination of theoretical calculations and studies of ion dissociation characteristics (section 3.4). For example, $[C,H_4,O]^{+\cdot}$ ions have been generated [35] in the following reactions:

$$(CH_2OH)_2 \rightarrow [C,H_4,O]^{+\cdot} + CH_2O + e$$

$$HOCH_2COOH \rightarrow [C,H_4,O]^{+\cdot} + CO_2 + e$$

$$HOCH_2CHO \rightarrow [C,H_4,O]^{+\cdot} + CO + e$$

The structures and heats of formation of the neutral species in these reactions are well known, and the heat of formation of the $[C,H_4,O]^{+\cdot}$ ion was obtained to be 815 ± 8 kJ mol^{-1} from the measured AE values of the above reactions. This value is significantly below the heat of formation of $[H_3COH]^{+\cdot}$ (845.3 kJ mol^{-1}). This indicates that another $[C,H_4,O]^{+\cdot}$ isomer should be involved. The $[C,H_4,O]^{+\cdot}$ isomer was found to be $[H_2COH_2]^{+\cdot}$ whose calculated heat of formation

is 798 kJ mol^{-1}, in good agreement with the above measured value. Structures of ions $[H_3COH]^{+\bullet}$ and $[H_2COH_2]^{+\bullet}$ were confirmed [35] by their collisional activation (CA) mass spectra (section 3.4.3) and their charge stripping (CS) mass spectra (section 3.4.4).

From results of AE measurements, reaction processes can be also studied. A simple example is that the fragmentation of benzonitrile,

$$[C_6H_5CN] \rightarrow [C_6H_4]^{+\bullet} + HCN + e$$

was found [22] to have unusually large kinetic shift based on the observation that the measured AE of the above reaction is reduced by ~ 0.3 eV when the mean fragmentation rate constant is dropped from 10^5 to 10^4 s^{-1}.

The application of ion thermochemistry to identify ionic and neutral species is not limited to an exact match between measured heats of formation and literature values. The measured AE can be used to eliminate impossible products from a fragmentation reaction. For instance, the major fragmentation of ionized aniline

$$[C_6H_5NH_2]^{+\bullet} \rightarrow [C_5H_6]^{+\bullet} + [H,C,N]$$

produces a [H,C,N] neutral species. But the AE of $[C_5H_6]^{+\bullet}$ was found [36,37] to lie about 0.8 eV above the calculated threshold if HCN is considered to be generated. Therefore the isomer of HCN, HNC, whose heat of formation is 0.6 ± 0.1 eV higher than $\Delta H_f^{\bullet}$(HCN), was proposed [37] to be the [H,C,N] neutral species. This result was supported by a collisionally induced

dissociative ionization (CIDI, section 3.4.5.5) experiment, [38] which clearly showed that HNC was indeed generated.

From the above examples, it can be concluded that ion thermochemistry plays an important role in identification of ionic and neutral species.

3.4 Ion Dissociation Characteristics

3.4.1 Introduction

Among ion thermochemistry, ion dissociation characteristics and theoretical calculations, ion dissociation characteristics are the key to identify ionic and neutral species in the gas phase. Ion dissociation characteristics involve the study of fragmentation reactions of gaseous ions and neutrals. These reactions concerning the topics of this thesis include metastable ion dissociation (MI) and reactions, caused by interactions between the fast moving ionic or neutral species and the stationary target gas atoms or molecules, including collisional activation (CA), charge stripping (CS), collisionally induced dissociative ionization (CIDI) and neutralization-reionization (NR). They show structural "pictures" (mass spectra) of a species of interest from different perspectives. Interpretation of these "pictures" may allow one to construct the full "picture" of the structure of the selected species. In the following, each of the above mentioned reactions and its applications will be described. It should be emphasized here that the study of each of these reactions may also involve the use of isotopically labelled compounds, the time-honoured method

that has proved to be of immense value in unravelling the complexities of reaction pathways.

3.4.2 Metastable Ion Dissociation

As outlined in section 2.1, metastable ion dissociation reactions have been observed in early mass spectrometry studies and first recognized by Hipple and Condon in 1945. As stated in section 3.2.2, these reactions take place with significant amount of internal energies and have rate constants from 10^4 to 10^6 s^{-1}.

The detection of stable ions and fragment ions formed in the ion source has been described in section 2.2.1. The detection of products (fragment ions or daughter ions) of metastable ion dissociation reactions depends upon where these reactions take place in a mass spectrometer. The reactions taking place within the magnetic or electrostatic analyzer cannot be observed because the equations of motion (equations (2-2) and (2-5)) do not apply to these ions insofar as they will not be refocused by either field. The fragment ions generated in the metastable ion dissociation reactions taking place in the field free regions in a mass spectrometer can be detected by determination of the proportional distributions of momentum or kinetic energy of the parent ion among the fragment ions.

For a mass spectrometer of reversed geometry, like the ZAB-2F instrument, the detection of the last type of fragment ions is illustrated as follows:

If a metastable ion M_1^{+*} dissociates to fragment ion M_2^+ and neutral M_3^*, the laws of conservation of momentum and energy have to be obeyed. Therefore the kinetic energy of the parent ion M_1^{+*} ($\frac{1}{2}m_1v_1^2 = zV$, equation (2-1)) is distributed proportionally between M_2^+ and M_3^*:

$$\frac{1}{2}m_2v_2^2 = m_2/m_1 \cdot zV \quad (3\text{-}5)$$

$$\frac{1}{2}m_3v_3^2 = m_3/m_1 \cdot zV \quad (3\text{-}6)$$

The momentum of $M_1^{+\bullet}$ ($m_1v_1 = zBr_B$, equation (2-3)) is also distributed proportionally between M_2^+ and $M_3^{\bullet}$:

$$m_2v_2 = m_2/m_1 \cdot zBr_B \quad (3\text{-}7)$$

$$m_3v_3 = m_3/m_1 \cdot zBr_B \quad (3\text{-}8)$$

Since the velocity of the particles is virtually unchanged, the kinetic energy and momentum of the products is related directly to instrument parameters, V (accelerating voltage), B (magnetic field strength) and r_B (central radii of the magnet). Thus, depending upon where is the reaction takes place, by scanning the relative parameter, one can obtain a metastable ion (MI) mass spectrum. For a metastable ion $M_1^{+\bullet}$ formed in the ion source, accelerated to V, its dissociation in the second field free region (see *Figure 2-1*) can be recorded by the scan of the electric field (E) of the electrostatic analyzer; its dissociation in the third field free region can be recorded by the scan of the magnetic field (B) of the second magnetic analyzer.

If an ion M_B^+ formed in a metastable reaction, $M_A^+ \rightarrow M_B^+ + M_C^{\bullet}$, taking place in the first field free region, it will be transmitted by the first magnetic analyzer as a species having an apparent mass of m_B^2/m_A. But it only has a fraction of the kinetic energy of $M_A^{+\bullet}$, $m_B/m_A \cdot zV$. Therefore, if M_B^+ dissociates to $M_D^+ + M_E$ in the second field free region, the product M_D^+ will be transmitted by the electrostatic analyzer at an electric field strength equal to ($m_D/m_B \cdot m_B/m_A \cdot$

zV) or more simply (m_D/m_A • zV). Therefore, if the apparent mass of M_B^+ (m_B^2/m_A) is the same as the mass of the source generated ion $M_1^{+\bullet}$, M_B^+ and $M_1^{+\bullet}$ will be both transmitted by the first magnetic analyzer, the MI mass spectrum of $M_1^{+\bullet}$ recorded by the scan of the electric field of the electrostatic analyzer will be complicated by the present of M_B^+ and its fragments. This kind of interference of M_B^+ can be recognized and will be also present in other experiments, like CA and CS, of $M_1^{+\bullet}$ performed in the second field free region. However this problem can be avoided if the MI or CA experiment of $M_1^{+\bullet}$ is done using the third field free region, because M_B^+ does not have the right kinetic energy to pass the electrostatic analyzer (which is usually kept at a field strength for transmitting source generated ions).

3.4.2.1 Metastable Peak Shape Study

Under conditions of good energy resolution, metastable peak shapes (peak shapes of fragment ions generated in metastable ion dissociation reactions) can be sensitive probes for the structure of metastable ions and they can also yield information on the partitioning of the internal energy of the metastable ion into the translational energy of the fragment ions. Upon fragmentation, part of the excess internal energy in the transition state of an ion (nonfixed kinetic shift, $\varepsilon^\ddagger$) and the reverse activation energy ($\varepsilon_r^\ddagger$) is released as kinetic energy (T). As a result, the shapes of metastable peaks are broadened. The magnitude of the peak broadening depends upon the amount of $\varepsilon^\ddagger$ and $\varepsilon_r^\ddagger$ involved in the dissociation.

Metastable peak shapes, which are recorded under conditions of good energy resolution, as shown in *Figure 3-11* fall into one of the following three categories. (a) Gaussian type peaks

may be represented as being roughly triangular in form. They are generally associated with small kinetic energy releases. (b) Dished and flat-topped peaks are associated with large kinetic energy releases due to a significant reverse activation energy, although the inverse statement is not necessarily true. The observed dish is produced by z-axial discrimination against the ion beam and is instrument dependent. (c) Composite peaks indicate the involvement of more than one transition state and/or the production of more than one isomeric fragment ion.

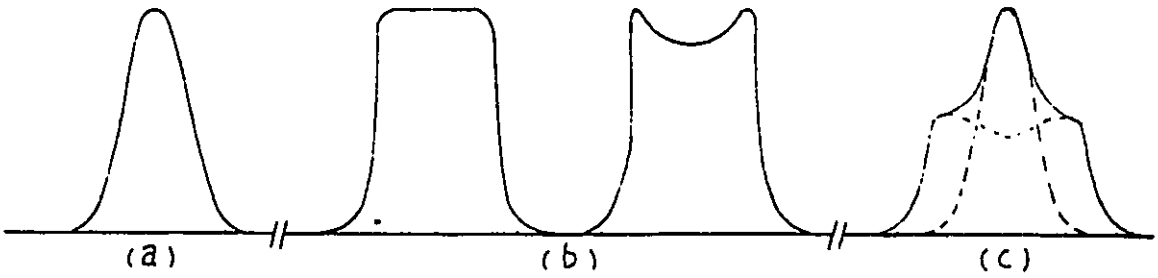

Figure 3-11 Common metastable peak shapes: (a) Gaussian, (b) Flat and dished-topped, and (c) Composite.

3.4.2.2 Applications

Applications of metastable ion dissociations include studies of metastable peak abundance ratios and metastable peak shapes.

The first semi-quantitative relationship between metastable peak abundance and the structure of a metastable ion was proposed by Shannon and McLafferty in 1966, [39] following a related study by Rosenstock et al. [40] The so-called "metastable abundance ratio test" was based on the premise that when two (or more) competing fragmentation from the same metastable ion

give reasonably intense metastable peaks, then the ratio of their abundances may be used as a criterion for the structure of the metastable ion. Thus, if metastable ions of a given m/z value, derived from different precursor species, all display the same metastable peaks having similar relative abundances, then it can be reasonably concluded that these metastable ions have the same reacting configurations (see also section 3.2.3). These peak abundances may be measured in terms of peak height or area. Usually, under conditions of low energy resolution peak heights should by used, while peak areas will be measured under high energy resolution. In either case, comparisons must be made under equivalent experimental conditions, such as ionizing electron energy, ion life time (reaction region) and energy resolution. For example, the ratio of fragment ions $[H_2COH]^+$ and $[C_3H_5]^+$ generated from dissociation of $[C_3H_7O]^+$ ions derived from diethyl ether changed from 3.6, when the dissociation took place in the first field free region in the MS-902S mass spectrometer, to 16.7, when the reaction was observed in the second field free region of the ZAB-2F mass spectrometer. [24]

As mentioned above, the study of metastable peak shapes requires good conditions of resolution of a mass spectrometer. The resolving power of a mass spectrometer may be considered in terms of energy and mass. Generally it is measured by the instrument's ability to separate two adjacent masses M_1^+ and M_2^+. As shown in *Figure 3-12* the resolution (R) of mass is defined as $R = m_1/\Delta m$ when $(h/H) \cdot 100 \leq 10$ and the resolution of energy is defined as ΔE.

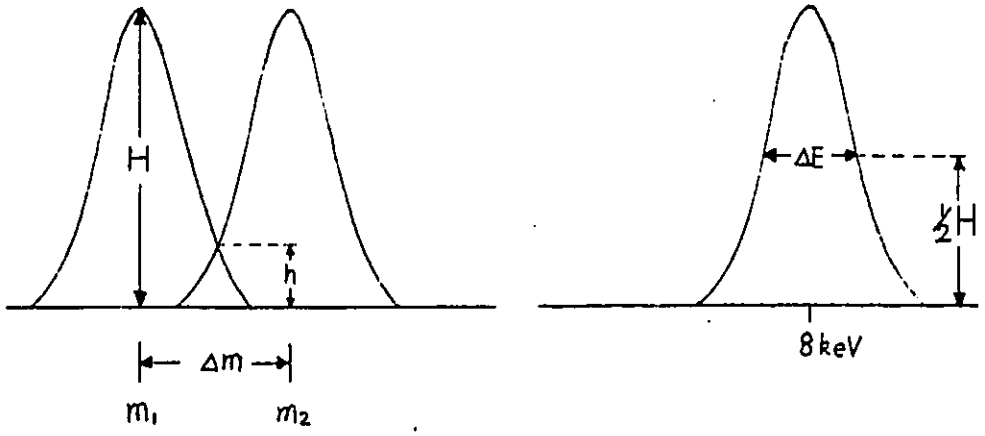

Figure 3-12 Measurements required for calculation of the mass and energy resolution. Δm is the mass difference between M_1^+ and M_2^+, H is peak height, h is the height of the overlap of peaks; ΔE is the energy spread at half the height of the mass selected ion beam.

Resolution in the ZAB-2F mass spectrometer may be increased (at the cost of ion transmission) by narrowing one or more of the variable slits (Y_1 to Y_6). Usually when only the first two analyzers are used, high mass resolution is achieved by narrowing Y_1, Y_5 and sometimes Y_3. Under such a condition, different ions having the same unit mass can be separated. For example, $[COOH]^+$ and $[C,H_3,N,O]^{+\cdot}$ having m/z values of 44.997454 and 45.021364 was separated by a resolution of R = 45/(45.021364 - 44.997454) = 1882. High energy resolution is obtained by narrowing Y_1 and Y_5. Values of $\Delta E < 4$ volts are usually acceptable.

Under high energy resolution, not only the shapes of metastable peaks can be recorded but also the kinetic energy releases associated with the metastable dissociations can be measured. Kinetic energy releases are commonly reported for the peak widths at their half-height, $T_{0.5}$, irrespective of the shape of the peak. For the metastable reaction $M_1^{+\cdot} \rightarrow M_2^+ + M_3^{\cdot}$, the $T_{0.5}$ associated with the metastable peak M_2^+ may be calculated by the following equation and is generally given in units of meV.

$$T_{0.5} = \frac{(\Delta E_2^2 - \Delta E_1^2) \times m_1^2}{16 \times m_2 \times m_3 \times V} \qquad (3\text{–}9)$$

where ΔE_2 and ΔE_1 are peak widths at half-height of the metastable peak M_2^+ and the main ion beam $M_1^{+\bullet}$, V is the accelerating voltage.

Combination of AE measurements as well as studies of metastable peak shapes and kinetic energy releases ($T_{0.5}$ values) of a metastable reaction provides important information about the reaction process. For example, [24] the AE for the metastable reaction $[phenol]^{+\bullet} \rightarrow [C_5H_6]^{+\bullet} + CO$ lies 0.9 eV above the calculated energy for formation of $[cyclopentadiene]^{+\bullet}$ + CO. The observation of a dished-topped metastable peak associated with large kinetic energy release ($T_{0.5}$ = 505 meV) for the reaction is in keeping with the reaction having an appreciable reverse activation energy.

3.4.3 Collisional Activation

The collisional activation of polyatomic cations has been observed in mass spectrometers in the early days of the development of the technique of mass spectrometry due to the poor vacuum in the earliest instruments. [41] However the process was of little interest until Jennings,[42] and Haddon and McLafferty [43] proposed the potential of collisional activation as a tool for

differentiation of ion structures. Today, collisional activation has become a very powerful technique for the elucidation of ion structures and is the basis for other ion dissociation characteristic experiments. [23,44]

3.4.3.1 Nature and Detection

When fast moving ions (ions having kilovolt translational energies) collide with atoms or molecules of stationary target gases (T), one type of interaction between the ions and the target gas is the convertion of a small fraction of the translational energy into internal excitation energy of the ions. This excitation may be considered as a Franck-Condon process (section 3.3.2), because the time of the encounter is sufficiently short. The amount of internal energy that an ion acquires by collisional excitation is sufficient to cause fragmentation of the ion,

$$M^+ \xrightarrow{T} (M^+)^* \rightarrow D^+ + N$$

a process known as collisional activation (CA) or collision induced dissociation (CID) or collision activated dissociation (CAD). CA experiments of mass selected ions are now routinely carried out on many mass spectrometers. The ZAB-2F mass spectrometer allows a variety of reaction regions for CA experiments. Collision gas may be introduced into the first field free region as well as one of the three collision gas cells located in the second and the third field free regions (see *Figure 2-1*). In most cases, the second collision gas cell is used (see *Figure 3-13*).

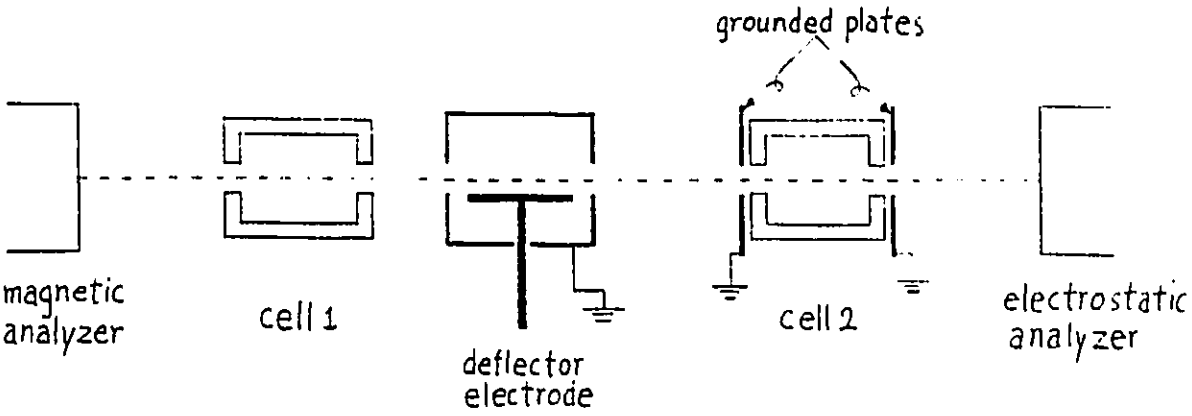

Figure 3-13 Brief layout of the second field free region of the ZAB-2F mass spectrometer.

In a typical CA experiment, the first magnetic analyzer is used to transmit an ion of interest formed in either the ion source or the first field free region, to the second field free region. Similar to an MI experiment, the distribution of translational energies of the mass selected ion M^+ to products, D^+ and N, is proportional to the mass of D^+ and N and can be recorded by the scan of the electrostatic analyzer as a collisional activation (CA) mass spectrum. The experimental set up for a CA experiment in the third field free region is the same as an equivalent MI experiment except that collision gas is introduced into the third collision gas cell.

3.4.3.2 Collision Gas and Gas Pressure

In a collision, the interaction between fast moving ions and stationary target gas atoms or molecules causes activation as well as charge stripping, charge exchange (neutralization), charge inversion and scattering of the ions. The proportion of each of the processes in a collision depends on the nature and pressure of the target gas.

He and O_2 are the most widely used collision target gases for CA experiments, because they have high target efficiency and they are readily obtainable in high purity and easily handled. However a large variety of collision target gases have been utilized. They fall mainly into two classes: "soft" agents (O_2, NO, Cl_2, NO_2) provide a smaller degree of fragmentation and "hard" agents (He, CH_4, SF_6) provide more, while N_2 is intermediate. Therefore the choice of collision target gas depends upon the information sought.

The factor which affects a CA mass spectrum the most is the pressure of the collision target gas. As the pressure is increased, multiple collision encounters increase and so does the yield of fragments resulting from high dissociation energy pathways. As a result, intensities of fragment signals increase but ion structure-characteristic information can be significantly reduced. For example,[23] ratios of signals at m/z 12, 13, 14 and 15 in the CA mass spectrum of allene ions, $[H_2C{=}C{=}CH_2]^{+\bullet}$, changed from m/z 12:13:14:15 = 48:47:100:13 to 100:42:25:2 when collision gas pressure was increased from 1.2×10^{-7} to 53×10^{-7} Torr. The structure-characteristic signal, m/z 14 ($[H_2C]^{+\bullet}$) was replaced by m/z 12 ($[C]^{+\bullet}$) and 13 ($[HC]^{+}$).

Normally the actual pressure of gas within the collision cell is not measured directly but is monitored at some nearby station in the mass spectrometer. Therefore instead of an absolute pressure of collision gas, the percentage of transmission of the main beam of (mass-selected) ions is usually reported and is used for convenience. The total collision (CA + other processes) probability is related to the collision gas pressure and the transmission of the main ion beam as illustrated in *Figure 3-14*.

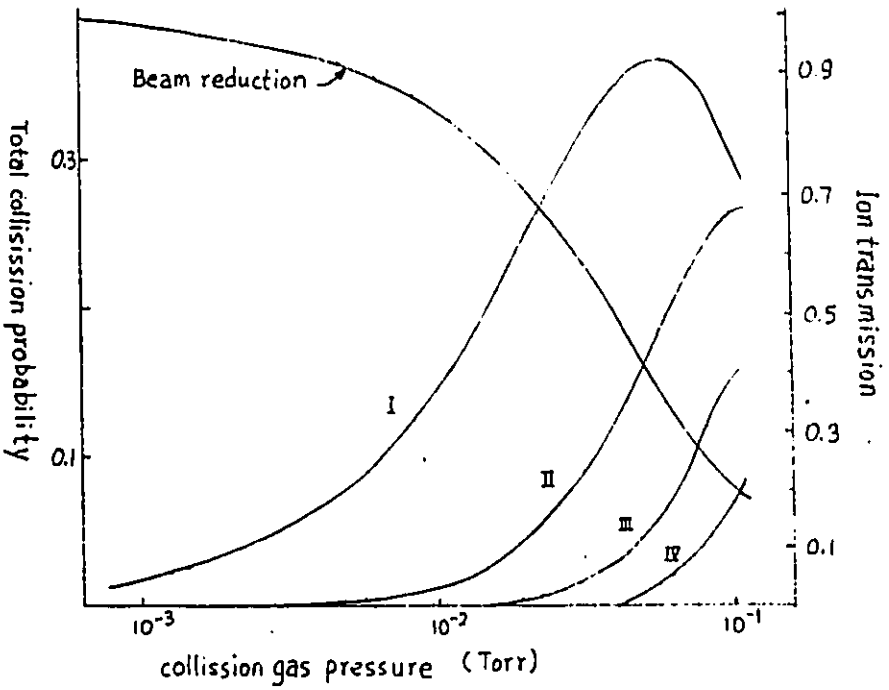

Figure 3-14 *Total collision probability, beam reduction (transmission) and the fraction of single (I), double (II), triple (III) and quadruple (IV) collisional processes as a function of collision gas pressure. Reproduced from Ref. 23.*

In most CA experiments collision gas pressure is adjusted to allow about 90% transmission of the main beam in order to avoid multiple collision encounters.

3.4.3.3 Applications

Unlike MI mass spectra which only give information of the reacting configurations of ions, CA mass spectra result from species having a large range of internal energies including non-decomposing and low energy species, so they provide more structure characteristic information.

Since CA processes only take place within the collision cell, the fragmentation arising from the CA processes can be separated from those arising from MI processes by a semi-

quantitative technique described below: The collision cell 2 in the ZAB-2F mass spectrometer may be charged by a voltage up to ± 5 keV. As a result an electric field parallel to the ion trajectories is generated and is kept within the cell by two grounded plates outside the cell (see *Figure 3-13*). When an ion enters this electric field, it will gain V′ eV translational energy if the cell is charged by a voltage of - V′ eV. After it leaves the cell, it will lose V′ eV translational energy and maintain its original translational energy. Therefore the translational energies of MI fragment signals will not be affected by the cell voltage because they are produced outside the cell. On the other hand, the translational energies of fragment ions arising from CA processes within the cell will be different from those ions produced from metastable ions. For a mass-selected ion M_1^+ generated with translational energy V in the ion source enters the cell charged by a voltage of - V′, its collisional activation dissociation to M_2^+ will produce a fragment signal of M_2^+ detected at a translational energy of $[(m_2/m_1) \bullet (V + V') - V']$, while those M_2^+ produced outside the cell will be detected at $[(m_2/m_1) \bullet V]$ in translational energy. *Figure 3-15* shows such a result.

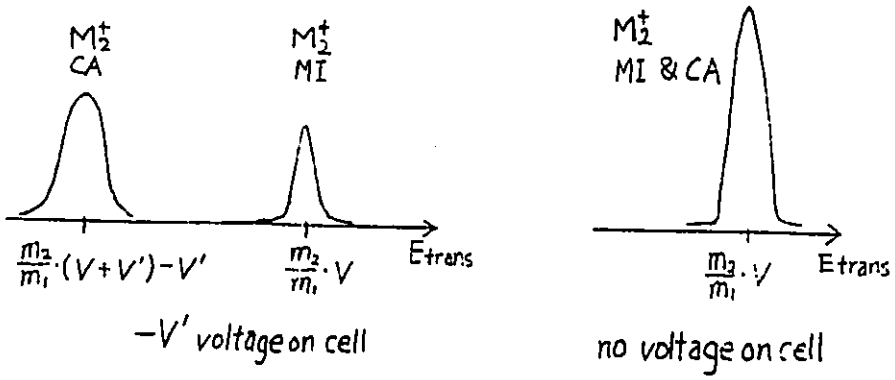

Figure 3-15 *CA mass spectra illustrating the use of a cell voltage of - V′ for separation of MI and CA signals.*

An important conclusion drawn from the early work of CA mass spectra is that CA mass spectra are relatively insensitive to the internal energy of the parent ion prior to collision. [44b,45] Hence, the reproducibility of CA mass spectra is better than MI mass spectra which are sensitive to the internal energy of a parent ion. CA mass spectra have been used extensively in ion structural studies since the early 1970s. Many cases have been noted in which CA mass spectra of isomeric ions were different. One example [46] related to the work of chapter 6 is the $[C_2,H_4,O_2]^{+\bullet}$ ions. Seven isomeric ions have been identified by their CA mass spectra (Table 3-1).

Table 3-1 Partial CA mass spectra of $[C_2,H_4,O_2]^{+\bullet}$ ions.

ion	m/z fragment ion									
	46	45	43	42	41	40	32	31	30	29
$[CH_3COOH]^{+\bullet}$	0.3	53	100	7.7	4.5	1.0	0	0.8	0	3.7
$[CH_2=C(OH)_2]^{+\bullet}$	8.7	47	36	100	10	1.9	0	10	1.3	18
$[H_2C=C=O(H_2O)]^{+\bullet}$	0.4	2.0	2.2	100	4.0	0.5	3.0	3.6	1.1	3.7
$[HOCH=CHOH]^{+\bullet}$	0.3	5.1	7.1	100	8.4	1.2	3.3	28	11	34
$[HCOOCH_3]^{+\bullet}$	1.0	3.5	0	0.8	2	0	100	54	9.5	27
$[HOCH_2CHO]^{+\bullet}$	0	0.3	0.5	1.2	0.4	0.2	100	30	2.7	12
$[CH_3OCOH]^{+\bullet}$	0	100	7	0	0	0	0	3	0	10

$[CH_3COOH]^{+\bullet}$ is characterized by m/z 43 ($[CH_3CO]^+$). $[CH_2=C(OH)_2]^{+\bullet}$, $[H_2C=C=O(H_2O)]^{+\bullet}$ and $[HOCH=CHOH]^{+\bullet}$ all give a major fragment at m/z 42 by loss of H_2O. $[CH_2=C(OH)_2]^{+\bullet}$ is easily recognized by its intense fragment signals at m/z 46, 45 and 43 (CH_2, $\dot{C}H_3$ and $HO^{\bullet}$ losses from $[CH_2=C(OH)_2]^{+\bullet}$). $[H_2C=C=O(H_2O)]^{+\bullet}$ and $[HOCH=CHOH]^{+\bullet}$ differ by the signal at m/z 31 ($[CH_2OH]^+$). $[HCOOCH_3]^{+\bullet}$ and $[HOCH_2CHO]^{+\bullet}$ share a major fragment at m/z 32 by loss of CO

but they are distinguished by the signals at m/z 46, 45 and 43. $[CH_3OCOH]^{+\bullet}$ is identified by its major fragment at m/z 45 by loss of $CH_3^{\bullet}$.

3.4.4 Charge Stripping

Charge stripping (CS) is another process caused by the interactions between the fast moving ions and the stationary target gases. In such a process a mass-selected ion M^+ loses an electron to form M^{2+}.

$$M^+ + T \rightarrow M^{2+} + T + e$$

This process was first reported by Beynon and co-workers in the early 1970s. [47] The experimental set up for CS experiments is the same as those of CA experiments. However, since the doubly charged ion (M^{2+}) falls at one-half the kinetic energy to charge ratio of the singly charged parent ion (M^+) and is of less energy spread (narrower in peak width), the signals resulting from CS may be easily distinguished from those from CA.

A number of factors affect the observation of charge stripping signals. These include: (a) the stability of M^{2+}; Since CS is also considered to be a vertical ionization process in the Franck-Condon sense (section 3.3.2), the stability of M^{2+} depends on its electronic structure formed in the process. (b) the nature and pressure of target gases; O_2 is found to be the most efficient target gas for CS because of its possibility of resonant electron capture to form O_2^-. [48] Other efficient target gases include He, NO and NO_2. The pressure effects of target gases on CS are similar to

those on CA. (c) the cross-section of competing processes such as CA and scattering relative to that for CS. [49]

The first report in which CS mass spectra were used in an ion structure characterization study appeared in 1975 in which isomeric $[C_6,H_6]^{+\cdot}$ ions were distinguished. [50] Since then, numerous other examples have been published, many cases of which have shown that the signals due to CS could be used to distinguish isomers when CA mass spectra could not. Two of such examples are $[C_3,H_6]^{+\cdot}$ [51] and $[C_5,H_{10}]^{+\cdot}$ [52].

3.4.5 Reactions of Neutrals

Reactions involving neutral species include collisionally induced dissociative ionization (CIDI) and neutralization-reionization (NR). From the previous sections (3.4.2, 3.4.3 and 3.4.4), it can be concluded that current mass spectrometric methodology is excellently suited for the generation and characterization of ions in the gas phase. This has led to the discovery of numerous ions of which the neutral counterparts had not yet been experimentally observed. In the 1980s mass spectrometric methodology has extended its application for the investigation of the neutral counterparts of (well-characterized) poly-atomic ions due to the pioneering work of Porter, McLafferty, Holmes, Terlouw and Schwarz. [53-56]

Fast neutrals can be generated in four ways:

(1) via fragmentation of a metastable mass-selected precursor ion.

$$M_1^+ \rightarrow M_2^+ + M_3 \qquad 3\text{-}1$$

(2) via collisional activation dissociation of mass-selected precursor ion; in most cases a mixed flux of neutrals is generated.

$$M_1^+ + T \rightarrow M_2^+ + M_3 + T \qquad 3\text{-}2$$

$$M_4^+ + M_5 + T$$

etc.

(3) via charge exchange neutralization of a mass-selected ion by collision with (stationary) target gases.

$$M_1^+ + N \rightarrow M_1 + N^+ \qquad 3\text{-}3$$

(4) via metastable or collision induced electron loss from a mass-selected anion.

$$M_1^- \nrightarrow M_1 + e \qquad 3\text{-}4$$

$$M_1^- + T \rightarrow M_1 + T + e$$

For the purpose of this thesis, reactions 3-1 to 3-3 are discussed.

3.4.5.1 Neutralization-Reionization

Reactions 3-1 and 3-2 have been described as metastable ion dissociation (3.4.2) and

collisional activation (3.4.3). Reaction 3-3 is also a result of one type of interaction between fast ions and stationary target gases, namely charge exchange neutralization. For a typical neutralization-reionization experiment this reaction takes place in collision gas cell 1 where neutralization target gas (N) is introduced (see *Figure 3-13*). Then the remaining precursor ions (M_1^+) will be deflected off their trajectories by the electrically charged deflector electrode. The neutral counterparts of the precursor ion, M_1, will pass the deflector electrode and enter collision gas cell 2 which is pressurized by collision target gas (R). The interaction between M_1 and R can cause collision induced (re)ionization of M_1 to form M_1^+ which in turn, can fragment. By the scan of the electrostatic analyzer, the signal of M_1^+ (recovery signal of the reionized neutral counterpart) and the signals of its fragmentation are recorded as a neutralization-reionization (NR) mass spectrum. An NR process refers to the following reaction sequence:

$$M_1^+ \xrightarrow{N} M_1 \xrightarrow{R} M_1^+ \rightarrow M_2^+ + M_3 \qquad 3\text{-}5$$

But an NR mass spectrum not only records the products from the above reaction sequence but also records the reionized neutrals produced from reactions 3-1 and 3-2 as well as the products of the following reaction sequence:

$$M_1^+ \xrightarrow{N} (M_1)^* \rightarrow M_2 + M_3 \xrightarrow{R} M_2^+ + M_3^+ \qquad 3\text{-}6$$

where a dissociative neutral counterpart, $(M_1)^*$, is generated in the neutralization step.

The reaction 3-1 involves collisionally induced dissociative ionization (CIDI) and will be

discussed later. The observation of a recovery signal of the neutral counterpart of a mass-selected precursor ion depends on the stability of the neutralized ion, M_1, formed in the neutralization step and the stability of the reionized neutral, M_1^+, in the reionization step.

3.4.5.2 Neutralization

The neutralization of a fast ion, M_1^+, is considered as a vertical Franck-Condon process since the encounter between the ion and the neutralization target gas (N) involves a time of only approximately 10^{-15} s. [55]

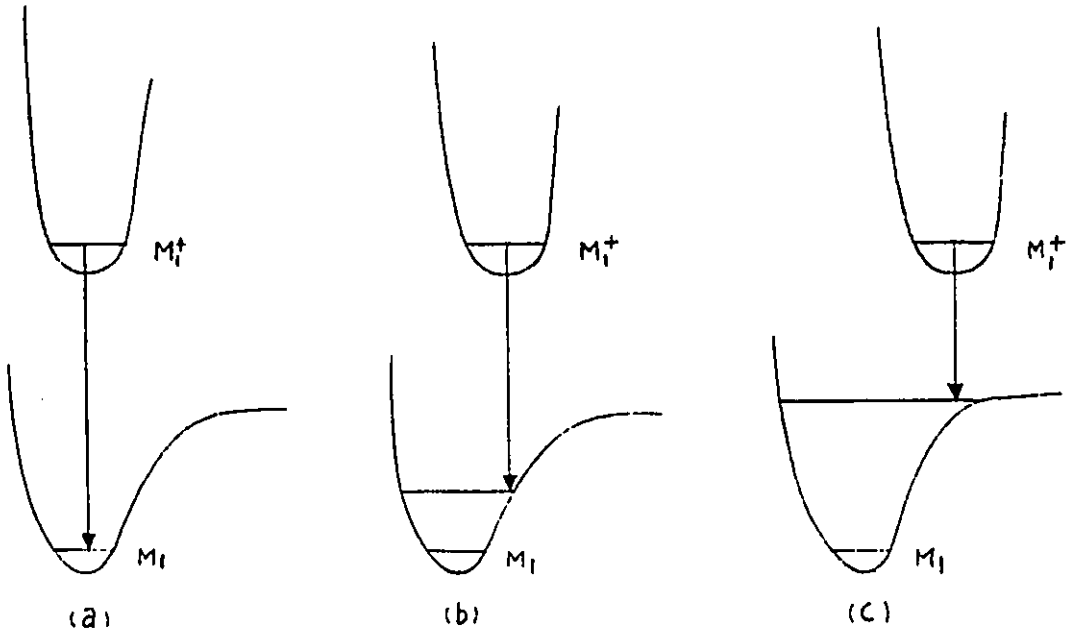

Figure 3-16 Vertical neutralization of ion M_1^+ to M_1, stable neutral (a), excited neutral (b) or no neutral (c).

Hence, the geometry of the ion does not change in the process, similar geometry of the ion and the corresponding (stable) neutral results in generation of the stable neutral while a difference in geometry leads to generation of an excited neutral or even no neutral. *Figure 3-16* shows possible results for the neutralization process of an ion, M_1^+, to the corresponding neutral M_1.

The efficiency of the neutralization process (charge exchange reaction 3-3) is strongly affected by the energy defect, Q_N, of the reaction.

$$Q_N = IE_v(N) - NE_v(M_1^+) \qquad (3\text{-}10)$$

where $IE_v(N)$ is the vertical ionization energy of the neutralization target gas molecule (N); $NE_v(M_1^+)$ is the vertical neutralization energy of the mass-selected ion M_1^+.

Three conditions should be considered in which the ground state of the neutral is generated:

(i) $Q_N \sim 0$, resonant charge exchange

In general, resonant charge exchange conditions are most efficient, for example, the $Ar^{+\cdot}/Ar$ charge exchange process has a reported efficiency of up to 40%, [57] and consequently the target gas should be selected to create these conditions.

(ii) $Q_N > 0$, endothermic charge exchange

For such processes the energy deficit will be supplied by the translational energy of the fast ions. Xe (IE = 12.1 eV) is a commonly used target gas for these processes and has proved to be very efficient for organic cations.

(iii) $Q_N < 0$, exothermic charge exchange

For such processes the excess energy will be stored in the neutrals as internal energy. The

use of alkali metal vapors as target gas for neutralization often results in the formation of excited neutral species because of the low IE of alkali metal atoms (e.g. IE(Na) = 5.1 eV, IE(K) = 4.3 eV). Neutrals thus produced are energy rich and may dissociate.

It has been concluded that both exothermic and very endothermic (with He (IE = 24.6 eV) as N) electron transfers usually produce neutrals with a considerable amount of internal energy, possibly enough for dissociation and/or rearrangement. However, due to the possible population of excited states, formation of an excited neutral may be resonant and therefore target gases with widely different IE can be very efficient. [58] For example, a stable electronic excited state of N_2 is accessed when $N_2^{+\cdot}$ is neutralized by NO (IE(N_2) = 15.6 eV, IE (NO) = 9.3 eV). [55] Since the IE's of most of the small organic species are about 10 eV, Xe, Hg, NO and c-C_3H_6 (cyclopropane), whose IE's are 12.1, 10.4, 9.3 and 9.9 eV respectively, are among the most widely used neutralization target gases. Alkali metals have also been found to be particularly suited to study of hypervalent species whose IE's may be of similar magnitude to those of the target gases. [55]

3.4.5.3 Reionization

In the collision cell 2, collision induced reionization of the neutrals will take place. There are two possible mechanisms for electron removal from a fast neutral: electron detachment, 3-7, and electron transfer, 3-8,

$$M_1 + R \rightarrow M_1^+ + R + e \qquad 3\text{-}7$$

$$M_1 + R \rightarrow M_1^+ + R^- \qquad 3\text{-}8$$

The electron detachment mechanism has been generally accepted as the major process. Collision induced ionization is also a vertical Franck-Condon process; therefore it is possible that, although the corresponding ion is stable, excitation to a repulsive part of the potential energy surface of the ion leads to (complete) dissociation of the ion due to a large geometry difference between the neutral and the corresponding ion. For example, the NR mass spectrum showed that the reionization of CCl_4 results in generation of $[CCl_3]^+ + Cl^\cdot$ and no recovery signal of CCl_4 was observed. [59] Another example of such a behaviour can be found in this thesis (OC_2O in chapter 5).

For the efficiency of collision induced ionization, it was found that for species with a low ionization energy (<7 eV) the efficiency increases with increasing electron affinity of the target gas due to an increasing contribution from electron transfer (reaction 3-8); for species with a higher ionization energy (>7 eV) the efficiency is not simply related to the electron affinity of the target gas. [59,60] It was also concluded that the extent of fragmentation of the reionized neutrals strongly depends on the target gas. The choice of target gas should be determined by the aim of the experiment. Ionization with O_2 is very efficient and is appropriate for examining the stability of neutral counterpart of the mass-selected ion. Ionization with He yields more fragments than with O_2 and is therefore well suited for structural analysis.

3.4.5.4 Target Gas Pressure

The pressure of the neutralization target gas (N) and reionization target gas (R) is of significant importance. Upon increasing the pressure of either N or R, the absolute abundance

of the signals in NR mass spectra increases. As in collisional activation processes, the disadvantage of major reduction of the main ion beam is the resulting complication of the NR mass spectrum due to multiple collision encounters. Therefore, intensity permitting, multiple collision conditions should be avoided and the pressures of both N and R are usually adjusted to allow 90% main beam transmission (single collision condition).

3.4.5.5 Collisionally Induced Dissociative Ionization

Since the metastable reaction 3-1 produces the neutral M_3, a collisionally induced dissociative ionization experiment can be considered as a neutralization-reionization experiment except that no neutralization target gas is introduced in collision cell 1. The reaction sequence for a CIDI experiment is shown as below:

$$\begin{array}{l} M_1^+ \xrightarrow{N} M_2^+ + M_3 \\ \qquad\qquad\quad \downarrow R \\ \qquad\qquad\quad M_3^+ \rightarrow M_4^+ + M_5 \end{array} \qquad 3\text{-}9$$

The efficiency of the collision induced (re)ionization process is the major factor governing the CIDI process and it is discussed in sections 3.4.5.3 and 3.4.5.4.

3.4.5.6 Applications

Collisionally induced dissociative ionization mass spectrometry has often been used

specifically to identify the neutral species produced in the fragmentation of metastable mass-selected ions. An example is the use of the CIDI mass spectra of HCN and HNC to identify metastable dissociation channels of ionized benzonitrile and aniline is given in section 3.3.8. Another example is that the unexpected loss of $CH_2OH^{\bullet}$ and $CH_3O^{\bullet}$ from ionized methyl acetate observed by a CIDI experiment has led to the intense investigation of the dissociation mechanism. [61]

The application of neutralization-reionization mass spectrometry includes identification of stable neutral species in the gas phase (which have eluded observation in condensed phase) and differentiation between isomeric ions. The elusive species accessed by NR mass spectrometry includes hypervalent radicals (e.g. $H_3^{\bullet}$, $H_3O^{\bullet}$), new, small organic molecules and carbenes (e.g. $(HO)_2CO$, H_2SO_3, HCOH) as well as neutral counterparts of ylid ions and distonic ions (e.g. CH_2ClH, $CH_2CH_2OH_2$) and they have been discussed in a critical review article. [55] More recently the neutral counterparts of protonated and deuterated dimethyl ether and methyl ethyl ether have been observed in this laboratory. [62] Sometimes the differences between the NR mass spectra of isomeric ions are more pronounced than those between the CA mass spectra, due to a significantly different degree of stability of their neutral counterparts. Many examples, (such as the $[C_2,H_4,Cl]^+$ system [59]), can be found, and in this thesis, the $[C,H_3,N,O]^{+\bullet}$ system (chapter 4) and the ions produced from fumaric acid (chapter 6) provide good examples.

3.5 Summary of Experimental Conditions

Ionization energies (IE) of neutral molecules and appearance energies (AE) of fragment

ions were obtained by the electron energy selector mass spectrometer and the MS-902S mass spectrometer. Experimental methods are outlined in section 3.3.7. For the electron energy selector mass spectrometer, H_2O was used as electron energy scale calibrant; for the MS-902S mass spectrometer, the electron energy scale was calibrated by diethyl ether for AE measurements of metastably generated ions and by benzene for AE measurements for ion source generated ions.

All ion dissociation experiments were performed with the ZAB-2F mass spectrometer. Ions were generated by 70 eV electron impact on precursor compounds and they were accelerated to 8 keV. Collisional activation (CA) and charge stripping (CS) mass spectra were recorded with O_2 or He as target gas. Neutralization-reionization (NR) experiments were performed using target gases Xe in collision Cell 1 for charge exchange neutralization of the mass-selected ions and O_2 in collision Cell 2 for reionization of the generated neutrals, unless otherwise stated. The beam deflector electrode was charged by a positive voltage of 1000 V. Gas pressures were adjusted to give a main ion beam transmission of 90% (90% T), unless otherwise stated. All metastable ion (MI), CA, CS and NR mass spectra were corrected for isotopic contributions from adjacent ions of lower mass. Unless otherwise stated, interference was negligible. MI contributions are corrected by the method described in section 3.4.3.3 for CA mass spectra, unless otherwise stated.

In the above experiments all beam defining slits were fully open to obtain maximum signal strength and to minimize energy resolving effects. Metastable peak shapes were recorded under higher energy resolution conditions with the main ion beam width at half height being 3 ± 1 V at an accelerating voltage of 8 kV. Kinetic energy releases, $T_{0.5}$, were obtained from the peak width at half-height and evaluated using equation (3-9).

Chapter 4 Isomeric $[C,H_3,N,O]^{+\bullet}$ Ions and Their Neutral Counterparts

4.1 Introduction

The subject matter of this chapter involves collaboration between the Theoretical Chemistry Group at Utrecht University and the Mass Spectrometry Laboratory at the University of Ottawa and has been published in *Organic Mass Spectrometry* **26**, 679 (1991).

Over the past few years mass spectrometric methodology has proved to be a powerful tool for distinguishing between isomeric ions [63]. Recently the $[C,H,N,O]^{+\bullet}$ system [64] has been examined. Three isomers: $[HNCO]^{+\bullet}$, $[HCNO]^{+\bullet}$ and $[CNOH]^{+\bullet}$ were identified. They could easily be distinguished by their collisional activation (CA) mass spectra. The kinetic energy releases of the metastable dissociations also allowed their differentiation. Next, protonation of HNCO and HCNO was examined [65]. By comparing the collisional activation (CA) mass spectra of these species with those of reference $[C,H_2,N,O]^+$ ions, it was established that HNCO yields $[H_2NCO]^+$, whereas HCNO protonates on the O-atom giving $[HCNOH]^+$. In this work the next series of ions, $[C,H_3,N,O]^{+\bullet}$ will be described. Once the structure of the ions was established, the neutralization-reionization (NR) technique [66] was used to assess the stability of their neutral counterparts. Theoretical calculations were performed to study the electronic structures of some of the $[C,H_3,N,O]^{+\bullet}$ ions and their neutral counterparts.

Table 4-1 lists the eight isomeric [C,H_3,N,O] structures which have been considered. Formamide, $H_2NC(H)O$ (1), is a well known compound and its thermochemical data have been determined accurately. $\Delta H_f^\bullet(H_2NC(H)O) = -186$ kJ mol^{-1} [67] and the adiabatic ionization energy is 10.13 eV. [68] Thus, $\Delta H_f^\bullet([H_2NC(H)O]^{+\bullet}) = 791$ kJ mol^{-1}. The enol of formamide, HNC(H)OH (2), has been calculated by ab initio molecular orbital theory to be 51 kJ mol^{-1} less stable than formamide. [69] To our knowledge the enol and its ionic counterpart have not been observed experimentally. MNDO calculations [70] predicted the ionized enol to be more stable than ionized formamide; $\Delta H_f^\bullet([HNC(H)OH]^{+\bullet}) = 801$ kJ mol^{-1} and $\Delta H_f^\bullet([H_2NC(H)O]^{+\bullet}) = 811$ kJ mol^{-1}. The latter value is fairly close to the experimental value, 791 kJ mol^{-1} (see above).

H_2NCOH (3) and H_3NCO (4) have not been considered as neutral species, but the ionic counterparts were calculated to be stable species in the gas phase [70,71]. Using the semi-empirical MINDO/3 method the heats of formation of $[H_2NCOH]^{+\bullet}$ and $[H_3NCO]^{+\bullet}$ were calculated to be 556 and 597 kJ mol^{-1} respectively [71a] with a barrier of 266 kJ mol^{-1} for the $[H_3NCO]^{+\bullet} \rightarrow [H_2NCOH]^{+\bullet}$ rearrangement [71b]; no bound solution was found [71a] for ionized formamide! In contrast, more recent MNDO calculations [70] gave $\Delta H_f^\bullet$ values for $[H_2NCOH]^{+\bullet}$, $[H_3NCO]^{+\bullet}$ and $[H_2NC(H)O]^{+\bullet}$ of 747, 772 and 811 kJ mol^{-1} respectively.

Early attempts to isolate nitrosomethane, H_3CNO (5), failed due to extensive isomerization to formaldoxime, H_2CNOH (6) [72], a more stable isomer [73]. It was later shown that monomeric nitrosomethane could be obtained by thermal decomposition of the trans-dimer [74]. A more recent study [75] has confirmed these results. However, it was also shown that heating cis-$(H_3CNO)_2$ gave formaldoxime up to ~80 °C and monomeric nitrosomethane above 95 °C [75]. Both methods were used to record the photoelectron spectrum of nitrosomethane. The adiabatic ionization energy was

measured to be 9.3 eV [75,76] and thus $\Delta H_f^\circ([H_3CNO]^{+\cdot}) = 967$ kJ mol^{-1} ($\Delta H_f^\circ(H_3CNO) = 70$ kJ mol^{-1} [74b]).

The photoelectron spectrum of formaldoxime has also been recorded and the adiabatic ionization energy has been determined to be 10.1 eV [75,77,78]. However, the heat of formation of neutral formaldoxime has not been determined accurately. Adeney et al. [73] calculated by ab initio molecular orbital theory that anti-formaldoxime is 41 kJ mol^{-1} more stable than nitrosomethane. Using the experimentally determined heat of formation of H_3CNO, 70 kJ mol^{-1} [74b], $\Delta H_f^\circ(H_2CNOH) \approx 29$ kJ mol^{-1} is obtained, which is the value given in Lias et al. [67]. However, using $\Delta H_f^\circ(H_3CC(NOH)C(NOH)CH_3) = -80$ kJ mol^{-1} [79] and Benson's additivity rules [80] the heat of formation of formaldoxime was estimated to be ca -9 kJ mol^{-1}, i.e. 79 kJ mol^{-1} lower than that of nitrosomethane. The latter value is in good agreement with the results from earlier ab initio calculations performed at a lower level of theory [81], where formaldoxime was calculated to be 81 kJ mol^{-1} more stable than nitrosomethane. Using $\Delta H_f^\circ(H_2CNOH) = -9$ kJ mol^{-1} $\Delta H_f^\circ([H_2CNOH]^{+\cdot})$ was obtained to be ~ 966 kJ mol^{-1}.

In the theoretical work of Adeney et al. [73] the $H_3CNO \rightarrow H_2CNOH$ rearrangement was also examined. It was proposed that it would take place via two 1,2-hydrogen shifts with formaldonitrone, $H_2CN(H)O$ (7), as intermediate. The heat of formation of $H_2CN(H)O$ was calculated to be 52 kJ mol^{-1} higher than that of nitrosomethane, but it was found to be separated from nitrosomethane and formaldoxime by high energy barriers (222 and 202 kJ mol^{-1} respectively).

The first structure assigned to nitrones was that of a three-membered heterocycle. This was soon discarded, but many reactions of nitrones involve the cyclic form, oxaziridines (8) [82].

For example, oxaziridines were proposed as intermediates in the photolytic rearrangement of nitrones into amides.

$$RCH{=}N(R')O \underset{\Delta}{\overset{h\nu}{\rightleftharpoons}} HR\overline{CONR'} \underset{\Delta}{\overset{h\nu}{\rightarrow}} RR'NC(H)O \text{ and/or } HR'NC(R)O \qquad 4\text{-}1$$

Some substituted oxaziridines have been isolated [83], but many oxaziridines are highly unstable and rearrange thermally and/or photolytically to the corresponding amides. Oxaziridine, $H_2\overline{CONH}$, has been calculated by ab initio methods to lie 327 kJ mol^{-1} higher in energy than formamide, but the barrier for rearrangement into formamide was expected to be very small [84]. So far formaldonitrone, oxaziridine and their molecular ions have eluded observation.

4.2 Results and Discussion

4.2.1.1 The Ions $[H_2NC(H)O]^{+\bullet}$ (1) and $[H_2NCOH]^{+\bullet}$ (3)

There was a very intense signal (base peak) at m/z 45 in the normal EI mass spectrum of formamide. Vertical ionization (by electron impact) of the formamide neutral molecule should yield the $[H_2NC(H)O]^{+\bullet}$ ion with the same geometry as the neutral molecule. The metastable $[H_2NC(H)O]^{+\bullet}$ ion generated only one signal at m/z 44 in its MI mass spectrum (Table 4-2). The dissociation characteristics of this ion are shown in its CA (*Figure 4-1a*) and CS (Table 4-3) mass spectra. The recovery signal (base peak) of the reionized neutral counterpart of this ion

presented in its NR mass spectrum (*Figure 4-3a*). The NR mass spectrum is similar to the CA mass spectrum except for a more intense m/z 28 signal.

The normal EI mass spectrum of methyl carbamate, $H_2NC(O)OCH_3$ (m/z 75), contained a peak at m/z 45, $[C,H_3,N,O]^{+\bullet}$, which was 23% of m/z 44 (base peak). Under high mass resolution it was found that a very small (<5%) contribution from $[COOH]^+$ presented. The AE of m/z 45 was measured using the electron energy selector mass spectrometer to be 11.44 ± 0.05 eV. Thus, $\Delta H_f^{\bullet}([H_2NCOH]^{+\bullet})$ was obtained to be ≤ 796 ± 5 kJ mol^{-1} ($\Delta H_f^{\bullet}(H_2NC(O)OCH_3)$ = -417 kJ mol^{-1} [85] and $\Delta H_f^{\bullet}(H_2CO)$ = -109 kJ mol^{-1} [67]). The latter number must be considered as an upper limit because a competitive shift (see section 3.3.4) is possible; there were three dissociation processes for ionized methyl carbamate with a lower AE (AE(m/z 47) = 11.16 ± 0.05 eV, AE(m/z 46) = 10.82 ± 0.05 eV and AE(m/z 44) = 11.24 ± 0.05 eV).

The MI, CA and CS mass spectra of this $[C,H_3,N,O]^{+\bullet}$ ion are shown in Table 4-2, *Figure 4-1b* and Table 4-3 respectively. Unfortunately, the m/z 46 ion generated from the metastable m/z 47 ion in the first field free region in the ZAB-2F mass spectrometer whose apparent $(m/z)^*$ is $46^2/47$ = 45.02 and whose translational energy is 8000 x 46/47 = 7830 eV will be selected by the magnetic analyzer at m/z 45 and appear at m/z 44 in the MI mass spectrum of the m/z 45 ion (The translational energy of the m/z 44 fragment ion is 8000 x 44/45 = 7822 eV). This metastably generated $(m/z)^*$ 45 ion also interfered the CS mass spectrum of the m/z 45 ion, since the doubly charged $(m/z)^*$ 45 ion, whose translational energy is very close to that of the doubly charged m/z 44 fragment ion, will also appear at m/z 22 in the CS mass spectrum. The $[C,H_3,N,O]^{+\bullet}$ ion was formed by hydrogen transfer and consequent H_2CO expulsion.

$$H_2NC(O)OCH_3 \rightarrow [C,H_3,N,O]^{+\bullet} + H_2CO + e \qquad 4\text{-}2$$

Three structures can be proposed for the m/z 45 ions: $[H_2NC(H)O]^{+\bullet}$ (H transfer to the carbonyl carbon atom), $[H_2NCOH]^{+\bullet}$ (H transfer to the carbonyl oxygen atom) and $[H_3NCO]^{+\bullet}$ (H transfer to the amine nitrogen atom). The first structure can easily be discarded due to the large differences between its MI, CA and CS mass spectra and those of ionized formamide (see Tables 2 and 3 and *Figure 4-1a*). Note that a significant part of the m/z 17 signal in the CA mass spectrum of the $[C,H_3,N,O]^{+\bullet}$ ion from methyl carbamate was produced by a slow (metastable) reaction. After correction for the MI contribution (established by putting a charge on the collision cell) the m/z 17: 16 ratio equalled 0.87: 1, i.e. m/z 16 was more intense than m/z 17. The latter ratio is remarkable because generation of m/z 17, $[H_3N]^{+\bullet}$, is energetically much more favourable than generation of m/z 16, $[H_2N]^+$. Note that m/z 17 must be $[H_3N]^{+\bullet}$; formation of $[HO]^+$ + $HCNH^{\bullet}$ has an energy requirement in excess of 1500 kJ mol^{-1}.

$$[H_3N]^{+\bullet} + CO \qquad \Sigma\Delta H_f^\circ = 823 \text{ kJ mol}^{-1}\ ^{67}$$

$$[H_2N]^+ + HCO^{\bullet} \qquad \Sigma\Delta H_f^\circ = 1309 \text{ kJ mol}^{-1}\ ^{67}$$

Therefore the $[C,H_3,N,O]^{+\bullet}$ ion from methyl carbamate is proposed to have the $[H_2NCOH]^{+\bullet}$ structure. The $[H_2NCOH]^{+\bullet}$ ion with significant amount of internal energy, i.e. the metastable ion, will isomerize into $[H_3NCO]^{+\bullet}$ and consequently dissociate into $[H_3N]^{+\bullet}$ + CO. The kinetic energy release, $T_{0.5}$(m/z 17) = 40 meV, of this dissociation revealed that this may not be a threshold

process. Since the $[H_3NCO]^{+\bullet} \rightarrow [H_3N]^{+\bullet} + CO$ reaction is expected to take place at its thermochemical threshold based on the recent theoretical calculation (section 4.2.1.2), the energy of the transition state for the $[H_2NCOH]^{+\bullet} \rightarrow [H_3NCO]^{+\bullet}$ isomerization reaction should be more than 823 kJ mol^{-1} (the lowest dissociation limit). The NR mass spectrum (*Figure 4-3b*) of the m/z 45 ion contained a fairly intense recovery signal of the reionized neutral counterpart of the m/z 45 ion and is similar to the CA mass spectrum of the m/z 45 ion except for a more intense m/z 28 signal. This observation is in keeping with the recent theoretical calculation which predicted H_2NCOH to be stable, but 163 kJ mol^{-1} higher in energy than $H_2NC(H)O$. The theoretical calculation also showed that H_3NCO dissociated spontaneously into $H_3N + CO$. The latter represents additional evidence that the $[C,H_3,N,O]^{+\bullet}$ ion from methyl carbamate does not have the $[H_3NCO]^{+\bullet}$ structure; the NR mass spectrum clearly indicates that the neutral counterpart of the $[C,H_3,N,O]^{+\bullet}$ ion is stable, which rules out the $[H_3NCO]^{+\bullet}$ structure.

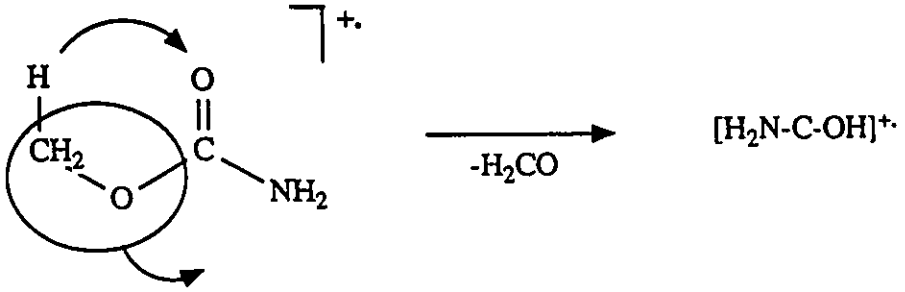

4-3

The normal EI mass spectrum of oxamic acid, $H_2NC(O)C(O)OH$ (m/z 89), contained a peak at m/z 45, which was 50% of m/z 44 (base peak). High mass resolution showed that m/z 45 was a doublet consisting of $[C,H_3,N,O]^{+\bullet}$ ion (72%) and $[C,H,O_2]^{+}$ ion (28%), most likely $[HOCO]^{+}$ (reactions 4-4a and 4-4b).

$$H_2NC(O)C(O)OH \rightarrow [C,H_3,N,O]^{+\bullet} + CO_2 + e \quad \text{4-4a}$$

$$\rightarrow [HOCO]^+ + H_2NCO^{\bullet} + e \quad \text{4-4b}$$

Oxamic acid molecular ion (m/z 89) produced only one peak at m/z 45 in its MI mass spectrum. This peak was of composite shape, containing a weak narrow signal and an intense broad component ($T_{0.5}$ = 313 meV). The AE of m/z 45 using electron energy selector mass spectrometer was measured to be 10.28 ± 0.05 eV. The latter threshold has to correspond with generation of $[C,H_3,N,O]^{+\bullet}$ because the estimated AE for generation of $[HOCO]^+$ is much higher, ca 11.6 eV; $\Delta H_f^{\bullet}(H_2NC(O)C(O)OH)$ = - 549 kJ mol^{-1} [86], $\Delta H_f^{\bullet}([HOCO]^+)$ = 589 kJ mol^{-1} [67] and $\Delta H_f^{\bullet}(H_2NCO^{\bullet}) \approx$ -21 kJ mol^{-1} [87]. Thus, the broad component of the composite m/z 45 MI signal was assigned to be the $[C,H_3,N,O]^{+\bullet}$ ion. The narrow component became relatively more intense upon introduction of a collision gas. Therefore, the small narrow component of m/z 45 was assigned to be the $[HOCO]^+$ ion generated by residual collision induced dissociation. The AE(m/z 45) leads to $\Delta H_f^{\bullet}([H_2NCOH]^{+\bullet}) \leq 837 \pm 5$ kJ mol^{-1} ($\Delta H_f^{\bullet}(H_2NC(O)C(O)OH)$ = - 549 kJ mol^{-1} [86] and $\Delta H_f^{\bullet}(CO_2)$ = -394 kJ mol^{-1} [67]), which is in keeping with the result using methyl carbamate as precursor. The heat of formation is an upper limit because the kinetic energy release is quite large ($T_{0.5}$ value = 313 meV) and indicates that there is a considerable barrier for the reverse reaction.

It now remains to elucidate the structure of the metastably generated $[C,H_3,N,O]^{+\bullet}$ ion. Since the generation of m/z 45 took place at a higher energy (AE(m/z 45) = 10.28 ± 0.05 eV, see above) than that required for generation of $[H_3N]^{+\bullet}$ + CO + CO_2 (estimated AE is 10.14 eV; $\Delta H_f^{\bullet}(CO_2)$ = -394 kJ mol^{-1} [67]) the $[H_3NCO]^{+\bullet}$ structure for the m/z 45 ions is unlikely. *Figure 4-2* shows the CA mass spectrum of the $[C,H_3,N,O]^{+\bullet}$ ions generated in the first field-free region of

the ZAB-2F mass spectrometer from the metastable molecular ion. This spectrum is close to that of $[H_2NCOH]^{+\cdot}$ corrected for the MI contribution (*Figure 4-1b*). Note that metastably generated ions have low internal energies and so there will be no MI contribution to the former CA mass spectrum. The NR mass spectrum of the m/z 45 ion is the same as that of the $[H_2NCOH]^{+\cdot}$ ion from methyl carbamate. Thus, ionized oxamic acid as well as ionized methyl carbamate produced $[H_2NCOH]^{+\cdot}$ and in both cases the fragmentation took place via a 1,4 hydrogen transfer (compare reactions 4-3 and 4-5).

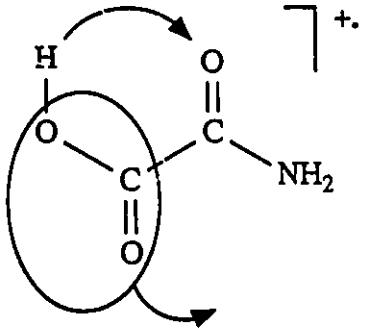

$$\xrightarrow[-CO_2]{} \quad [H_2N\text{-}C\text{-}OH]^{+\cdot} \qquad 4\text{-}5$$

The normal EI mass spectrum of propionamide, $H_2NC(O)CH_2CH_3$ (m/z 73), was dominated by m/z 44, $[H_2NCO]^+$, but a small signal at m/z 45 was also present (5.1% of m/z 44). The m/z 45 signal was partly due to the $^{13}C/^{15}N$ contributions from m/z 44. Fortunately, the isotopic interference was negligible in the MI mass spectrum of these m/z 45 ions. The MI (Table 4-2) and CA, CS and NR are compatible with those of the $[H_2NCOH]^{+\cdot}$ ion from methyl carbamate and the $T_{0.5}$ values of m/z 17 are within experimental error the same, 43 and 40 meV respectively. Again, fragmentation took place via a 1,4 hydrogen shift producing $[H_2NCOH]^{+\cdot}$.

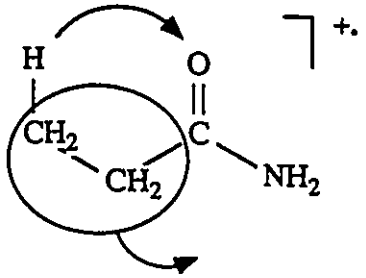

$$\xrightarrow[-H_2C=CH_2]{} \quad [H_2N\text{-}C\text{-}OH]^{+\cdot} \qquad 4\text{-}6$$

4.2.1.2 Theoretical calculations of $[H_2NC(H)O]^{+\bullet}$ (1), $[HNC(H)OH]^{+\bullet}$ (2), $[H_2NCOH]^{+\bullet}$ (3) and $[H_3NCO]^{+\bullet}$ (4)

Thus, despite considerable effort as detailed above, the ion $[H_3NCO]^{+\bullet}$ was not observed. To obtain more information about the relative stabilities of $[H_2NC(H)O]^{+\bullet}$, $[H_2NCOH]^{+\bullet}$ and $[H_3NCO]^{+\bullet}$ ab initio molecular orbital calculations were performed using the program system GAMESS [88]. The calculations were done by RHF calculations in the standard 4-31G basis in order to determine optimum geometries for the isomers and the transition states. After determining the geometries, single point Configuration Interaction (CI) calculations were performed using the 6-31 G^{**} basis. The results are given in Table 4-4. They show that the ions $[H_2NC(H)O]^{+\bullet}$ (1), $[H_2NCOH]^{+\bullet}$ (3) and $[H_3NCO]^{+\bullet}$ (4) are close in energy and that they are separated by high barriers. Ion $[H_2NC(H)O]^{+\bullet}$ (1) has a low-lying excited state which is also in a potential well. In contrast with the MNDO calculations mentioned in the Introduction [70], ion $[H_2NCOH]^{+\bullet}$ (3) is not the most stable of the three isomers. Using the experimentally determined heat of formation of $[H_2NC(H)O]^{+\bullet}$, 791 kJ mol^{-1} as the base value, the present calculations give $\Delta H_f^{\bullet}([H_2NCOH]^{+\bullet}) = 798$ kJ mol^{-1} which is in remarkably good agreement with experiment, ≤ 796 kJ mol^{-1}. For ion $[H_3NCO]^{+\bullet}$ a heat of formation of 804 kJ mol^{-1} is obtained. Using the latter value and $\Delta H_f^{\bullet}([H_3N]^{+\bullet}) + \Delta H_f^{\bullet}(CO) = 823$ kJ mol^{-1} [67], it becomes clear that the ionic complex $[H_3NCO]^{+\bullet}$ is only weakly bound. According to the calculations the reaction $[H_3NCO]^{+\bullet} \rightarrow [H_3N]^{+\bullet} + CO$ has only a small energy barrier. Although the RHF calculation leads to a small reverse activation energy, the results of CI calculations suggest that there is no barrier for this reaction. However, any transition state connecting ion (4) with (1), (2) or (3) was not found,

these transitions can only take place at very high energies. The isomerization requiring the lowest energy is the transition $[H_2NC(H)O]^{+\bullet}$ (1) → $[H_2NCOH]^{+\bullet}$ (3). The latter result is in keeping with the different kinetic energy releases for $H^\bullet$ loss from metastable $[H_2NC(H)O]^{+\bullet}$ and $[H_2NCOH]^{+\bullet}$ ions (see Table 4-2). The decomposition requires 87 kJ mol^{-1} less energy ($\Delta H_f^\bullet([H_2NCO]^+ + \Delta H_f^\bullet(H^\bullet)$ = 890 kJ mol^{-1} [65]) than the isomerization (1) → (3), so ions (1) and (3) fragment before they isomerize. The calculations show that the ion $[HNC(H)OH]^{+\bullet}$ (2) is stable. But to our knowledge, no experimental evidence was found for the existence of this ion.

These results may be compared to the results for the neutral molecules. For H_3NCO the RHF method does not lead to a significant minimum; the geometry search leads to a slight minimum at a very long CN distance. As for the corresponding ions, the neutral isomers $H_2NC(H)O$ ($1^\bullet$) and H_2NCOH ($3^\bullet$) are separated by a high barrier.

4.2.2 The Ions $[H_3CNO]^{+\bullet}$ (5) and $[H_2CNOH]^{+\bullet}$ (6)

A signal due to $[C,H_3,N,O]^{+\bullet}$ was present in the normal EI mass spectrum of nitromethane, H_3CNO_2 (m/z 61); m/z 45 was 10% of m/z 30 (base peak). The MI mass spectrum of the m/z 45 ion is included in Table 4-2 and contained only a signal at m/z 30, $[NO]^+$. The kinetic energy release accompanying this dissociation is very small, $T_{0.5}$ = 0.5 meV. The CA mass spectrum (*Figure 4-1c*) is also dominated by m/z 30, but a smaller signal at m/z 15, $[H_3C]^+$, is also present. Based on this information the $[C,H_3,N,O]^{+\bullet}$ ion was proposed to have the $[H_3CNO]^{+\bullet}$ structure. The NR mass spectrum (*Figure 4-3c*) of the $[H_3CNO]^{+\bullet}$ ion contained a recovery signal of the

reionized neutral counterpart of this m/z 45 ion.

Thermal decomposition of the trans-dimer of nitrosomethane (see structure below) is known to produce monomeric nitrosomethane (see Introduction). Indeed, the normal EI mass spectrum of the dimer and its decomposition products contained a very intense signal at m/z 45 (93% of m/z 30, base peak). Generation of these m/z 45 ions required 9.32 ± 0.05 eV (measured by the electron energy selector mass spectrometer) which is identical to the IE of nitrosomethane, 9.3 eV [75,76]. Moreover, the MI and CA mass spectra of the m/z 45 ion is close to those of the $[H_3CNO]^{+\bullet}$ ion from nitromethane; the only significant difference is slightly more intense signals at m/z 28 and 44. Thus, thermal decomposition of the trans-dimer of nitrosomethane yielded (predominantly) H_3CNO, which was subsequently ionized. However, the NR mass spectrum of the m/z 45 ion from the trans-dimer of nitrosomathane differed significantly from that of $[H_3CNO]^{+\bullet}$ (see *Figure 4-3c*). Intense signals appeared at m/z 45, 44 and 28. This observation and the above result of CA experiment indicated the co-generation of ion $[H_2CNOH]^{+\bullet}$ (see below).

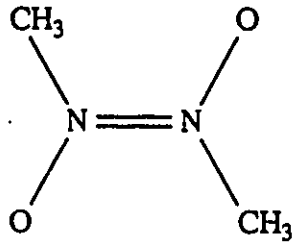

trans-dimer of nitrosomethane

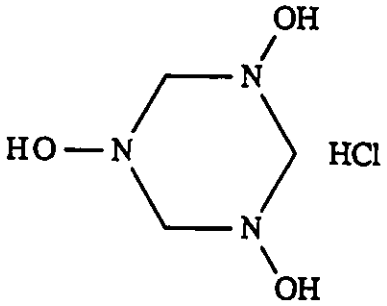

trimeric formaldoxime hydrochloride

Thermolysis of trimeric formaldoxime hydrochloride and ionization of the products also

yielded a $[C,H_3,N,O]^{+\bullet}$ ion; m/z 45 was the base peak and also the highest mass ion in the normal EI mass spectrum. Like the MI mass spectrum of ion $[H_3CNO]^{+\bullet}$, the MI mass spectrum (Table 4-2) of this ion was dominated by m/z 30, $[NO]^+$. However, the kinetic energy releases for the fragmentation processes are markedly different, 0.5 meV for $[H_3CNO]^{+\bullet}$ versus 35 meV for this ion. In addition, the MI mass spectrum of the m/z 45 ions from trimeric formaldoxime hydrochloride also contained a (small) signal at m/z 28 (most likely a $[C,H_2,N]^+$ isomer). The CA (*Figure 4-1d*) and CS (Table 4-3) mass spectra are also distinctly different from those of $[H_3CNO]^{+\bullet}$. The CA mass spectrum of the $[C,H_3,N,O]^{+\bullet}$ ion from trimeric formaldoxime hydrochloride contained signals at m/z 14 ($[CH_2]^{+\bullet}$), 18 ($[H_2O]^{+\bullet}$) and 31 ($[NOH]^+$), which can be considered as dissociation characteristics of $[H_2CNOH]^{+\bullet}$. Therefore, it was proposed that trimeric formaldoxime hydrochloride simply depolymerized upon heating and that the produced formaldoxime, H_2CNOH, was thereafter ionized. The NR mass spectrum (*Figure 4-3d*) of the $[H_2CNOH]^{+\bullet}$ ion is similar to the CA mass spectrum. The recovery signal of the reionized neutral counterpart of the $[H_2CNOH]^{+\bullet}$ ion was the base peak in the spectrum.

The MI mass spectra of $[H_3CNO]^{+\bullet}$ and $[H_2CNOH]^{+\bullet}$ show that fairly high energetic $[H_2CNOH]^{+\bullet}$ ions, i.e. metastable ions, isomerized into $[H_3CNO]^{+\bullet}$ prior to fragmentation, with the isomerization as the rate determining step. Thus, the energy of the transition state has to be > 1130 kJ mol^{-1} ($\Delta H_f^\bullet([NO]^+) + \Delta H_f^\bullet(CH_3^\bullet)$)[67]. There is no sign of communication between these two isomers and $[H_2NC(H)O]^{+\bullet}$, $[H_2NCOH]^{+\bullet}$ and $[H_3NCO]^{+\bullet}$.

4.3 Conclusions

A combination of mass spectrometry and ab initio molecular orbital theory was used to identify $[H_3,C,N,O]^{+\bullet}$ ions in the gas phase. Theory predicted that $[H_2NC(H)O]^{+\bullet}$ is slightly more stable than $[H_2NCOH]^{+\bullet}$ and $[H_3NCO]^{+\bullet}$, and that these three isomers are separated by high energy barriers. The isomeric ions could easily be distinguished via their metastable ion, collisional activation and charge stripping mass spectra. Ion $[H_2NCOH]^{+\bullet}$ was generated via 1,4 hydrogen transfer in $[H_2NC(O)OCH_3]^{+\bullet}$, $[H_2NC(O)C(O)OH]^{+\bullet}$ and $[H_2NC(O)CH_2CH_3]^{+\bullet}$. H transfer to the amine group, generating the $[H_3NCO]^{+\bullet}$ ion, was not observed. However, it was proposed that metastable fragmentation of $[H_2NCOH]^{+\bullet}$ took place via $[H_3NCO]^{+\bullet}$ with the isomerization as rate determining step. A high barrier for isomerization had to be invoked to explain the $[H_3CNO]^{+\bullet}$ and $[H_2CNOH]^{+\bullet}$ CA and CS mass spectra. However, metastable $[H_2CNOH]^{+\bullet}$ ions of high internal energy did isomerize into $[H_3CNO]^{+\bullet}$ prior to fragmentation.

Neutralization-reionization mass spectrometry was used to identify the neutral counterparts of these $[H_3,C,N,O]^{+\bullet}$ ions as stable species in the gas phase. Theory predicted the H_3NCO complex to be unstable.

4.4 Experimental

Appearance energy (AE) measurements were recorded with the electron energy selector

mass spectrometer by Dr. F.P. Lossing. The measurements were described in section 3.5. Dissociation characteristic experiments were performed with the ZAB-2F mass spectrometer. Detailed description of the experiments including metastable ion (MI), collision activation (CA), charge stripping (CS) and neutralization-reionization (NR) experiments can be found in section 3.5. Theoretical calculations were performed by Dr. P.J.A. Ruttink at Utrecht University, The Netherlands.

All compounds, except the trans-dimer of nitrosomethane, were commercially available and showed no detectable impurities. The trans-dimer of nitrosomethane was obtained via pyrolysis of t-butyl nitrite [89]. Needle-like prisms were obtained after recrystallisation with n-propanol. The melting point was 120 °C, identical with the literature value [89].

Table 4-1. Eight isomeric [C,H_3,N,O] isomers and the heats of formation (in kJ mol^{-1}) of the neutrals and their ionic counterparts. Results of theoretical calculations are given in brackets. See text for details.

[C,H_3,N,O] isomer		ΔH_f°(neutral)	ΔH_f°(ion)
H_2N-C(H)=O	**1**	-186 [67]	791 [68]
			(811 [70])
HN=C(H)-OH	**2**	(-135 [69])	(801 [70])
H_2N-C-OH	**3**	-	(747 [70])
H_3N-C=O	**4**	-	(772 [70])
H_3C-N=O	**5**	70 [74b]	967 [75,76]
H_2C=N-OH	**6**	-9 [a]	966 [75,77,78]
		(29 [73], -11 [81])	
H_2C=N(H)-O	**7**	(122 [73])	-
$H_2\overline{C}$-O-$\overline{NH}$	**8**	(141 [84])	-

a. Estimated by additivity [80], see text.

Table 4-2. Metastable ion mass spectra of $[C,H_3,N,O]^{+\bullet}$ ions from various precursors. The kinetic energy releases, $T_{0.5}$ (in meV), for the various metastable processes are presented in brackets. All data are corrected for isotopic contributions from ions of lower mass; relative intensities are peak heights under conditions of low energy resolution.

precursor	neutral	fragment ion, m/z.				proposed structure for
	lost	44	30	28	17	the $[C,H_3,N,O]^{+\bullet}$ ions
$H_2NC(H)O$	-	100 (33)	-	-	-	$[H_2NC(H)O]^{+\bullet}$
$H_2NC(O)OCH_3$	CO	a	-	-	a (40)	$[H_2NCOH]^{+\bullet}$
$H_2NC(O)CH_2CH_3$	C_2H_4	100 (10)	-	-	64 (43)	$[H_2NCOH]^{+\bullet}$
H_3CNO_2	O	-	100 (0.5)	< 1	-	$[H_3CNO]^{+\bullet}$
$[H_3,C,N,O]$ [b]	-	c	100 (0.6)	1	-	$[H_3CNO]^{+\bullet}$ + $[H_2CNOH]^{+\bullet}$
$[H_3,C,N,O]$ [d]	-	5	100 (35) [e]	10 (63) [e]	-	$[H_2CNOH]^{+\bullet}$

a. The spectrum contained signals at m/z 44 and 17 in the ratio 100: 29. However, part of the "m/z 44" signal (ca 50%) was due to the metastable process m/z 47 → m/z 46 + H$^{\bullet}$ taking place in the first field-free region.

b. Produced by thermolysis of the trans-dimer of nitrosomethane.

c. The spectrum contained signals at m/z 44, 30 and 28 in the ratio 145: 100: 1. However, a large part of the "m/z 44" signal (> 90%) was due to the metastable process m/z 47 → m/z 46 + H$^{\bullet}$ taking place in the first field-free region.

d. Produced by thermolysis of trimeric formaldoxime hydrochloride.

e. These decompositions showed a large collision cross section and so $T_{0.5}$ values should be regarded as upper limits.

Table 4-3. Charge stripping mass spectra of $[C,H_3,N,O]^{+\bullet}$ ions from various precursors. O_2 (90% T) was used as target gas. All data are corrected for isotopic contributions from ions of lower mass.

precursor	neutral lost	CS mass spectrum		proposed structure for
		m/z 22	22.5	the $[C,H_3,N,O]^{+\bullet}$ ions
$H_2NC(H)O$	-	100	64	$[H_2NC(H)O]^{+\bullet}$
$H_2NC(O)OCH_3$	CO	23	100	$[H_2NCOH]^{+\bullet}$
H_3CNO_2 [a]	O	36	100	$[H_3CNO]^{+\bullet}$
$[H_3,C,N,O]$ [a,b]	-	c	c	$[H_3CNO]^{+\bullet}$ + $[H_2CNOH]^{+\bullet}$
$[H_3,C,N,O]$ [a,d]	-	100	54	$[H_2CNOH]^{+\bullet}$

a. The absolute abundances of the charge stripping signals are much smaller than in the other two spectra; compare *Figure 4-1c* and *4-1d* with *Figure 4-1a* and *4-1b*.

b. Produced by thermolysis of the trans-dimer of nitrosomethane.

c. Interference from the metastable process m/z 47 → m/z 46 + $H^{\bullet}$ prevented the measurement of these peaks.

d. Produced by thermolysis of trimeric formaldoxime hydrochloride.

Table 4-4. Calculated relative energies, absolute energies and transition state energies along with geometries of $[H_2NC(H)O]^{+\bullet}$, $[HNC(H)OH]^{+\bullet}$, $[H_2NCOH]^{+\bullet}$ and $[H_3NCO]^{+\bullet}$ and their neutral counterparts, based on RHF/4-31 G optimized geometries. The experimental enthalpies for (**1**) and (**3**) are 791 and ≤796 kJ mol^{-1}, respectively. For (**1**$^{\bullet}$) and (**9**$^{\bullet}$) are -186 and -156 kJ mol^{-1}, respectively. Bond lengths are in ångstroms and angles are in degrees.

isomer	geometry	E_{rel} (kJ mol^{-1})	E_{abs} (kJ mol^{-1})[a]
1a $[H_2NC(H)O]^{+\bullet}$	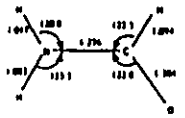	0	791
1b	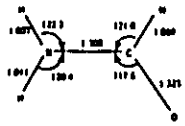	38	829
2 $[HNC(H)OH]^{+\bullet}$	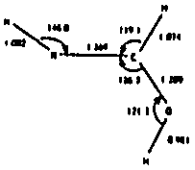	76	867
3 $[H_2NCOH]^{+\bullet}$	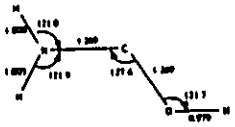	6	797
4 $[H_3NCO]^{+\bullet}$	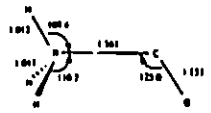	12	803
TS **1a-3**	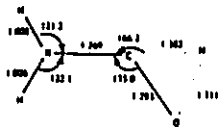	187	978
TS **1a-2**	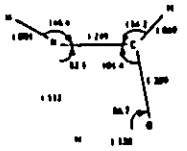	269	1060
TS **2-3**	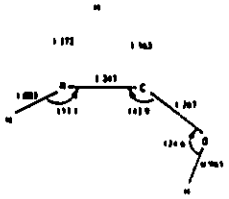	287	1078

(Table 4-4 continue)

isomer	geometry	E_{rel} (kJ mol^{-1})
4 $[H_3NCO]^{+\bullet}$		0
TS **4-9**	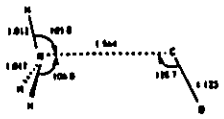	1
9 $[H_3N]^{+\bullet}$ + CO		7

isomer	geometry	E_{rel} (kJ mol^{-1})	E_{abs} (kJ mol^{-1})[b]
1$^{\bullet}$ $H_2NC(H)O$	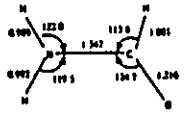	0	-186
3$^{\bullet}$ H_2NCOH	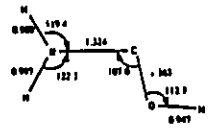	163	-23
TS **1**$^{\bullet}$-**3**$^{\bullet}$	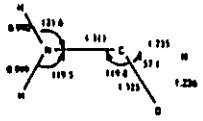	323	137
9$^{\bullet}$ H_3N + CO		26	-160

a. Base on the experimental heat of formation of (**1**).

b. Base on the experimental heat of formation of (**1**$^{\bullet}$).

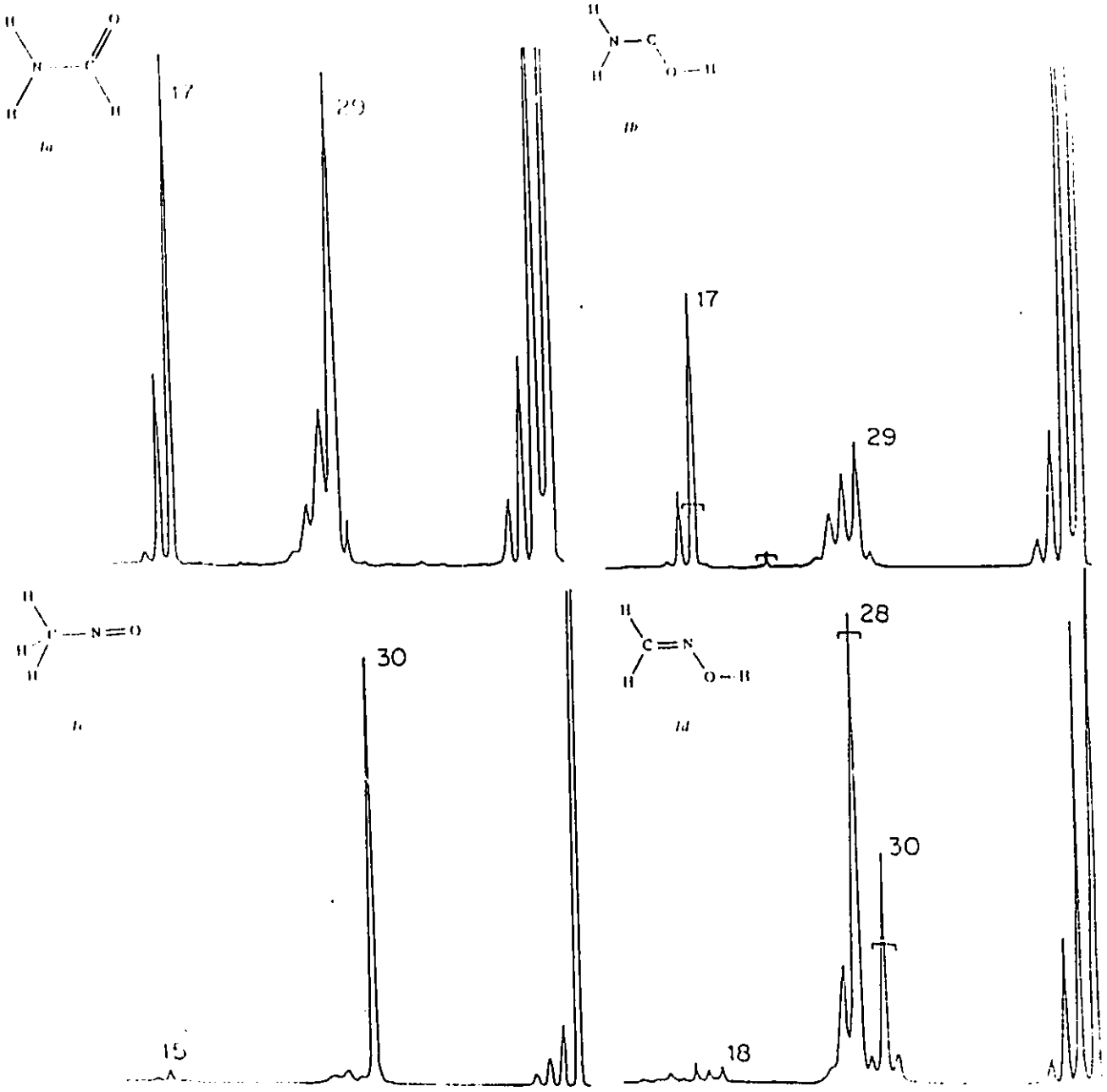

Figure 4-1. *O_2 (90% T) collisional activation mass spectra of ionized $H_2NC(H)O$ (a), the $[C,H_3,N,O]^{+\bullet}$ ions from $H_2NC(O)OCH_3$ (b) and H_3CNO_2 (c) and the ionized $[C,H_3,N,O]$ product molecules from thermolysis of trimeric formaldoxime hydrochloride (d). The signals remaining <u>below</u> the bars are corrected for contributions of metastable ions, except for the charge stripping peak (m/z 22.5) in 1b which is a ^{13}C contribution from m/z 44.*

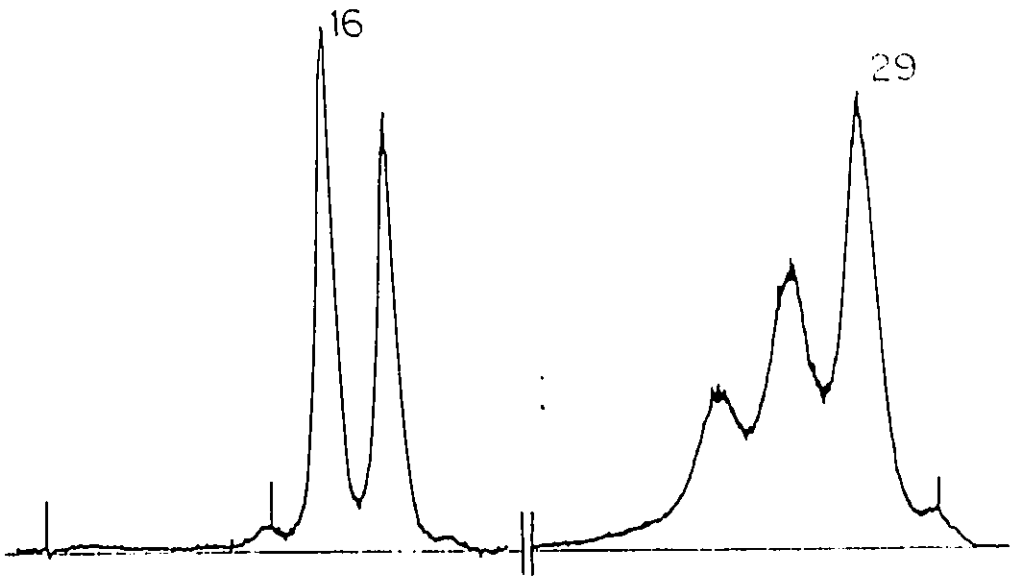

Figure 4-2. O_2 (80% T) collisional activation mass spectrum of the $[C,H_3,N,O]^{+\bullet}$ ion generated via metastable fragmentation of $H_2NC(O)C(O)OH$ molecular ion in the first field-free region of the mass spectrometer (m/z $45^2/89$ = 22.8 was mass-selected).

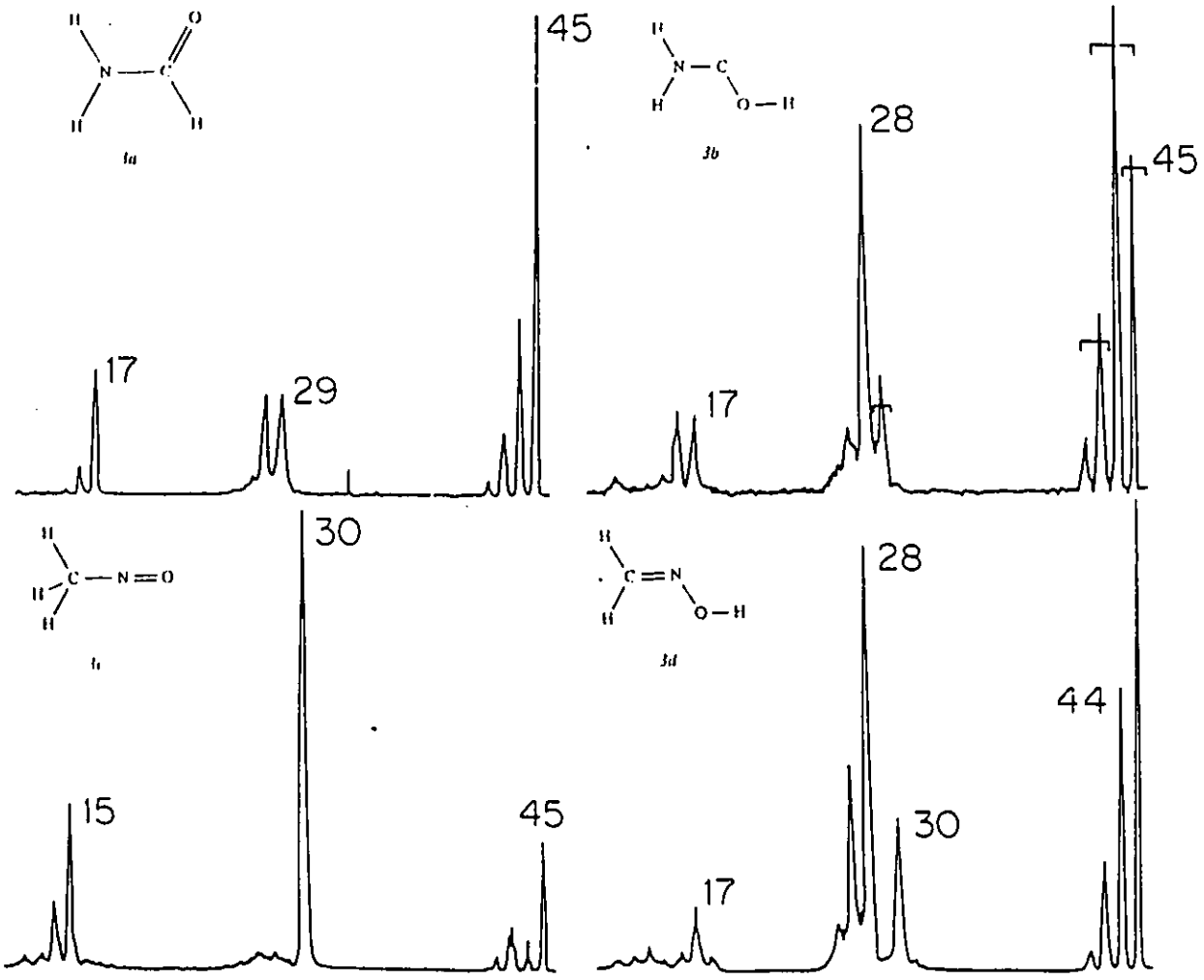

Figure 4-3. Neutralization-reionization mass spectra of ionized $H_2NC(H)O$ (a), the $[C,H_3,N,O]^{+\bullet}$ ions from $H_2NC(O)OCH_3$ (b) and H_3CNO_2 (c) and the ionized $[C,H_3,N,O]$ product molecules from thermolysis of trimeric formaldoxime hydrochloride (d). Xe (90% T) was the charge exchange neutralization agent and O_2 (90% T) the reionization target gas. Isotopic contributions from m/z 44 are indicated with bars.

Chapter 5 Oxides of Carbon

5.1 Introduction

Linear and quasi-linear cumulenes of the general structure AC_nB (A,B = lone pair, H_2, O, S; $n \geq 2$) have been subjects of both experimental and theoretical interest for more than a century. There are several reasons for the exceptional interest in these molecules: they have been postulated as key intermediates in the formation of interstellar species; they have unusual spectroscopic properties, reactivity and stability, as well as their unique electronic structures. Unfortunately, quite a few of these molecules have such a high reactivity that they cannot be produced even as a transient. This is especially true for cumulenes containing an even number of carbon atoms, which are believed to be considerably less stable than their odd-numbered analogues [90,91] and have often eluded experimental identification. However, quite a few hydrocumulenes, e.g. allene and ketene, have been successfully generated and identified. Recently, neutralization-reionization mass spectrometry (NRMS)[92] has proven itself as a powerful tool for studying elusive molecules in the gas phase. Several cumulenes including dithiocumulenes SC_nS (n = 2,4), [93,94] oxycumulene OC_4O [95] and mixed S/O cumulene SC_2O [96] have been accessed in the gas phase by NRMS. All efforts, beginning as early as 1913, to prepare a chemically bound OC_2O, the first member of the even-numbered oxycumulenes, ethylenedione have proven unsuccessful. Therefore, the aim of this work is to investigate three

oxides of carbon, OC_2O, OC_3O (carbon suboxide) and C_2O (carbonyl carbene) in the gas phase by NRMS.

5.2 Result and Discussion

5.2.1 OC_2O

The study of OC_2O began in 1913 when Staudinger and Anthes [97] observed the reaction of oxalyl bromide, $(COBr)_2$, with potassium metal. But their study and the later pyrolysis and photolysis experiments on bridged α-diketones [98,99] did not provide direct evidence for the existence of OC_2O, although OC_2O is expected to be a kinetically extremely stable species on the basis of *ab initio* calculations. [90] Two reasons [96] were suggested for this failure: (i) The OC_2O species have not been generated in the bound triplet ground state, $^3\Sigma_g^-$, but rather in the singlet state $^1\Sigma_g^+$, which is predicted to dissociate spontaneously to two ground-state CO molecules. (ii) The lifetime of the stable $^3\Sigma_g^-$ OC_2O species may be drastically shortened by an efficient spin-orbit coupling if a potential-curve crossing is available not too far from the minimum. On the other hand, the ionic counterpart of OC_2O, $[OC_2O]^{+\cdot}$, is experimentally accessible and has been the object of electron spin resonance (ESR),[100] molecular beam photoionization, [101] high-pressure mass spectrometry [102] and drift tube mass spectrometry [103] experiments.

Besides the experimental efforts, *ab initio* theoretical calculations have been used to investigate the electronic structures of OC_2O. It was predicted by most of the calculations[90,91,104-107]

that OC_2O has a triplet ground state, $^3\Sigma_g^-$. The heat of formation of this triplet ground state was calculated to be from -100 to 87 kJ mol^{-1} by various methods. [90,104-107] This triplet ground state was found [90,104] to be linear and to have considerably higher energy than two separated CO molecules in their ground singlet state, $^1\Sigma$. Its linear dissociation to two ground state CO molecules was predicted [104] to be symmetry forbidden and accordingly to have a high activation energy. Its lowest spin-allowed dissociation limit was dissociation to a CO molecule in the ground state $^1\Sigma$ plus a CO molecule in the lowest excited state $^3\Pi$. However, the OC_2O ($^3\Sigma_g^-$) lay 309 kJ mol^{-1} below this dissociation limit. Several bent singlet excited states were also found for OC_2O. They were at least 80 kJ mol^{-1} higher in energy than the triplet ground state and might dissociate to two separated CO molecules with little or no activation energy.

The ion $[OC_2O]^{+\bullet}$ was predicted to have a trans geometry in its ground state by a theoretical calculation. [100] Its heat of formation was measured to be from 1013 to 1050 kJ mol^{-1} by various techniques. [101-103] In this work, AE of $[OC_2O]^{+\bullet}$ generated from oxalic acid, $(COOH)_2$ and oxalyl chloride, $(COCl)_2$, were measured by the MS-902S mass spectrometer. From these two compounds, close values of $\Delta H_f^\bullet([OC_2O]^{+\bullet})$ were obtained to be 939 ± 10 kJ mol^{-1} and 942 ± 10 kJ mol^{-1} respectively. Table 5-1 summarizes these data for $\Delta H_f^\bullet([OC_2O]^{+\bullet})$. The $\Delta H_f^\bullet([OC_2O]^{+\bullet})$ obtained in this work is lower than those reported in the previous works. The recent values are believed reliable. The reliability of the AE experiments were examined carefully. In the experiment with oxalic acid, the following reaction

$$(COOH)_2 \rightarrow [OC_2O]^{+\bullet} + H_2O + O + e \qquad 5\text{-}1$$

was considered to take place in the ion source. Under high mass resolution, three peaks were resolved at m/z 56. The three peaks from low mass to high mass corresponded to $[OC_2O]^{+\cdot}$, $[C_3H_4O]^{+\cdot}$ and $[C_4H_8]^{+\cdot}$. The lowest mass peak, corresponding to $[OC_2O]^{+\cdot}$, was selected and its ionization efficiency curve was recorded. The lost neutrals in reaction 5-1 were most probably H_2O + O rather than 2HO$^{\cdot}$. This is based on the following reason: it was observed that the metastable molecular ion of oxalic acid, $[(COOH)_2]^{+\cdot}$, lost CO_2 to form $[C(OH)_2]^{+\cdot}$. [109] This result indicated that the molecular ion should have a cyclic structure with intramolecular hydrogen bonding between the two hydroxyl groups and the losses of two HO$^{\cdot}$ groups are not likely as a result. In the experiment of oxalyl chloride, the ion source reaction

$$(COCl)_2 \rightarrow [OC_2O]^{+\cdot} + 2Cl^{\cdot} + e \qquad 5\text{-}2$$

was studied. The peak at m/z 56 was a singlet under high mass resolution. The reason for the difference in $\Delta H_f^{\cdot}([OC_2O]^{+\cdot})$ between this work and the previous works may be that excited $[OC_2O]^{+\cdot}$ species were generated in the previous works.

There was a intense signal at m/z 56, 17% of m/z 63 (O=C^{+}-Cl, base peak) in the normal EI mass spectrum of oxalyl chloride. There was no fragment signal in the MI mass spectrum of this m/z 56 ion. The CA mass spectrum of this m/z 56 ion is shown in Table 5-2. The fragment signals at m/z 44 ($[CO_2]^{+\cdot}$), 40 ($[C_2O]^{+\cdot}$, 28 ($[CO]^{+\cdot}$), 24 ($[C_2]^{+\cdot}$), 16 ($[O]^{+\cdot}$) and 12 ($[C]^{+\cdot}$) indicate that the m/z 56 ion should have the $[O=C=C=O]^{+\cdot}$ structure. This m/z 56 ion had quite a large collision cross-section that gave intense CA fragment signals even with the very inefficient collision target gas Xe. Other precursors, oxalic acid, 2,3-butanedione and the product of reaction

of high pressure carbon monoxide, also had signals at m/z 56 in their EI mass spectra. These m/z 56 ions were weak in terms of intensity but yielded closely similar CA mass spectra (Table 5-2) to that of the m/z 56 ion from oxalyl chloride. Therefore these m/z 56 ions were also assigned to have the $[O=C=C=O]^{+\bullet}$ structure. The result confirms that the reaction [102,103]

$$[CO]^{+\bullet} + 2CO \rightarrow [OC_2O]^{+\bullet} + CO \qquad 5\text{-}3$$

takes place when high pressure CO was introduced in the ion source. Unfortunately, $[C_4H_8]^{+\bullet}$ ions were found to be a usual back ground signal in the ZAB-2F mass spectrometer. It gave weak fragment signals at m/z 55 ($[C_4H_7]^+$), 41 ($[C_3H_5]^+$) and 39 ($[C_3H_3]^+$) in the CA mass spectra of the $[OC_2O]^{+\bullet}$ ion. The weak recovery signals in all the NR mass spectra (Table 5-3) of the m/z 56 from oxalyl chloride were found to be the reionized neutral counterparts of the $[C_4H_8]^{+\bullet}$ ions. The signals at m/z 55, 41 and 39, which were related to the $[C_4H_8]^{+\bullet}$ ions, also presented as minor signals in the NR mass spectra. Hence, there was no recovery signal for the reionized neutral counterpart of the $[OC_2O]^{+\bullet}$ ion. The generation of the fragment signals at m/z 44, 40, 28, 24, 16 and 12 in the NR mass spectra except for the He/O_2 NR mass spectrum remains to be explained.

Three possible sources of the above fragment signals are considered. The first possible source is the neutrals formed in the CA process taking place along with the neutralization process in collision Cell 1 (see also section 3.4.5.1). Part of the fragment signals at m/z 28, 16 and 12, the $[CO]^{+\bullet}$ and its fragments $[O]^{+\bullet}$ and $[C]^{+\bullet}$, are from this source because they were the only signals in the He/O_2 NR mass spectrum (Table 5-3). Since He is not an efficient neutralization target gas but a very efficient collision target gas, it will cause collisional activation dissociation

of the mass selected $[OC_2O]^{+\bullet}$ ion, rather than neutralization. The second possible source is the dissociative OC_2O neutral molecule. This source, mostly OC_2O in singlet states, may also generate part of the $[CO]^{+\bullet}$, $[O]^{+\bullet}$ and $[C]^{+\bullet}$. But the rest of the fragment signals at m/z 44, 40 and 24 should not be from this source because the dissociation energies for their production from the neutral molecule are high and the endothermic neutralization process with Xe as target gas cannot provide enough energy for the dissociations. The third and only possible source left is dissociative reionized OC_2O. This reionized OC_2O should certainly yield the above fragmention signals with the exception of part of the $[CO]^{+\bullet}$, $[O]^{+\bullet}$ and $[C]^{+\bullet}$ signals. Therefore, it can be concluded that stable OC_2O neutral species were generated in the neutralization process in collision Cell 1 and successfully travelled to collision Cell 2 but when reionized they produced highly excited $[OC_2O]^{+\bullet}$ ions which completely dissociated. Under normal experimental conditions, the lifetime of these stable OC_2O species was calculated to be ~ 1 μs.

5.2.2 C_2O and OC_3O

Carbon suboxide, OC_3O, was prepared by Diels and Wolf [110] in 1906 by treating diethyl malonate with a large excess of phosphorous pentoxide. The early studies on OC_3O have been reviewed by Reyerson and Kobe. [111] Since then it has been the object of numerous infrared and Raman, [112-115] photochemical, [116-119] electron diffraction, [120,121] electron spectroscopy (ESCA), [122-124] ultraviolet absorption, [125-127] carbon-13 nuclear magnetic resonance (NMR), [128] and high pressure mass spectrometry [129] experiments as well as theoretical calculations. [130-135] As a product of the reactions of carbon suboxide, carbonyl carbene, C_2O, has been studied by a variety of

experimental techniques including matrix-isolation infrared, [136,137] photochemical, [116-118,138,139] electron spin resonance (ESR), [140,141] high pressure mass spectrometry [129] and ion cyclotron resonance (ICR) mass spectrometry [142] as well as theoretical calculations. [143-146]

The heats of formation of OC_3O and $[OC_3O]^{+\cdot}$ were reported to be -94 and 929 kJ mol^{-1} respectively. [108] Both linear and bent structures were suggested for OC_3O on the basis of theoretical calculations [130-135] and electron spectroscopy (ESCA) experiments. [120,122] The heat of formation of C_2O was determined to be 386 ± 19 kJ mol^{-1} in the experiments [116,117] and was calculated [144] to be 372 kJ mol^{-1}. $\Delta H_f^{\bullet}([C_2O]^{+\cdot})$ was calculated to be ≤ 1476 kJ mol^{-1} by the appearance energy measurement [129] of the reaction

$$OC_3O \rightarrow [C_2O]^{+\cdot} + CO + e \qquad 5\text{-}4$$

and 1421 ± 42 kJ mol^{-1} by the ICR mass spectrometry study [142] on the reaction

$$([CO]^{+\cdot})^{\bullet} + CO \rightarrow [C_2O]^{+\cdot} + O \qquad 5\text{-}5$$

In this work, the appearance energy of $[C_2O]^{+\cdot}$ formed in the ion source, reaction 5-4, was measured to be 14.7 ± 0.1 eV by the MS-920S mass spectrometer and 14.48 ± 0.05 eV by the electron energy selector mass spectrometer. These results lead to $\Delta H_f^{\bullet}([C_2O]^{+\cdot})$ to be ≤ 1433 ± 10 and ≤ 1412 ± 5 kJ mol^{-1} respectively. These values are in good agreement with the previous results.

There were intense signals at m/z 68 and 40 in the normal EI mass spectrum of the pyrolysis products of malonic acid mixed with phosphorous pentoxide (reaction 5-6). The rest of the relatively intense signals in the spectrum were m/z 44, 32, 28, 24, 16, 14 and 12. The signal at m/z 44 corresponded to the decarboxylation product, CO_2, in the pyrolysis reaction (reaction 5-6b).

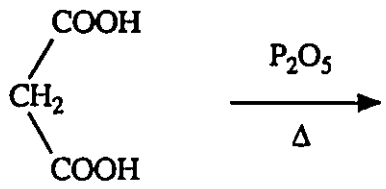

$$OC_3O + 2H_2O \qquad \text{5-6a}$$

$$CO_2 + CH_3COOH \qquad \text{5-6b}$$

The metastable m/z 68 ion gave a signal at m/z 40 ($[C_2O]^{+\cdot}$) in its MI mass spectrum with little kinetic energy release ($T_{0.5}$ = 1.8 meV). The CA mass spectrum (Table 5-4) of the m/z 68 ion was dominated by this signal and other characteristic fragment signals at m/z 52 ($[C_3O]^{+\cdot}$), 36 ($[C_3]^{+\cdot}$), 28 ($[CO]^{+\cdot}$), 24 ($[C_2]^{+\cdot}$) and 12 ($[C]^{+\cdot}$). In the NR mass spectrum (Table 5-5) of the m/z 68 ion its reionized neutral counterpart gave a recovery signal at m/z 68 and the same fragment signals as those in its CA mass spectrum. Therefore, the m/z 68 ion was assigned the $[O=C=C=C=O]^{+\cdot}$ structure. The m/z 40 ion did not fragment metastably. Its CA mass spectrum (Table 5-4) contained characteristic fragment signals at m/z 28 ($[CO]^{+\cdot}$), 24 ($[C_2]^{+\cdot}$) and 12 ($[C]^{+\cdot}$). Its reionized neutral counterpart and these fragment signals appeared in the NR mass spectrum (Table 5-5) of the m/z 40 ion. This leads to the assignment of the structure $[C=C=O]^{+\cdot}$ to the m/z 40 ion.

5.3 Conclusions

Three elusive molecules OC_2O, OC_3O and C_2O as well as their ionic counterparts were identified by tandem mass spectrometry. As predicted by theoretical calculations OC_2O was generated as a stable neutral molecule and had a highly dissociative ionic counterpart. Neutral molecules OC_3O and C_2O along with their ionic counterparts were found to be stable species in the gas phase. For OC_3O and C_2O which have recovery signals in their NR mass spectra, vertical neutralization of the ions should yield neutral counterparts in their ground states having the same geometry of the ions and vertical (re)ionization of the neutral counterparts should result the ions in their ground states with the same geometry. For OC_2O which has no recovery signal in its NR mass spectra, it is believed that neutralization of the ion yielded its neutral counterpart in the ground state but the (re)ionization of the linear ground state neutral counterpart did not produce the ground state ion which is expected to have a trans geometry. More information (probably provided by high level *ab initio* molecular orbital calculations) of the dissociative $[OC_2O]^{+\bullet}$ ion and its dissociation channels is needed to confirm this conclusion.

5.4 Experimental

Appearance energy (AE) measurements were performed with the MS-902S mass spectrometer and the electron energy selector mass spectrometer. The measurements were described in section 3.5. Dissociation characteristic experiments were performed with the ZAB-2F

mass spectrometer. Detailed description of the experiments including metastable ion (MI), collision activation (CA) and neutralization-reionization (NR) experiments can be found in section 3.5.

All compounds, except carbon suboxide, were commercially available and showed no detectable impurities. Carbon suboxide was synthesized by pyrolysis of malonic acid in phosphorous pentoxide. [112] By-products like carbon dioxide and acetic acid were introduced into the ion source of the mass spectrometer along with carbon suboxide and did not interfere with the CA and NR mass spectra of OC_3O and C_2O.

Table 5-1 Experimental data of heat of formation of $[OC_2O]^{+\cdot}$.

method	ref.	result	$\Delta H_f^\circ([OC_2O]^{+\cdot})$ kJ mol^{-1}
Photoionization	101	Binding energy ($[CO]^{+\cdot}$-CO) = 0.97 ± 0.04 eV	1038 ± 4
High Pressure MS	102(a)	AE($[OC_2O]^{+\cdot}$) = 12.8 ± 0.3 eV	1013 ± 29
High Pressure MS	102(c)	$[CO]^{+\cdot}$ + 2CO → $[OC_2O]^{+\cdot}$ + CO, $-\Delta H \geq 106.2$ kJ mol^{-1}	≤1025
Drift tube MS	103(b)	Binding energy ($[CO]^{+\cdot}$-CO) = 0.8 eV	1054
AE Measurement	this work	AE($[OC_2O]^{+\cdot}$) from $(COOH)_2$ = 17.4 ± 0.1 eV	≤938 ± 10
AE Measurement	this work	AE($[OC_2O]^{+\cdot}$) from $(COCl)_2$ = 15.7 ± 0.1 eV	≤942 ± 10

Table 5-2 CA mass spectra of $[OC_2O]^{+\cdot}$ ions from different precursors. Collision target gas pressures were adjusted to allow 90% beam transmission.

precursor	target gas	fragment ion (m/z)					
		44	40	28	24	16	12
CO + CO	O_2	1.6	17.1	100	1.2	0.4	3.3
$(COCH_3)_2$	O_2	2.9	17.8	100	1.4	<0.1	2.5
$(COOH)_2$	O_2	2.0	16.3	100	1.3	<0.1	2.0
$(COCl)_2$	O_2	2.4	18.2	100	1.4	0.3	3.1
$(COCl)_2$	Xe	0.1	5.2	100	0.2	<0.1	1.8
$(COCl)_2$	He	0.7	15.2	100	2.0	0.3	1.0

Table 5-3 NR mass spectra of the $[OC_2O]^{+\cdot}$ ions from oxalyl chloride. Neutralization target gas (N) and reionization target gas (R) pressures were adjusted to allow 90% beam transmission.

target gas (N/R)	fragment ion (m/z) [a]					
	44	40	28	24	16	12
Xe/O_2	0.2	0.7	100	0.7	2.9	7.3
O_2/O_2	0.5	0.7	100	1.2	5.6	10.8
$c\text{-}C_3H_6/O_2$	<0.1	3.2	100	1.2	4.0	7.2
Xe/He	<0.1	1.0	100	1.0	4.9	10.5
He/O_2	-	-	100	<0.1	6.7	6.7

a. The recovery signals at m/z 56 and weak fragment signals at m/z 55, 41, and 39 were all due to the interference of the back ground $[C_4H_8]^{+\cdot}$ ions.

Table 5-4 CA mass spectra of the $[OC_3O]^{+\bullet}$ and $[C_2O]^{+\bullet}$ ions from carbon suboxide. Collision target gas (O_2) pressure was adjusted to allow 90% beam transmission.

parent ion (m/z)	fragment ion (m/z)							
	52	40	36	34 [a]	28	24	16	12
68	8.4	100	0.4	5.9	10.9	5.0	-	2.9
40	-	-	-	-	100	18.1	1.1	28.7

a. This is a charge stripping signal, m/z 68 $^{2+}$, of the molecular ion.

Table 5-5 NR mass spectra of the $[OC_3O]^{+\bullet}$ and $[C_2O]^{+\bullet}$ ions from carbon suboxide. Neutralization target gas (Xe) and reionization target gas (O_2) pressures were adjusted to allow 90% beam transmission.

parent ion (m/z)	fragment ion (m/z)								
	68	52	40	36	34 [a]	28	24	16	12
68	463	31.6	100	3.0	3.0	43.0	16.7	-	13.3
40	-	-	323	-	-	100	19.4	1.6	24.2

a. This signal relates to the charge stripping signal, m/z 68^{2+}, of the molecular ion.

Chapter 6 Fragmentation Mechanisms of Ionized Maleic and Fumaric Acids

6.1 Introduction

The EI mass spectra of maleic acid (Z-HOOCCH=CHCOOH), maleic acid-2,3-d_2, fumaric acid (E-HOOCCH=CHCOOH) and fumaric acid-2,3-d_2 were examined earlier by Holmes et al[147]. Fragmentation mechanisms proposed for these compounds were based on the interpretation of the EI mass spectra. It was observed that the fragmentation of maleic and fumaric acids were strikingly different. The experiments were done at the time when tandem mass spectrometry was still under development. Since then no other study has reexamined the fragmentation mechanisms. Therefore in this work, tandem mass spectrometry was used to reinvestigate the fragmentation mechanisms of maleic and fumaric acids and their 2,3-d_2 and carboxyl-d_2 isotopomers.

6.2 Result and Discussion

In the following sections results of thermodynamic measurements and the examination of the dissociation characteristics of ionized maleic and fumaric acids and their primary fragment ions will be presented. The aim of the investigation is to assign structures to these ions and to identify their fragmentation mechanisms.

6.2.1 Maleic Acid

Usually Z,E-isomers containing one double bond are very similar in their heats of formation, ionization energies and EI mass spectra. For example, the thermodynamic data (Table 6-1) and EI mass spectra[148] of Z,E-3-hexene and Z,E-2-butenoic acids are very close. But maleic and fumaric acids show significant differences in their ionization energies (Table 6-1) and normal EI mass spectra (*Figure 6-1 and 6-17*). Similar differences can be found between ortho-benzenedicarboxylic acid and its meta- and para- isomers (see Table 6-1 and ref. 148). In these two systems, maleic acid and o-benzenedicarboxylic acid have the lowest heat of formation and ionization energy. This can be explained by the intramolecular hydrogen bonding between the two carboxyl groups in the compounds and the resulting ring structures stabilize these two molecules.

The normal EI mass spectra of maleic acid (*Figure 6-1a*) and maleic acid-2,3-d_2 (*Figure 6-1b*), which were introduced to the ion source of the ZAB-2F by the direct probe inlet system, are closely similar to those of ref. 147 also obtained by a direct inlet system. In that previous work, the temperature effect on the EI mass spectrum of maleic acid was examined. It was found that intense dehydration took place in a glass tube indirect inlet system at ~ 200 °C, but neither dehydration nor decarboxylation was observed with variation of the probe heater temperature from 80 to 250 °C, using the direct inlet system. In the present work the temperature effect on the normal mass spectrum of unlabelled maleic acid has also been studied. It was found that the relative abundances of major fragment ions at m/z 99 ($[M-OH]^+$), 98 ($[M-H_2O]^{+\cdot}$), 88 ($[M-CO]^{+\cdot}$), 72 ($[M-CO_2]^{+\cdot}$) and 45 ($[COOH]^+$) did not change over a range of probe heater temperatures from

70 to 130°C. But over a higher temperature range from 130 to 190°C the abundances of the ions at m/z 99, 72 and 45 increased relative to the abundances of ions at m/z 98 and 88 which did not change. These results indicate that neither thermal dehydration nor decarbonylation takes place in the ion source and the product of thermal decarboxylation, m/z 72, is contributing to the normal EI mass spectrum at high probe heater temperatures. It was also found that at 200°C the ratio of $[M+1]^+ : [M]^{+\cdot} = 1 : 1$, indicating that the reaction

$$RCOOH + [RCOOH]^{+\cdot} \rightarrow [RCOOH_2]^+ + RCOO^{\cdot}$$

was taking place in the source, in agreement with the previous observation[147]. The $[M+1]^+$ ion may lose H_2O to give an ion also at m/z 99 which contributes to the normal EI mass spectrum. The increase of abundance of the m/z 45 ion may also result from the products of ion-molecule reactions taking place in the ion source at high temperatures, as well as from fragmentation of m/z 72.

In the normal EI mass spectrum of maleic acid (*Figure 6-1*) the abundance of the molecular ion at m/z 116 was weak and there were major fragment ions at m/z 98, 88 and 72, which were generated from the metastable molecular ion. In the following the experimental results and fragmentation mechanisms of the molecular ions (m/z 116), major fragment ions (m/z 98, 88 and 72) and other important fragment ions (m/z 99, 70, 69 and 60) of the three isotopomers of maleic acid are presented. These ions are identified by their m/z values corresponding to the unlabelled maleic acid and represent the ions from all the three acids.

m/z 116, the molecular ion

The intensity of the molecular ion is weak, 3% of m/z 45 (base peak), in the EI mass

spectrum of unlabelled maleic acid. The IE was measured using the MS-902S mass spectrometer (see section 2.2.2 and 3.3.7.2) to be 9.98 ± 0.1 eV for the unlabelled acid and 10.05 ± 0.1 eV for the carboxyl-d_2 acid. Taking the IE of 10.0 ± 0.1 eV for maleic acid and $\Delta H_f^\bullet$(Z-HOOCCH=CHCOOH) = -679.4 kJ mol^{-1} [150] the upper limit of $\Delta H_f^\bullet$([Z-HOOCCH=CHCOOH]$^{+\bullet}$) was calculated to be 285 ± 10 kJ mol^{-1} (see Table 6-2).

The molecular ion has three metastable dissociation channels, $[M-H_2O]^{+\bullet}$, $[M-CO]^{+\bullet}$ and $[M-CO_2]^{+\bullet}$ (Table 6-3). The temperature effect on the metastable peak abundances has also been studied for maleic acid-carboxyl-d_2. It was found that the relative abundance of the $[M-CO_2]^{+\bullet}$ ion increased by a factor of ~4 by increasing the probe heater temperature from 100 to 240 °C but the relative abundance of the $[M-D_2O]^{+\bullet}$, $[M-HDO]^{+\bullet}$ and $[M-CO]^{+\bullet}$ ions did not change over this temperature range. These results are similar to those found for the normal EI mass spectrum.

The CA mass spectrum of the molecular ion of unlabelled maleic acid is shown in *Figure 6-2*. In the spectrum, there were a few weak CA signals that appeared and the metastable peaks at m/z 88 and 72 did not increase substantially. The NR mass spectrum (*Figure 6-3*) of the molecular ion contained only very weak signals of fragment ions and no recovery signal for the reionized neutral counterpart of the molecular ion. The low intensity of the molecular ion or/and its dissociative neutral counterpart may be the reason(s) for the absence of the recovery signal.

As mentioned above, the structure of the molecular ion may be cyclic. In this ring structure the intramolecular hydrogen bonding can be between two hydroxyl groups or/and between a hydroxyl group and a carbonyl group of the two carboxyl groups (see structures in below). The proposed mechanisms of the metastable dissociations of the molecular ion may be shown by maleic acid-carboxyl-d_2. The observation of D_2O and HDO losses from the molecular

ion of maleic acid-carboxyl-d_2 and H_2O and HDO losses from the molecular ion of maleic acid-2,3-d_2 implies that there are two channels corresponding to the water loss:

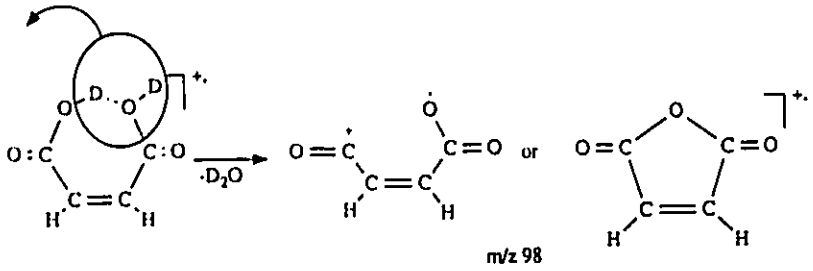

6-1

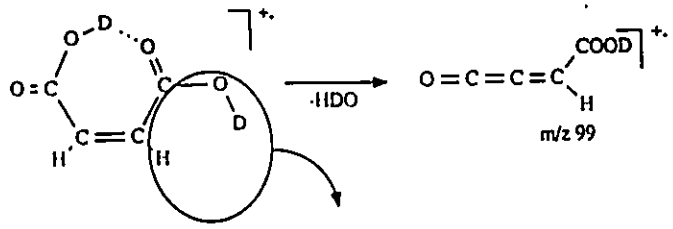

6-2

The molecular ion may also lose CO by two ways:

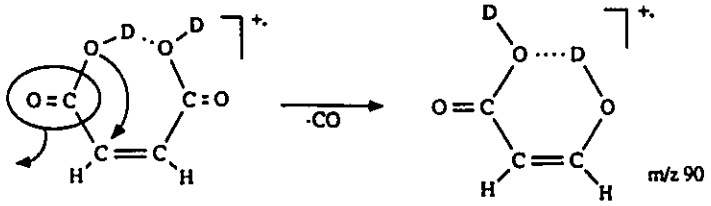

6-3

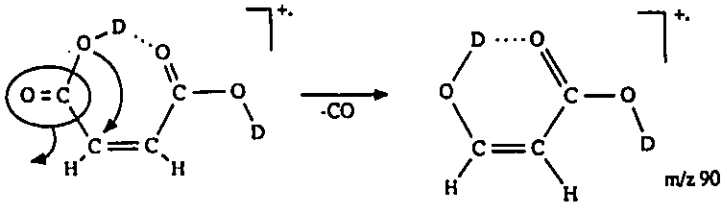

6-4

There are also two possible paths proposed for the decarboxylation of the molecular ion:

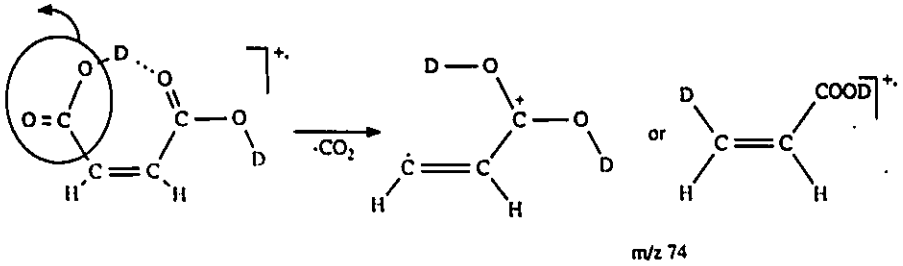

6-5

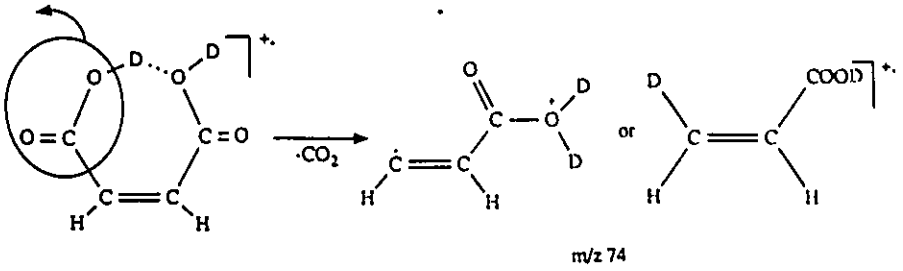

6-6

m/z 99, the M-OH ion

The abundance of this ion is 11% of m/z 45 (base peak) in the normal EI mass spectrum of unlabelled maleic acid. This ion was not produced by the metastable molecular ion but was produced by a direct bond cleavage reaction, HO˙ loss from the energised molecular ion in the ion source. The mechanism of maleic acid-carboxyl-d_2 losing DO˙ in the ion source is shown as below:

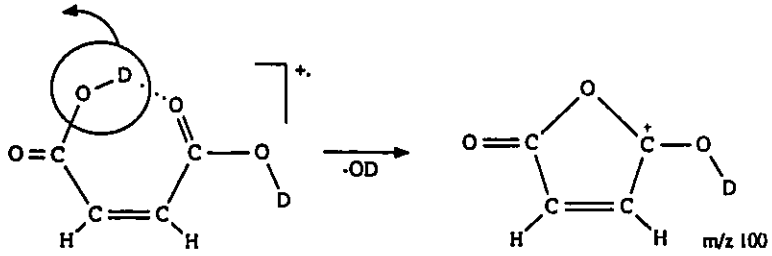

6-7

The AE of this ion source reaction was measured using the MS-902S mass spectrometer to be 11.2 ± 0.1 eV. This leads to the $\Delta H_f^{\bullet}([C_4H_2DO_3]^+) \leq 365 \pm 10$ kJ mol^{-1} ($\Delta H_f^{\bullet}$(Z-HOOCCH=CHCOOH]) = -679.4 kJ mol^{-1} [150] and $\Delta H_f^{\bullet}$(HO˙) = 38.9 kJ mol^{-1} [149]). The deuterated m/z 99 ion (m/z 100) from maleic acid-carboxyl-d_2 had two metastable peaks at m/z 81 (HDO loss) and 72 (CO loss) in its MI mass spectrum. The CA mass spectrum of the m/z 99 ion from unlabelled maleic acid is shown in *Figure 6-4*. There was no signal in the NR mass spectrum of the m/z 99 ion.

The m/z 99 ion may well have the ring structure because its metastable loss of CO has quite a high reverse energy barrier ($T_{0.5}$ = 685 meV). An open chain structure like O=$^+$CCH=CHCOOD will be expected to have smaller barrier for its CO loss, e.g. the similar ion O=$^+$C-CH=CH_2 loses CO metastably with little barrier ($T_{0.5}$ = 2.1 meV)[151]. Hence, the metastable loss of HDO from the proposed cyclic ion possibly follows a similar mechanism to that of the molecular ion (reation 6-2). The mechanisms of the two metastable dissociation channels of this ion are shown as below:

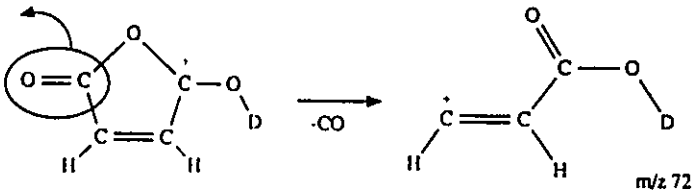

6-8

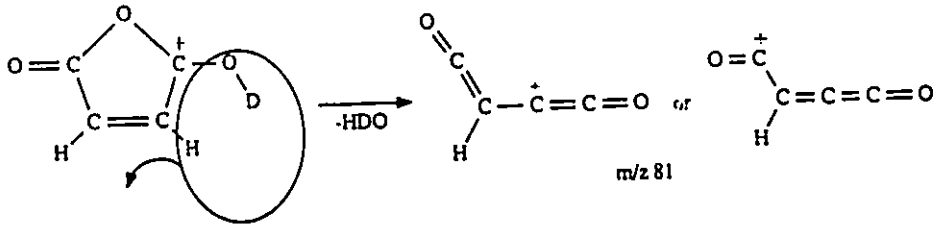

6-9

m/z 98, the M-H_2O ion

The abundance of this ion is 5% of m/z 45 (base peak) in the normal EI mass spectrum of unlabelled maleic acid. This ion can be generated from the metastable molecular ion (reactions 6-1 and 6-2). The AE of metastable reactions 6-1 and 6-2, could not be measured due to the metastable peaks being too weak. Instead, the AE of generating m/z 99 ($[C_4HDO_3]^{+\bullet}$) from reaction 6-1 and m/z 98 ($[C_4H_2O_3]^{+\bullet}$) from reaction 6-2 in the ion source were measured using

the MS-902S mass spectrometer to be 10.9 ± 0.1 eV and 10.5 ± 0.1 eV respectively. Using $\Delta H_f^{\bullet}$(Z-HOOCCH=CHCOOH) = -679.4 kJ mol^{-1} [150] and $\Delta H_f^{\bullet}(H_2O)$ = -241.6 kJ mol^{-1}, [149] $\Delta H_f^{\bullet}([C_4HDO_3]^{+\bullet})$ and $\Delta H_f^{\bullet}([C_4H_2O_3]^{+\bullet})$ were calculated to be ≤ 609 ± 10 kJ mol^{-1} and ≤ 579 ± 10 kJ mol^{-1} respectively. There were two major metastable peaks corresponding to CO and CO_2 losses and a weak metastable peak corresponding to ĊOOH loss in the MI mass spectrum of the m/z 98 ion (Table 6-4). There was also a signal corresponding to H_2O loss in the spectrum. But this signal is an interference signal because it was found to be an artifact in all three isotopomers of maleic acid. The CA mass spectrum of the m/z 98 ion from unlabelled maleic acid is shown in *Figure 6-5*. All the m/z 98 ions were too weak to give any signals in the NR mass spectra.

The structure proposed for the $[C_4HDO_3]^{+\bullet}$ ion is $[DOOCCH=C=C=O]^{+\bullet}$. The heat of formation of this ion was estimated to be 606 kJ mol^{-1} by the established method [152] by substituting -COOH on $[H_2C=C=C=O]^{+\bullet}$ using the $[H_2C=CH_2]^{+\bullet}$-$[H_2C=CHCOOH]^{+\bullet}$ pair of ions as an energy comparison standard. This value is in good agreement with the experimental value, ≤ 609 ± 10 kJ mol^{-1} (Table 6-2). The structure of $[C_4H_2O_3]^{+\bullet}$ is proposed to be the distonic ion O=C^{+}-CH=CHCOO$^{\bullet}$. But the presence of the maleic anhydride radical cation is also possible even though the metastable maleic anhydride radical cation gives only one fragment (m/z 54). Therefore the $[C_4H_2O_3]^{+\bullet}$ ions probably have these two structures and the measured heat of formation, ≤ 579 ± 10 kJ mol^{-1}, should correspond to the O=C^{+}-CH=CHCOO$^{\bullet}$ ion because the heat of formation of ionized maleic anhydride is much higher, 643.7 kJ mol^{-1} [149] (Table 6-2). The CA and NR mass spectra of the molecular ion of maleic anhydride are shown in *Figure 6-6* and *6-7* respectively. The dissociation characteristics of the maleic anhydride radical cation and its neutral counterpart can be seen by signals at m/z 54 (HĊ=CH-$^{+}$C=O), 44 ($[CO_2]^{+\bullet}$), 41

(HC⁺=C=O), 28 ([CO]⁺˙) and 26 ([HC≡CH]⁺˙) in the spectra. The metastable dissociations of $[C_4HDO_3]^{+\cdot}$, $[C_4H_2O_3]^{+\cdot}$ and the maleic anhydride radical cation are shown in Table 6-4. The mechanisms of these dissociations are proposed as below:

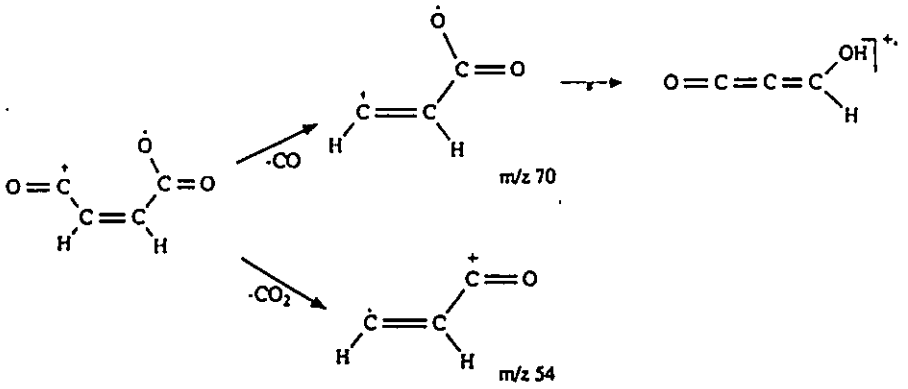

6-10

6-11

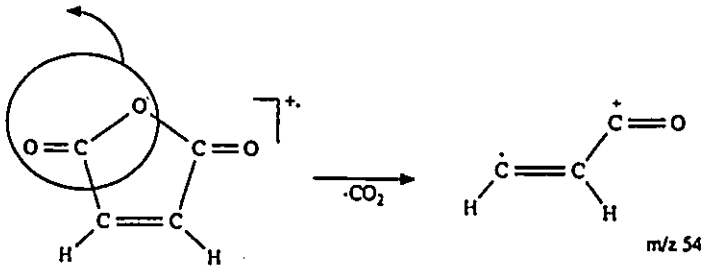

6-12

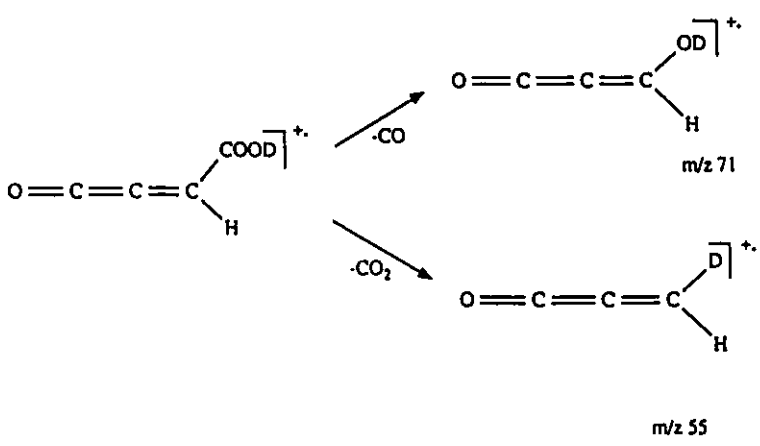

6-13

6-14

m/z 88, the M-CO ion

The abundance of this ion is 2% of m/z 45 (base peak) in the normal EI mass spectrum of unlabelled maleic acid. This ion can be generated from the metastable molecular ion (reaction 6-3 and 6-4). The AE of the $[M-CO]^{+\bullet}$ ion, $[C_3H_2D_2O_3]^{+\bullet}$, produced in the ion source from Z-DOOCCH=CHCOOD was measured using the MS-902S mass spectrometer to be 10.6 ±0.1 eV. This value leads to $\Delta H_f^{\bullet}([C_3H_2D_2O_3]^{+\bullet}) \leq 451 \pm 10$ kJ mol^{-1} ($\Delta H_f^{\bullet}$(Z-HOOCCH=CHCOOH) = - 679.4 kJ mol^{-1} [150] and $\Delta H_f^{\bullet}$(CO) = - 108.7 kJ mol^{-1}) [149]. The heat of formation of the $[M-CO]^{+\bullet}$ ion generated from metastable $[E-HOOCCH=CHCOOH]^{+\bullet}$ (fumaric acid) in the first field free region in the MS-920S mass spectrometer was obtained to be $\leq 531 \pm 10$ kJ mol^{-1}. Therefore the former $[M-CO]^{+\bullet}$ ion is 80 kJ mol^{-1} lower in energy than the latter. This indicates that the $[M-CO]^{+\bullet}$ ion from Z-DOOCCH=CHCOOD should have the proposed ring structures in reactions 6-3 and 6-4 and the $[M-CO]^{+\bullet}$ ion from E-HOOCCH=CHCOOH may well have an open chain structure, $[E-HOOCCH=CHOH]^{+\bullet}$ (see *m/z 88* in section 6.2.2). As in the molecular ion of Z-HOOCCH=CHCOOH, the ring structure has a quantitatively similar effect in stabilizing the ion (The $[Z-HOOCCH=CHCOOH]^{+\bullet}$ ion is 70 kJ mol^{-1} lower in energy than the $[E-HOOCCH=CHCOOH]^{+\bullet}$ ion).

There were three peaks, m/z 70 (H_2O loss), m/z 60 (CO loss) and m/z 42 (CO and H_2O or HCOOH loss), in the MI mass spectrum (Table 6-5) of the m/z 88 ion from unlabelled maleic acid. The intensity of the m/z 88 ion was too weak for an NR experiment. The CA mass spectrum of the m/z 88 ion was dominated by a signal at m/z 70 (*Figure 6-8*).

The mechanism of H_2O loss from the m/z 88 ion can be shown by the metastable dissociation of m/z 90 ion from maleic acid-carboxyl-d_2 (see also reactions 6-3 and 6-4):

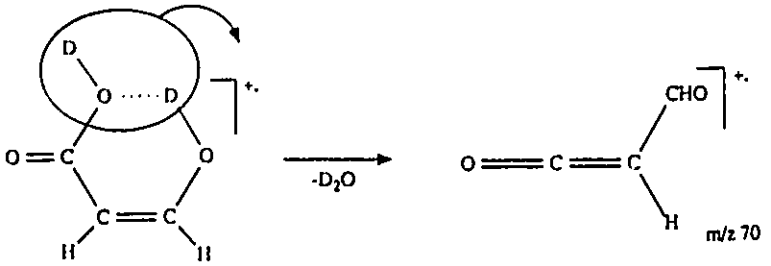

6-15

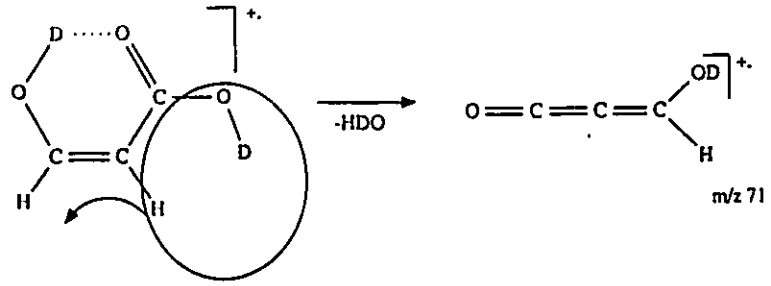

6-16

The m/z 42 ion may be generated directly from the m/z 88 ion by HCOOH loss and/or from the dissociative m/z 60 ion by H_2O loss. The m/z 60 ion was identified to be water-ketene complex $[H_2C{=}C{=}O(H_2O)]^{+\cdot}$ by its characteristic CA mass spectrum [153] (see also section ***m/z 60***). The generation of the m/z 60 ion from the m/z 88 ion may be explained by the mechanism of m/z 90 → m/z 62 from maleic acid-carboxyl-d_2:

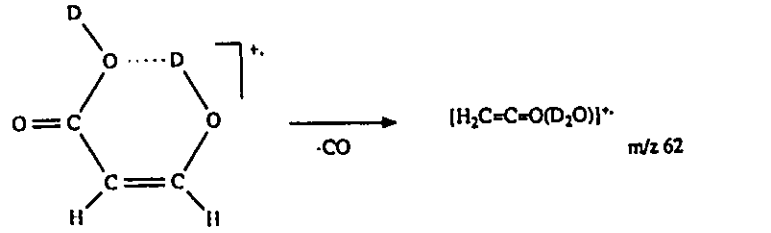

6-17

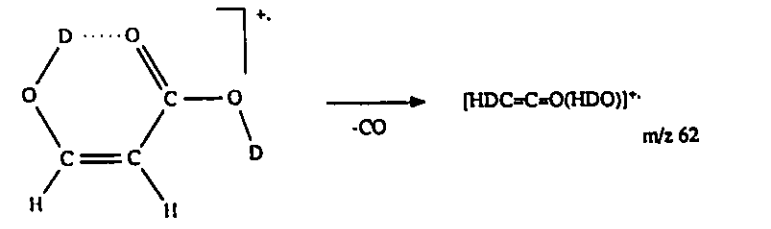

6-18

m/z 72, the M-CO_2 ion

The abundance of this ion is 73% of m/z 45 (base peak) in the normal EI mass spectrum of unlabelled maleic acid. This ion can also be generated from the metastable molecular ion (reaction 6-5 and 6-6). Four structures were considered for the m/z 72 ion.

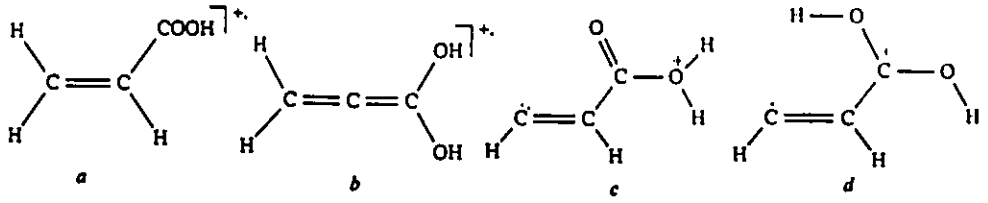

a *b* *c* *d*

The AE of the ion source reaction, m/z 116 → m/z 72 ($[C_3H_4O_2]^{+\cdot}$) from unlabelled maleic acid was measured using the MS-902S mass spectrometer to be 10.6 ± 0.1 eV. The $\Delta H_f^{\bullet}([C_3H_4O_2]^{+\cdot})$ was calculated to be ≤ 738 ± 10 kJ mol^{-1} ($\Delta H_f^{\bullet}$(Z-HOOCCH=CHCOOH) = -679.4 kJ mol^{-1} [150] and $\Delta H_f^{\bullet}(CO_2)$ = -392.9 kJ mol^{-1} [149]). In order to discuss the significance of this thermochemical result in relation to ions ***a***, ***b***, ***c*** and ***d***, it is necessary also to describe the dissociation characteristics of the m/z 72 ion. The MI, CA and NR mass spectra of the m/z 72 ion are shown in Table 6-6, *Figure 6-9* and *6-10* respectively. There were three signals at m/z 71 ($H^{\bullet}$ loss), m/z 55 ($HO^{\bullet}$ loss) and m/z 44 (CO loss) in the MI mass spectrum. The NR mass spectrum contained a recovery signal of the reionized neutral counterpart of the m/z 72 ion.

The heat of formation of ion ***a*** ($[H_2C{=}CHCOOH]^{+\cdot}$) is 698.1 kJ mol^{-1} [149]. The MI mass spectrum of ion ***a*** contained only two peaks at m/z 71 and m/z 44 (Table 6-6). The absence of the signal at m/z 55 indicates that the m/z 72 ions from maleic acid could not be <u>solely</u> ion ***a***. The possible co-generation of ion ***a*** in the m/z 72 ions is likely because of the similarities of the kinetic energy releases ($T_{0.5}$ values) and CA mass spectra between ion ***a*** and the m/z 72 ion (see

Table 6-6, *Figure 6-11 and 6-9*). Ion ***a*** gave a recovery signal of its reionized neutral counterpart in its NR mass spectrum (*Figure 6-12*).

Ion ***b*** was generated by a McLafferty rearrangement reaction from metastable ionized α-ethyl acrylic acid, $[H_2C=(C_2H_5)COOH]^{+\bullet}$:

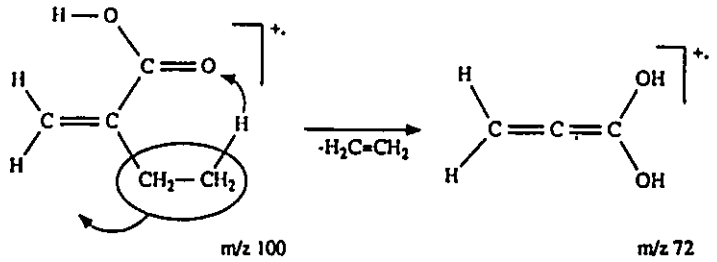

6-19

Unfortunately 16% of these m/z 72 ions were found to be $[C_4H_8O]^{+\bullet}$ (also m/z 72) which was generated by CO loss from the molecular ion (m/z 100). The fragments of the $[C_4H_8O]^{+\bullet}$ appeared in the MI and CA mass spectra of the $[C_3H_4O_2]^{+\bullet}$ ion (Table 6-6 and *Figure 6-13*). The heat of formation of ion ***b*** <u>metastably</u> generated from the above reaction in the first field free region in the MS-902S mass spectrometer was measured to be ≤ 606 ± 10 kJ mol^{-1} ($H_2C=C(C_2H_5)COOH \rightarrow b + H_2C=CH_2$, metastable peak AE = 10.9 ± 0.1 eV, $\Delta H_f^{\bullet}(H_2C=C(C_2H_5)COOH)$ = - 388.7 kJ mol^{-1} [149] and $\Delta H_f^{\bullet}(H_2C=CH_2)$ = - 58.5 kJ mol^{-1} [149]). This value was in fair agreement with the value of 623 kJ mol^{-1} estimated by the established method [152] by substituting -OH on $[H_2C=C=CH_2]^{+\bullet}$ using $[H_2C=CH_2]^{+\bullet}$-$[H_2C=CHOH]^{+\bullet}$-$[H_2C=C(OH)_2]^{+\bullet}$ ions as standards for comparison. However the significant differences between ion ***b*** and the m/z 72 ion from unlabelled maleic acid in their heats of formation and kinetic energy releases ($T_{0.5}$ values) indicates that ion ***b*** cannot be the structure of the m/z 72 ion.

The heats of formation of ions ***c*** and ***d*** could be estimated as following: the AE of reaction $H_2C=CHCOOC_2H_5 \rightarrow [C_3H_5O_2]^+ + H_2C=\dot{C}H$ was measured by the electron energy selector

mass spectrometer to be 11.18 ± 0.05 eV. The $[C_3H_5O_2]^+$ ion was considered to be $H_2C{=}CH^+C(OH)_2$ based on the mechanism established by Harrison et al[154]. The MI mass spectrum of this ion contained only one intense signal at m/z 55 (H_2O loss) and confirmed that this ion had the above structure. The AE leads to $\Delta H_f^\bullet(H_2C{=}CH^+C(OH)_2) \leq 437 \pm 5$ kJ mol^{-1} ($\Delta H_f^\bullet(H_2C{=}CHCOOC_2H_5) = -377$ kJ mol^{-1} and $\Delta H_f^\bullet(H_2C{=}\dot{C}H) = 264$ kJ mol^{-1}). [149] Adding Δ_1 = 46 kJ mol^{-1} ($\Delta_1 = \Delta H_f^\bullet(H_2C{=}^+CH) - \Delta H_f^\bullet([H_2C{=}CH_2]^{+\bullet}) = 1112 - 1066 = 46$ kJ mol^{-1} [149]) to 437 ± 5 kJ mol^{-1}, the heat of formation of ion ***d*** is obtained to be ≤ 483 ± 5 kJ mol^{-1}. Adding Δ_2 = 111 kJ mol^{-1} ($\Delta_2 = \Delta H_f^\bullet(H_3CCOO^+H_2) - \Delta H_f^\bullet(H_3CC^+(OH)_2) = 426 - 315 = 111$ kJ mol^{-1} [154]) to this value, 483 kJ mol^{-1}, the heat of formation of ion ***c*** is obtained to be ≤ 594 ± 5 kJ mol^{-1}. Even though these heats of formation of ions ***c*** and ***d*** are quite different from the measured heat of formation of the m/z 72 ion, ions ***c*** and ***d*** are considered to be the main structures of the m/z 72 ion. The reasons for this are: (1) The measured heat of formation is only the upper limit; (2) It is possible that energy rich or excited ions of ions ***c*** and ***d*** are generated, since the kinetic energy release for reactions 6-5 and 6-6 is significant ($T_{0.5}$ = 88 meV). The structure of the $[72\text{-}H]^+$ ion is proposed to be $[HC{=}CHCOOH]^+$. And structures, $H_2C{=}CH\text{-}^+C{=}O$ and $[H_2C{=}CHOH]^{+\bullet}$ are proposed for the $[72\text{-}HO^\bullet]^+$ and $[72\text{-}CO]^{+\bullet}$ ions respectively. Deuterium mixing in ions ***c*** and ***d*** should lead to the separation of H$^\bullet$ and D$^\bullet$ losses as well as HO$^\bullet$ and DO$^\bullet$ losses from the m/z 74 ion from maleic acid-carboxyl-d_2 and maleic acid-2,3-d_2. The reaction sequence for the metastable dissociations of ions ***c*** and ***d*** are shown as below:

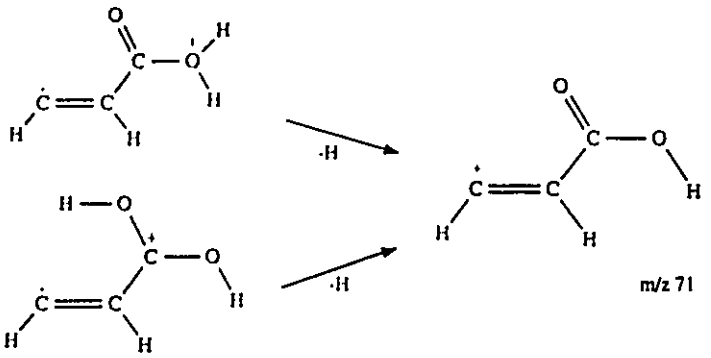

6-20

6-21

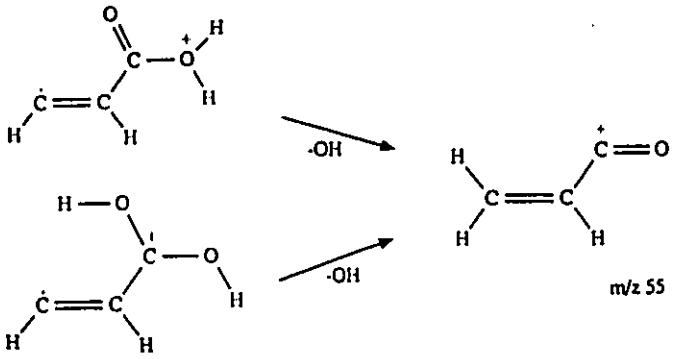

6-22

6-23

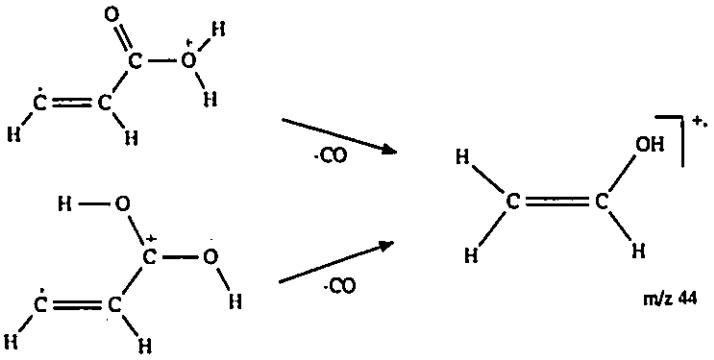

6-24

6-25

In the following, some important secondary fragment ions, which are ions generated from the molecular ion by two steps, will be discussed. Because more than one step is needed to

produce these ions from the molecular ion, the AE measurements of the reactions to generate these ions may be less reliable. Therefore, no thermochemical data were measured for these ions.

m/z 70

The abundance of this ion is 3% of m/z 45 (base peak) in the normal EI mass spectrum of unlabelled maleic acid. The isotopomers of this ion can be generated from maleic acid-carboxyl-d_2 metastably from the m/z 98 and m/z 99 ions (reactions 6-10 and 6-13) and the m/z 90 ion (reactions 6-15 and 6-16).

Fortunately, the dissociation characteristics of the ion allowed structures to be assigned to the m/z 70 ion. There was only one peak at m/z 69 ($T_{0.5}$ = 17 meV) in the MI mass spectrum of the m/z 70 ion from unlabelled maleic acid. However, the m/z 71 ion generated from the metastable m/z 72 ion in the first field free region in the ZAB-2F mass spectrometer whose appearant $(m/z)^*$ is $71^2/72 = 70.01$ and whose translational energy is 8000 x 71/72 = 7889 eV will be also selected by the magnetic analyzer at m/z 70 and appear at m/z 69 in the MI mass spectrum of the m/z 70 ion (The translational energy of the m/z 69 fragment ion is 8000 x 69/70 = 7886 eV). If the magnetic analyzer and the electrostatic analyzer are both used to select an ion, the ion will be selected by both its momentum and translational energy so that the above interference can be avoided. An MI experiment was done by using the third field free region in the ZAB-2F mass spectrometer (see section 3.4.2) and this confirmed that there was a peak at m/z 69. The CA mass spectrum of the m/z 70 ion (*Figure 6-14*) was also obtained by using the collision cell in the third field free region. There was no signal in the NR mass spectrum of the

m/z 70 ion.

Three structures were considered for the m/z 70 ions.

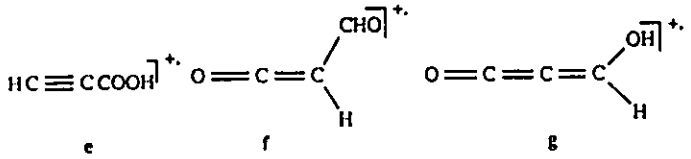

Ion *e* was easily ruled out because it had three peaks at m/z 69, 53 and 42 in its MI mass spectrum and a relatively high heat of formation, $\Delta H_f^{\bullet}([e]^{+\bullet})$ = 891 kJ mol^{-1} [149] (Table 6-2).

Ions *f* and *g* are the structures proposed for the m/z 70 ions. The heats of formation of ions *f* and *g* were both estimated to be 677 kJ mol^{-1} by the established method [152]. For ion *f*, -CHO was substituted in $[H_2C{=}C{=}O]^{+\bullet}$ using the $[H_2C{=}CH_2]^{+\bullet}$-$[H_2C{=}CHCHO]^{+\bullet}$ pair of ions as standard for comparison. For ion *g*, -OH was substituted in $[H_2C{=}C{=}C{=}O]^{+\bullet}$ using the $[H_2C{=}CH_2]^{+\bullet}$-$[H_2C{=}CHOH]^{+\bullet}$-$[H_2C{=}C(OH)_2]^{+\bullet}$ ions as standards for comparison. Both ions *f* and *g* may lose $^{\bullet}$H metastably to give O=C=CH-$^{+}$C=O ion (m/z 69). A mixture of ions *f* and *g* may give the above CA mass spectrum. The peaks at m/z 29 ($^{+}$CHO) and m/z 41 ($HC^{+}{=}C{=}O$) may arise from ion *f*. The peak at m/z 53 ($HC^{+}{=}C{=}C{=}O$) may arise from ion *g*. Both ions *f* and *g* may yield peaks at m/z 42 ($[H_2C{=}C{=}O]^{+\bullet}$) and 28 ($[CO]^{+\bullet}$).

m/z 69

The abundance of this ion is 3% of m/z 45 (base peak) in the normal EI mass spectrum of unlabelled maleic acid. This ion can be generated from the metastable m/z 70 ion. This ion lost only CO metastably to give $HC^{+}{=}C{=}O$ at m/z 41, possibly with a small reverse energy

barrier ($T_{0.5}$ = 38 meV). This metastable peak also dominated the CA mass spectrum of the m/z 69 ion (*Figure 6-15*). There was no signal in the NR mass spectrum of the m/z 69 ion.

The structure proposed for this ion is O=C=CH-$^{+}$C=O. Its heat of formation was estimated to be 510 kJ mol^{-1} by the established method [152] by substituting CO in $[H_2C{=}C{=}O]^{+\bullet}$ using the $[H_2C{=}CH_2]^{+\bullet}$-$[H_2C{=}C{-}C{=}O]$ pair of ions as standard for comparison.

m/z 60

The intensity of this ion is very weak, 0.5% of m/z 45 (base peak) in the normal EI mass spectrum of unlabelled maleic acid. This ion can be generated from the metastable m/z 88 ion (reactions 6-17 and 6-18) and was identified to be the water-ketene complex, $[H_2C{=}C{=}O(H_2O)]^{+\bullet}$ whose heat of formation was 579 ± 5 kJ mol^{-1} [153]. The H_2O loss from the metastable $[H_2C{=}C{=}O(H_2O)]^{+\bullet}$ ion was found to be a threshold process ($T_{0.5}$ = 0.2 meV). The MI mass spectrum of the m/z 60 ion also contained a peak corresponding to H_2O loss. Unfortunately the m/z 60 ion was too weak for a metastable peak shape study and no $T_{0.5}$ value was measured for this metastable peak. However, the CA mass spectrum of the m/z 60 ion (*Figure 6-16*) is similar to that of the $[H_2C{=}C{=}O(H_2O)]^{+\bullet}$ ion and allows the identification of the m/z 60 ion. There was no signal in the NR mass spectrum of the m/z 60 ion.

6.2.2 Fumaric Acid

The normal EI mass spectrum of fumaric acid (*Figure 6-17a*) and fumaric acid-2,3-d_2

(*Figure 6-17b*) which were introduced to the ion source of the ZAB-2F mass spectrometer by the direct probe inlet system, are closely similar to those of the previous result [147] obtained by both direct and indirect inlet systems. The temperature effect on the normal EI mass spectrum of unlabelled fumaric acid has been studied. In agreement with the previous work [147], no evidence of thermal degradation was found. The relative abundances of major fragment ions at m/z 99 ($[M\text{-}OH]^+$), 98 ($[M\text{-}H_2O]^{+\cdot}$), 88 ($[M\text{-}CO]^{+\cdot}$), 81 ($[M\text{-}H_2O\text{-}HO^{\cdot}]^+$), 72 ($[M\text{-}CO_2]^{+\cdot}$) and 45 ($[COOH]^+$) changed only slightly over a range of probe heater temperatures from 170 to 300 °C. In the normal EI mass spectrum of fumaric acid the molecular ion is seen to be more stable than that of maleic acid, although it has a higher heat of formation (see Table 6-2). Only two major fragment ions at m/z 98 and 88 can be generated from the metastable molecular ion. However, most of these fragment ions showed dissociation characteristics similar to those from maleic acid. Indeed, most of the fragment ions were found to have the same structures as those from maleic acid. In the following, this result is presented in detail. The ions being discussed are identified by their m/z values corresponding to unlabelled fumaric acid and represent the ions from all the three isotopomers of fumaric acid.

m/z 116, the molecular ion

As mentioned above, the molecular ion is quite intense, 54% of m/z 98 (base peak), in the normal EI mass spectrum of unlabelled fumaric acid. The IE of fumaric acid was measured using the MS-902S mass spectrometer to be 10.6 ± 0.1 eV, in good agreement with the literature value 10.7 eV [150]. The heat of formation of the molecular ion was reported to be 355 kJ mol^{-1} (Table 6-2).

The molecular ion had only two metastable dissociation channels, $[M-H_2O]^{+\bullet}$ and $[M-CO]^{+\bullet}$ (Table 6-3). The MI and CA mass spectra of the molecular ion of unlabelled fumaric acid did not change significantly over a range of probe heater temperature form 170 to 300 °C. This observation confirms that no thermal degradation takes place in the ion source. The CA mass spectrum of the molecular ion is shown in *Figure 6-18*. The low mass region of the spectrum is similar to that of the molecular ion of maleic acid (*Figure 6-2*). The NR mass spectrum (*Figure 6-19*) of the molecular ion of fumaric acid-carboxyl-d_2 contained a weak recovery signal for the reionized neutral counterpart of the molecular ion. The spectrum is very similar to the normal EI mass spectrum (*Figure 6-17c*) except for the absence of the $[M-CO]^{+\bullet}$ signal. The reasons for this may be: (i) if the neutral counterpart of the molecular ion loses CO, then the $[M-CO]^{+\bullet}$ signal will be absent because the reionized neutral counterpart of the $[M-CO]^{+\bullet}$ gives a very weak recovery signal in its NR mass spectrum (see ***m/z 88, the M-CO ion***); (ii) if the reacting configuration of the molecular ion, which leads to the generation of the $[M-CO]^{+\bullet}$ ion, does not have a stable neutral counterpart, which probably has different geometry from that leads to the recovery signal, then the $[M-CO]^{+\bullet}$ signal will not be present; (iii) if the reionized neutral counterpart of the molecular ion is energy rich, then its dissociations to $[M-H_2O]^{+\bullet}$ and $[M-OH]^{+\bullet}$ may be a lot faster than to $[M-CO]^{+\bullet}$ whose generation involves the parent ions' rearrangement (transfer of an -OH group) so that the product of the slow reaction ($M^{+\bullet}$-CO) will not be observed.

The molecular ion is considered to have the same geometry as the neutral fumaric acid, i.e. an open chain structure. It may also lose CO metastably to generate $[E\text{-}HOCH{=}CHCOOH]^{+\bullet}$. The observation of H_2O and HDO losses from the molecular ion of fumaric acid-2,3-d_2 as well

as D_2O and HDO losses from the molecular ion of fumaric acid-carboxyl-d_2 indicates that rearrangement should be involved in the loss of water from the molecular ion. The proposed mechanisms of the metastable dissociations of the metastable molecular ion of fumaric acid-carboxyl-d_2 are shown as below:

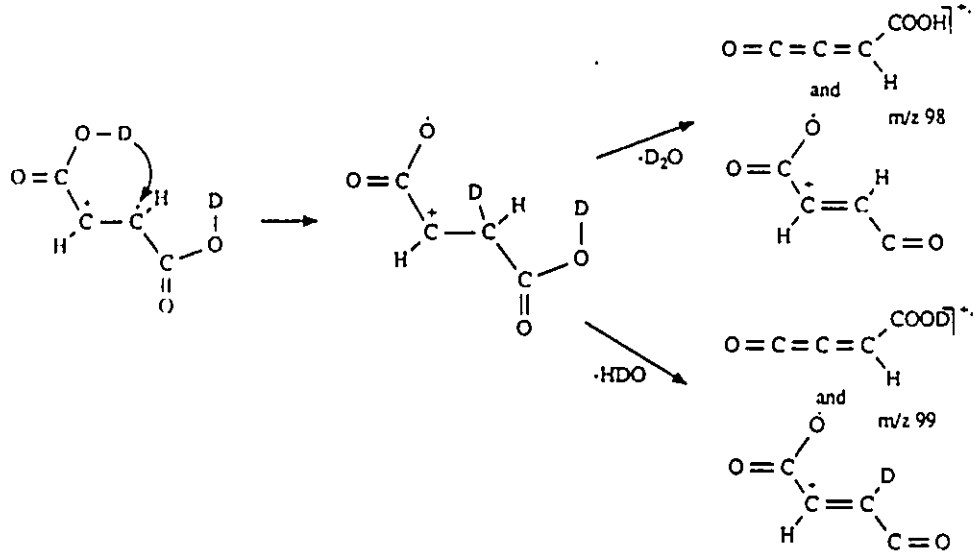

6-26

6-27

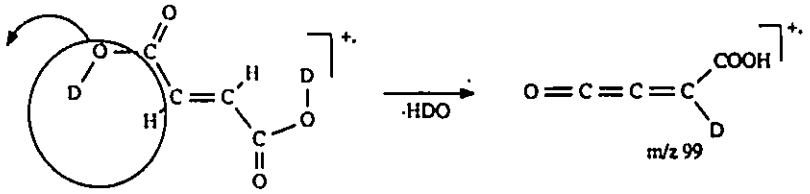

6-28

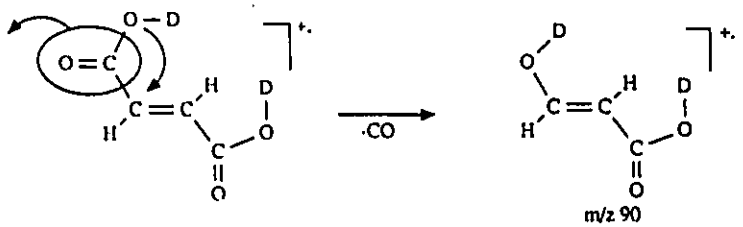

6-29

m/z 99, the M-OH ion

The abundance of this ion is 49% of m/z 98 (base peak) in the normal EI mass spectrum of unlabelled fumaric acid. The generation of this ion is also from a direct bond cleavage reaction in the ion source:

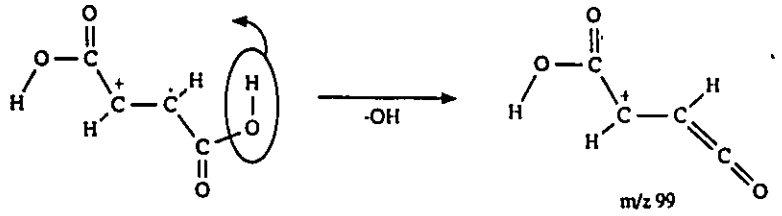

6-30

The AE of the source reaction of HO$^{\bullet}$ loss from fumaric acid-2,3-d_2 was measured using the MS-902S mass spectrometer to be 11.5 ± 0.1 eV. This leads to $\Delta H_f^{\bullet}([C_4HD_2O_3]^+) \leq 397 \pm 10$ kJ mol^{-1} ($\Delta H_f^{\bullet}$(E-HOOCCH=CHCOOH) = - 675.8 kJ mol^{-1} [150] and $\Delta H_f^{\bullet}$(HO$^{\bullet}$) = 38.9 kJ mol^{-1} [149]). The m/z 99 ion also lost H_2O and CO metastably as did that of maleic acid. The CA mass spectrum of the m/z 99 ion from unlabelled fumaric acid and the NR mass spectrum of the deuterated m/z 99 ion (m/z 100) from fumaric acid-carboxyl-d_2 are shown in *Figure 6-20* and *6-21* respectively. The CA mass spectrum is similar to that of the m/z 99 ion from maleic acid. The recovery signal of the m/z 99 ion is the base peak in the NR mass spectrum.

The m/z 99 ion is not likely to have the ring structure as that of the m/z 99 ion from maleic acid even though its CA mass spectrum and $T_{0.5}$ values of its metastable peaks are similar to the latter. This is because this m/z 99 ion has higher heat of formation than the m/z 99 ion from maleic acid (397 vs 365 kJ mol^{-1}). The proposed structure of this m/z 99 ion and the mechanisms of its two dissociation channels are shown as below:

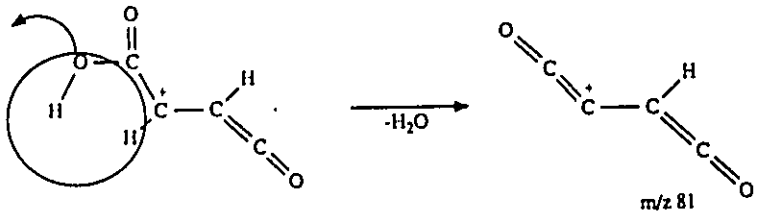

6-31

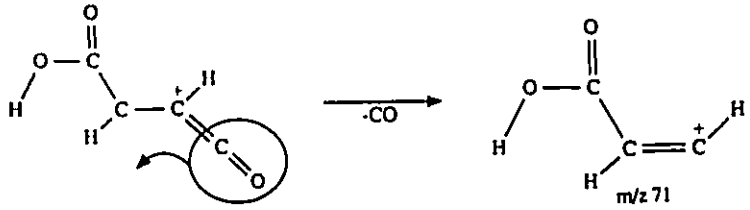

6-32

m/z 98, the M-H_2O ion

This ion is the base peak in the normal EI mass spectrum of unlabelled fumaric acid. It can be generated from the metastable molecular ion. The AE of the ion source reactions of the molecular ion of fumaric acid-2,3-d_2 losing H_2O and HDO were measured using the MS-902S mass spectrometer to be 11.3 ± 0.1 and 10.9 ± 0.1 eV respectively. The AE of the m/z 98 ion generated from the metastable molecular ion of unlabelled fumaric acid in the first field free region in the MS-902S mass spectrometer was measured to be 11.3 ± 0.1 eV. Surprisingly the AE for the source reaction is lower than that for the first field free region metastable reaction. This may be because the collisional induced dissociation process taking place in the ion source lowered the AE of the reactions. (See the CA mass spectrum of the molecular ion, *Figure 6-18*. Note that the cross-section for collisional induced dissociation of the m/z 98 ion generated from

the molecular ion is substantial). Using $\Delta H_f^{\bullet}$(E-HOOCCH=CHCOOH) = - 675.8 kJ mol^{-1} [150] and $\Delta H_f^{\bullet}(H_2O)$ = - 241.6 kJ mol^{-1} [149], the upper limits of $\Delta H_f^{\bullet}([C_4H_2O_3]^{+\bullet})$ and $\Delta H_f^{\bullet}([C_4HDO_3]^{+\bullet})$ were calculated to be ~ 655 ± 10 and ~ 616 ± 10 kJ mol^{-1} respectively (Table 6-2). The m/z 98 ion had three metastable peaks at m/z 70 (CO loss), 54 (CO_2 loss) and 53 (HOOĊ loss) in its MI mass spectrum (Table 6-4). These metastable signals were confirmed by the appearance of the appropriate reionized neutral signals in the CIDI mass spectrum of the m/z 98 ion. The metastable peak for H_2O loss in the MI mass spectrum was also found to be artifact. The CA mass spectrum of the m/z 98 ion from unlabelled fumaric acid is shown in *Figure 6-22*. The NR mass spectra of the deuterated m/z 98 ions, $[C_4H_2O_3]^{+\bullet}$ and $[C_4HDO_3]^{+\bullet}$, from fumaric acid-carboxyl-d_2 are shown in *Figure 6-23* and *6-24* respectively. The two spectra are very similar and contain intense recovery signals of the reionized neutral counterparts of these ions.

As with the m/z 98 ion of maleic acid, two structures, $[HOOCCH=C=C=O]^{+\bullet}$, and the distonic ion, $O=C^{+}\text{-}CH=CH\text{-}COO^{\bullet}$, are proposed for the m/z 98 ions. The existence of maleic anhydride radical cation can be ruled out because the significant differences between the m/z 98 ion from fumaric acid and the molecular ion of maleic anhydride in both their CA and NR mass spectra (compare *Figure 6-22* to *6-24* with *Figure 6-6* and *6-7*). The measured heats of formation of these m/z 98 ions are higher than that of the m/z 98 ion from maleic acid. This indicates that the m/z 98 ions are energy rich. As a result, the metastable loss of HOOĊ from this energised $[HOOCCH=C=C=O]^{+\bullet}$ ion is more intense than the $[HOOCCH=C=C=O]^{+\bullet}$ ion from maleic acid (see Table 6-4). The mechanisms of the metastable dissociation reactions of the above two species are shown in reactions 6-10 to 6-14 (see ***m/z 98, the M-H_2O ion*** in 6.2.1 Maleic Acid). The mechanism of the HOOĊ loss from $[HOOCCH=C=C=O]^{+\bullet}$ ion is shown as below:

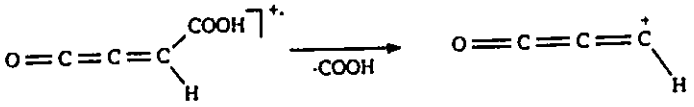

6-33

m/z 88, the M-CO ion

The abundance of this ion is 33% of m/z 98 (base peak) in the normal mass spectrum of unlabelled fumaric acid. This ion can be generated from the meastable molecular ion (reaction 6-29). The AE of this metastable reaction in the first field free region in the MS-902S mass spectrometer was measured to be 11.4 ± 0.1 eV. This leads to the heat of formation of the m/z 88 ion, $\Delta H_f^{\bullet}([C_3H_4O_3]^{+\bullet})$, to be ≤ 531 ± 10 kJ mol^{-1} ($\Delta H_f^{\bullet}$(E-HOOCCH=CHCOOH) = - 675.8 kJ mol^{-1} [150] and $\Delta H_f^{\bullet}$(CO) = - 108.7 kJ mol^{-1} [149]). As did the m/z 88 ion from maleic acid, this m/z 88 ion gave three metastable peaks at m/z 70 (H_2O loss), m/z 60 (CO loss) and m/z 42 (CO and H_2O or HCOOH loss) in the MI mass spectrum (Table 6-5). The $T_{0.5}$ values of these metastable peaks from both m/z 88 ions are very close but the relative abundances are quite different (see Table 6-5). Also the CA mass spectrum (*Figure 6-25*) of this m/z 88 ion is similar to that of the m/z 88 ion from maleic acid. The NR mass spectrum of the deuterated m/z 88 ion (m/z 90) from fumaric acid-carboxyl-d_2 is shown in *Figure 6-26*. The spectrum contained a weak recovery signal for the reionized neutral counterpart of the m/z 88 ion.

As mentioned above, the structure proposed for the m/z 88 ion is [E-HOCH=CHCOOH]$^{+\bullet}$. $\Delta H_f^{\bullet}$([E-HOCH=CHCOOH]$^{+\bullet}$) was estimated to be 493 kJ mol^{-1} (see Table 6-2) by the established method [152] by substituting -OH on [H_2C=CHCOOH]$^{+\bullet}$ using [H_2C=CH_2]$^{+\bullet}$-[H_2C=CHOH]$^{+\bullet}$-[H_2C=$C(OH)_2$]$^{+\bullet}$ ions as standards for comparison. This value is 38 kJ mol^{-1} lower than the

experimental value, 531 ± 10 kJ mol^{-1}. However, the generation of energy rich m/z 88 ions is possible because the $T_{0.5}$ value of the metastable dissociation of the molecular ion to the m/z 88 ion is quite large (162 meV). The m/z 42 ion may be generated directly from the m/z 88 ion by HCOOH loss and/or from the dissociative m/z 60 ion by H_2O loss. The m/z 60 ion was identified to be also the the water-ketene complex, $[H_2C{=}C{=}O(H_2O)]^{+\cdot}$ (see section ***m/z 60***). The mechanisms of the metastable dissociations of the m/z 88 ion can be shown by its isotopomer (m/z 90) from fumaric acid-carboxyl-d_2:

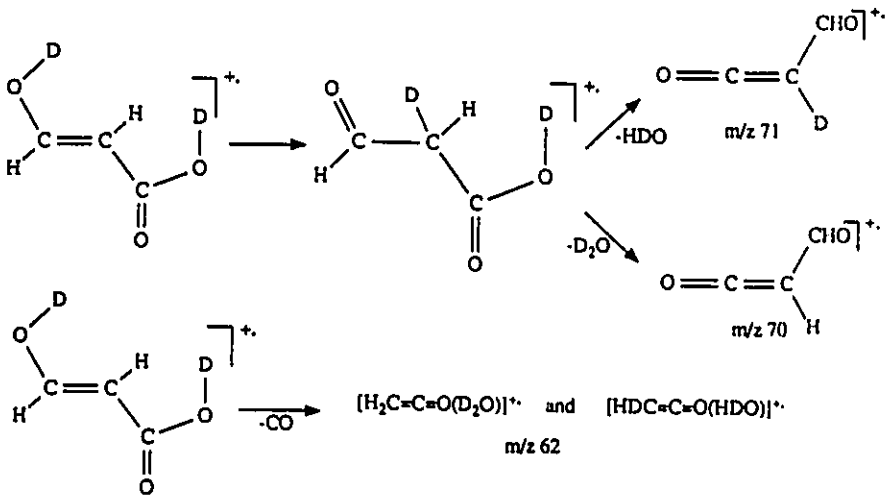

6-34

6-35

6-36

m/z 72, the M-CO_2 ion

The abundance of this ion is 23% of m/z 98 (base peak) in the normal EI mass spectrum of unlabelled fumaric acid. Different from the m/z 72 ion from maleic acid, this ion cannot be

generated from the metastable molecular ion. The AE of the ion source generated deuterated m/z 72 ion (m/z 74, $[C_3H_2D_2O_2]^{+\bullet}$) from fumaric acid-2,3-$d_2$ was measured using the MS-902S mass spectrometer to be 10.2 ± 0.1 eV. This leads to $\Delta H_f^\bullet([C_3H_2D_2O_2]^{+\bullet}) \leq 700 \pm 10$ kJ mol^{-1} ($\Delta H_f^\bullet$(E-HOOCCH=CHCOOH) = - 675.8 kJ mol^{-1} [150] and $\Delta H_f^\bullet(CO_2)$ = - 392.9 kJ mol^{-1} [149]). The MI mass spectrum including relative abundances and $T_{0.5}$ values of the metastable peaks (Table 6-6), CA and NR mass spectra (*Figure 6-27* and *6-28*) are closely similar to those of the m/z 72 ion from maleic acid. Therefore, this ion should have the same structure, i.e. ions ***a***, ***c*** and ***d***, as the m/z 72 ion from maleic acid (see section ***m/z 72, the M-CO$_2$ ion*** in 6.2.1 Maleic Acid). The reaction sequence from metastable dissociations of these ions are shown in reactions 6-20 to 6-25.

In the following, secondary fragment ions, m/z 82, 81, 70, 69 and 60, will be discussed. As with the secondary fragment ions from maleic acid, no thermochemical data were measured for these ions.

m/z 82

The abundance of this ion is 6% of m/z 98 (base peak) in the normal EI mass spectrum of unlabelled fumaric acid. This ion can be generated by consecutive losses of two HO$^\bullet$ from the molecular ion in the ion source:

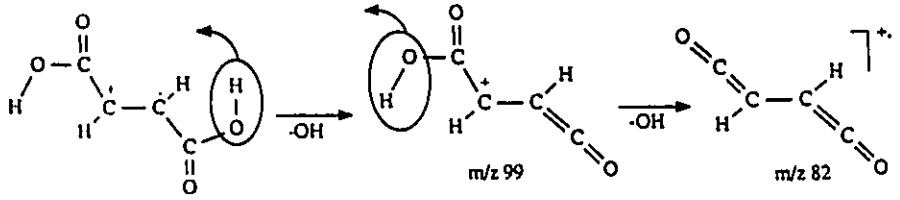

6-37

It loses CO metastably to yield m/z 54 ($[H_2C=C=C=O]^{+\bullet}$ or $O=C^{+}\text{-}CH=^{\bullet}CH$) with a small reverse energy barrier ($T_{0.5}$ = 19 meV). This ion can be characterized by its CA and NR mass spectra (*Figure 6-29* and *6-30*). A strong recovery signal of the reionized neutral counterpart of the m/z 82 ion presented in the NR mass spectrum. The proposed structure for this ion is shown in reaction 6-36. The dissociation characteristics of this ion are signals at m/z 54 ($[H_2C=C=C=O]^{+\bullet}$), 41 ($HC^{+}=C=O$), 38 ($[C_3H_2]^{+\bullet}$), 28 ($[CO]^{+\bullet}$) and 26 ($[HC\equiv CH]^{+\bullet}$) in its CA and NR mass spectra.

m/z 81

The abundance of this ion is 20% of m/z 98 (base peak) in the normal EI mass spectrum of unlabelled fumaric acid. This ion can be generated from the metastable m/z 99 ion (reaction 6-31). It had only one metastable dissociation channel, namely CO loss with a large reverse energy barrier ($T_{0.5}$ = 274 meV). The dissociation characteristics of this ion can be seen in its CA and NR mass spectra (*Figure 6-31* and *6-32*). A recovery signal of the reionized neutral counterpart of this ion also appeared in the NR mass spectrum. The structure proposed for this ion is $O=C=C^{+}\text{-}CH=C=O$, an isomer of the protonated butatrienedione ($[O=C=C=C=C=O + H]^{+}$). Signals at m/z 53 ($HC^{+}=C=C=O$), 41 ($HC^{+}=C=O$), 40 ($[C=C=O]^{+\bullet}$), 37 ($[HC=C=C]^{+}$), 28 ($[CO]^{+\bullet}$ and 25 ($HC\equiv C^{+}$) in the CA and NR mass spectra are the dissociation characteristics of the m/z 81 ion.

m/z 70 and m/z 69

The abundances of the m/z 70 and 69 ions are 12% and 6% respectively in the normal EI mass spectrum of unlabelled fumaric acid. The m/z 70 ion can be generated from the

metastable m/z 98 and 88 ions (reactions 6-10, 6-13, 6-34 and 6-35) and it loses H$^{\bullet}$ metastably to yield the m/z 69 ion. Same structures are proposed to these ions as those of the m/z 70 and 69 ions from maleic acid (see sections ***m/z 70*** and ***m/z 69*** in 6.2.1 Maleic Acid). This is based on the similarities in the MI and CA mass spectra for the ions generated from fumaric acid and maleic acid. Table 6-7 shows the comparison of the MI mass spectra of these ions. The CA mass spectra of the m/z 70 and 69 ion are shown in *Figure 6-33* and *6-34* respectively. These ions gave recovery signals of their neutral counterparts in their NR mass spectra (*Figure 6-35* and *6-36*).

m/z 60

The abundance of this ion is 2% of m/z 98 (base peak) in the normal EI mass spectrum of unlabelled fumaric acid. As the m/z 60 ion from maleic acid, this ion can be generated from the metastable m/z 88 ion (reaction 6-36) and was identified to be the water-ketene complex, $[H_2C{=}C{=}O(H_2O)]^{+\bullet}$ [153]. The H_2O loss from the metastable m/z 60 ion was also found to be a threshold process ($T_{0.5}$ = 0.8 meV). The CA mass spectrum of this m/z 60 ion (*Figure 6- 37*) is very close to that of the $[H_2C{=}C{=}O(H_2O)]^{+\bullet}$ ion. Not so surprisingly, the deuterated m/z 60 ion (m/z 62) from fumaric acid-carboxyl-d_2 gave a weak recovery signal of its reionized neutral counterpart in its NR mass spectrum (*Figure 6-38*) as did the $[H_2C{=}C{=}O(H_2O)]^{+\bullet}$ ion generated from dihydroxyacetone [153] (see *Figure 6-39*). However, the recovery signal was weak and the NR mass spectrum was dominated by signals at m/z 42 ($[H_2C{=}C{=}O]^{+\bullet}$) and 43 ($[HDC{=}C{=}O]^{+\bullet}$).

6.3 Conclusions

Tandem mass spectrometry was used to identify molecular ions and major fragment ions of maleic and fumaric acids. The different unimolecular dissociations of the two molecular ions were in agreement with the previous study [147]. A ring structure with intramolecular hydrogen bonding between the two carboxyl groups was proposed for the molecular ion of maleic acid. This ring structure was retained in some of the major fragment ions from maleic acid. On the other hand, the molecular ion of fumaric acid has an open chain structure. Unlike other Z,E-isomers, these two molecular ions do not intercovert in the gas phase. Most of the major fragment ions were assigned structures of substituted ketene or methylene ketene for both maleic and fumaric acids. These ions were formed by consecutive losses of H_2O of CO from the molecular ions. Isotopic labelling experiments showed that H_2O losses from the molecular ions and related fragment ions involved different processes but no hydrogen scrambling was found. The same structures were proposed for the fragment ions at m/z 98, 70, 69 and 60 from both maleic and fumaric acids.

Neutralization-reionization mass spectrometry (NRMS) was used to identify the neutral counterparts of the molecular ions and major fragment ions. All the discussed ions from fumaric acid were found to have stable neutral counterparts in the gas phase. Their NR mass spectra are more suitable for identifying them than their CA mass spectra. But in maleic acid, the molecular ion gave only fragmention signals and the m/z 72 ion gave both recovery and fragment signals in their NR mass spectra. The weak intensities and/or the unstable neutral counterparts may be the reason(s) for this observation.

The dissociation characteristics of the ions having m/z values higher than 60 were not reported in any references, therefore the assignment of the structures was based on the result of thermodynamic experiments and dissociation characteristics. The proposed structures may be confirmed by generation of the corresponding structures from other proper precursors and by high level theoretical calculations.

6.4 Experimental

Appearance energy (AE) and ionization energy (IE) measurements were performed with the MS-902S mass spectrometer and the electon energy selector mass spectrometer. The measurements were discribed in section 3.5. Dissociation characteristic experiments were performed with the ZAB-2F mass spectrometer. Detailed discription of the experiments including metastable ion (MI), collision activation (CA) and neutralization-reionization (NR) experiments can be found in section 3.5.

All compounds except fumaric acid-2,3-d_2, fumaric acid-carboxyl-d_2, maleic acid-carboxyl-d_2 and α-ethyl acrylic acid were commercially available and showed no detectable impurities. Fumaric acid-2,3-d_2 was prepared by the method of Atkinson et al.[155] The carboxyl-d_2 labelled acids were prepared by exchanging the carboxyl hydrogens with deuterium in D_2O. α-ethyl acrylic acid was prepared by oxidation of α-ethyl acrolein by the method of Campaigne and LeSuer.[156]

Table 6-1 Thermodynamic data of gaseous Z,E-3-hexene, Z,E-2-butenoic acid, o,m,p-benzenedicarboxylic acid and Z,E-2-buten-dicarboxylic acid (maleic and fumaric acid). All data are taken from ref. 149 unless otherwise stated.

molecule	IE (eV)	$\Delta H_f^\bullet$ neutral (kJ mol^{-1})	$\Delta H_f^\bullet$ ion (kJ mol^{-1})
Z-3-hexene	8.95	-46.8	815.1
E-3-hexene	8.96	-50.6	813.0
Z-2-butenoic acid	10.08	-346.9	627.0
E-2-butenoic acid	9.9	-351.1	606.1
m-benzene dicarboxylic acid	9.98	-696	267
p-benzene dicarboxylic acid	9.86	-718	233
o-benzene dicarboxylic acid	9.5 ± 0.1 [a]	-675 [b]	240 ± 10 [a]
maleic acid	10.0 ± 0.1 [a]	-679.4 [c]	285 ± 10 [a]
fumaric acid	10.7 10.6 ± 0.1 [a]	-675.8 [c]	355

a. This work.

b. Estimated by adding the heat of sublimation of m-benzene dicarboxylic acid to the heat of formation of solid state o-benzene dicarboxylic acid.

c. From ref. 150.

Table 6-2 Heats of formation of the molecular ions and major fragment ions from maleic and fumaric acids.

structure	m/z	ΔH_f° (kJ mol^{-1})			
		estimated	literature	measured (precursor) (maleic acid)	(fumaric acid)
[maleic acid]$^{+\cdot}$	116	-	-	285 ± 10	-
[fumaric acid]$^{+\cdot}$	116	-	355[a]	-	345 ± 10
	99	-	-	365 ± 10	397 ± 10
	98	-	-	-	655 ± 10
	98	-	-	-	616 ± 10
[HOOCCH=C=C=O]$^{+\cdot}$	98	606	-	609 ± 10	-
O=C^{+}-HC=CH-COO$^{\cdot}$	98	-	-	579 ± 10	-
[maleic anhydride]$^{+\cdot}$	98	-	643.7[a]	-	-
[E-HOHC=CHCOOH]$^{+\cdot}$	88	493	-	-	531 ± 10
[Z-HOHC=CHCOOH]$^{+\cdot}$	88	493	-	451 ± 10	-
	72	-	-	738 ± 10	700 ± 10
[H_2C=CHCOOH]$^{+\cdot}$	72	-	698.1[a]	-	-
[H_2C=C=C(OH)$_2$]$^{+\cdot}$	72	606			
		(623 ± 10)[b]			
HĊ=CHC^{+}(OH)$_2$	72	483			
HĊ=CH(C=O)$^{+}$OH$_2$	72	594			
[HC≡CCOOH]$^{+\cdot}$	70	-	891[a]		
[(HO)HC=C=C=O]$^{+\cdot}$	70	677			
[(CHO)HC=C=O]$^{+\cdot}$	70	677			
O=C^{+}-HC=C=O	69	510			
[H_2C=C=O(H_2O)]$^{+\cdot}$	60	-	579 ± 5[c]		

a. Ref. 149.
b. Measured from α-ethyl acrylic acid.
c. Ref. 153.

Table 6-3 MI mass spectra of ***m/z 116, the molecular ions*** from maleic acid, fumaric acid and their 2,3-d_2 and carboxyl-d_2 isotopemers. Kinetic energy releases ($T_{0.5}$ values, in meV) are in parentheses.

parent ion, m/z	fragment ion, m/z						
	100	99	98	90	88	74	72
maleic acid, 116	-	-	11 (24)	-	50 (164)	-	100 (58)
maleic acid-2,3-d_2, 118	29 (24)	35 (25)	-	93 (173)	-	100 (88)	-
maleic acid-carboxyl-d_2, 118	-	28 (26)	8 (24)	100 (156)	-	35 (88)	-
fumaric acid, 116	-	-	25 (27)	-	100 (162)	-	-
fumaric acid-2,3-d_2, 118	36 (20)	43 (20)	-	100 (185)	-	-	-
fumaric acid-carboxyl-d_2, 118	-	30	8	100	-	-	-

Table 6-4 MI mass spectra of ***the m/z 98, M-H_2O ions*** from maleic anhydride, maleic acid, fumaric acid and their 2,3-d_2 and carboxyl-d_2 isotopomers. Kinetic energy releases ($T_{0.5}$ values, in meV) are in parentheses.

precursor, m/z	neutral loss	parent ion, m/z	fragment ion, m/z 72	71	70	56	55	54	53
maleic acid, 116	H_2O	98	-	-	100 (21)	-	-	37 (293)	4 (7)
maleic acid -2,3-d_2, 118	H_2O	100	53 [a] (617) [b]	-	-	100 (262)	-	-	-
	HDO	99	-	100 [a] (529) [c]	-	-	58 (270)	-	-
maleic acid -carboxyl-d_2, 118	HDO	99	-	100 [a] (532) [d]	-	-	8 (70)	-	3 (18)
	D_2O	98	-	-	95 [a] (603) [e]	-	-	100 (271)	5 (8)
maleic anhydride, 98	-	98	-	-	-	-	-	100 (255)	
fumaric acid, 116	H_2O	98	-	-	100 (13)	-	-	18 (59)[f]	5 (13)
fumaric acid -2,3-d_2, 118	H_2O	100	100 (17)	-	-	6 -	-	2 -	-
	HDO	99	-	100 (10)	-	-	16 -	-	1 -
fumaric acid carboxyl-d_2, 118	HDO	99	-	100 (11)	-	-	10 (43)	-	4 (20)
	D_2O	98	-	-	100 (10)	-	-	20 (105)[g]	2 (34)

a. Part of the signal is artifact.
b. The metastable peak is composite. This $T_{0.5}$ corresponds to the broad component. And the $T_{0.5}$ corresponding to the narrow component is 113 meV.
c. The metastable peak is composite. This $T_{0.5}$ corresponds to the broad component. And the $T_{0.5}$ corresponding to the narrow component is 24 meV.
d. The metastable peak is composite. This $T_{0.5}$ corresponds to the broad component. And the $T_{0.5}$ corresponding to the narrow component is 66 meV.
e. The metastable peak is composite. This $T_{0.5}$ corresponds to the broad component. And the $T_{0.5}$ corresponding to the narrow component is 41 meV.
f. The metastable peak is composite. This $T_{0.5}$ corresponds to the narrow component. And the $T_{0.5}$ corresponding to the broad component is 591 meV.
g. The metastable peak is composite. This $T_{0.5}$ corresponds to the narrow component. And the $T_{0.5}$ corresponding to the broad component is 862 meV.

Table 6-5 MI mass spectra of ***the m/z 88, the M-CO ions*** from maleic acid, fumaric acid and their 2,3-d_2 and carboxyl-d_2 isotopomers. Kinetic energy releases ($T_{0.5}$ values, in meV) are in parentheses.

precursor, m/z	neutral loss	parent ion, m/z	fragment ion, m/z 72	71	70	62	60	44	43	42
maleic acid, 116	CO	88	-	-	100	-	48	-	-	69
maleic acid-2,3-d_2, 118	CO	90	75	98	-	100	-	21	41	-
maleic acid -carboxyl-d_2, 118	CO	90	-	100 (6)	63 (14)	72 (185)	-	-	55 (29)	33 (39)
fumaric acid, 116	CO	88	-	-	97 (7)	-	100 (188)	-	-	75 (36)
fumaric acid -2,3-d_2, 118	CO	90	89	93	-	100	-	24	60	-
fumaric acid -carboxyl-d_2, 118	CO	90	-	100	42	68	-	-	30	20

Table 6-6 MI mass spectra of ***m/z 72, the M-CO_2 ions*** from acrylic acid, α-ethylacrylic acid, maleic acid, fumaric acid and their 2,3-d_2 and carboxyl-d_2 isotopomers. Kinetic energy releases ($T_{0.5}$ values, in meV) are in parentheses.

precursor, m/z	neutral loss	parent ion, m/z	fragment ion, m/z 73	72	71	57	56	55	54	46	44	43
maleic acid, 116	CO_2	72	-	-	100 (132) [a]	-	-	32 (44)	-	-	44 (322)	-
maleic acid-2,3-d_2, 118	CO_2	74	100 (232)	21 (246)	-	26 (37)	9 (33)	-	-	47 (316)	-	-
maleic acid -carboxyl-d_2, 118	CO_2	74	100 (268)	30 (258)	-	27 (36)	23 (45)	-	-	47 (336)	-	-
acrylic acid, 72	-	72	-	-	100 (247)	-	-	-	-	-	54 (217)	-
α-ethylacrylic acid, 100	CO/C_2H_4	72	-	-	95 (23)	61 (231)	-	100 (72)	11 (85)	-	14 (435)	43 (26)
fumaric acid, 116	CO_2	72	-	-	100 (289)	-	-	27 (63)	-	-	25 (368)	-
fumaric acid -2,3-d_2, 118	CO_2	74	100	22	-	33	23	-	-	44	-	-
fumaric acid -carboxyl-d_2, 118	CO_2	74	100 (266)	31 (269)	-	42 (40)	37 (36)	-	-	53 (375)	-	-

a. The metastable peak is composite. This $T_{0.5}$ value corresponds to the broad component. The $T_{0.5}$ value for the narrow component is 73 meV.

Table 6-7 MI mass spectra of the m/z 70 and 69 ions from maleic and fumaric acids.

precursor	parent ion	kinetic energy release ($T_{0.5}$ in meV)	
		m/z 69	m/z 41
maleic acid	70	17	-
fumaric acid	70	11	-
maleic acid	69	-	38
fumaric acid	69	-	44

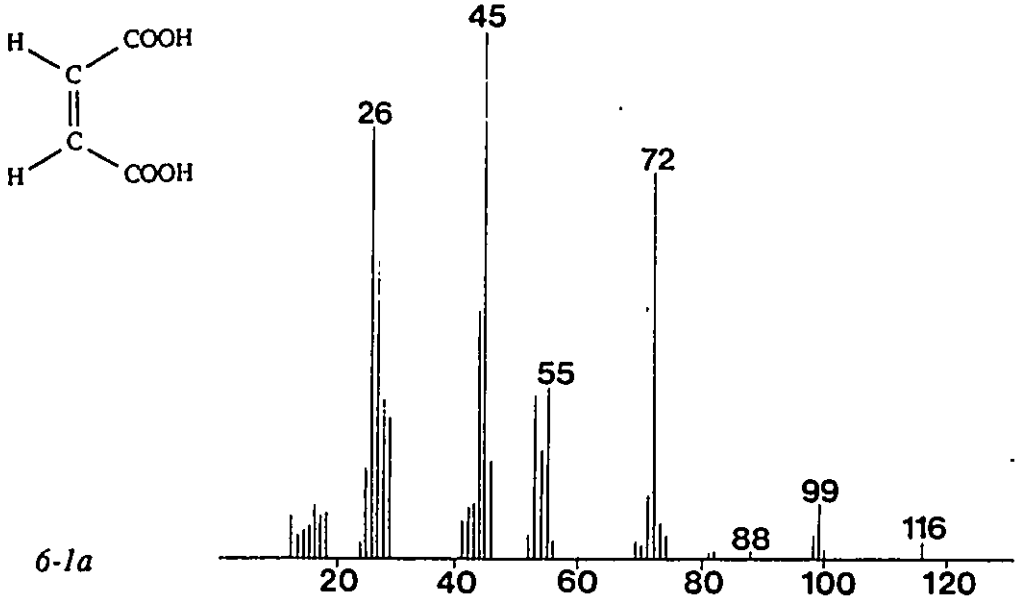
H
COOH
C
C
H
COOH
45
26
72
55
99
88
116
20
40
60
80
100
120

6-1a

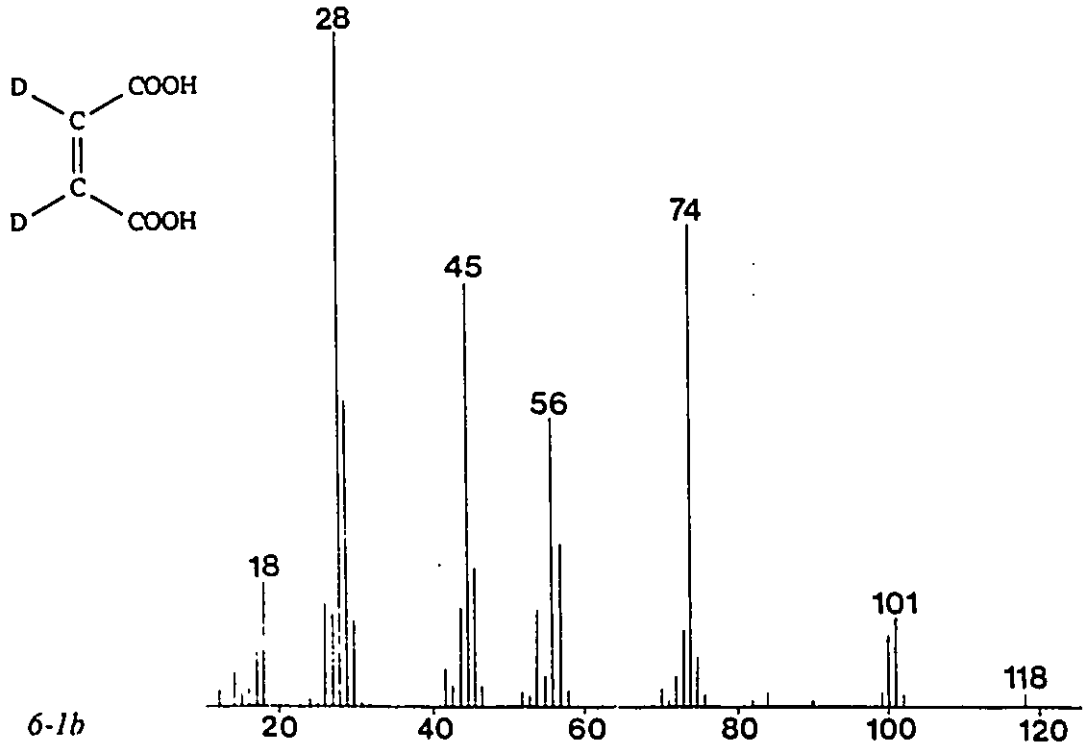
D
COOH
C
C
D
COOH
28
74
45
56
18
101
118
20
40
60
80
100
120

6-1b

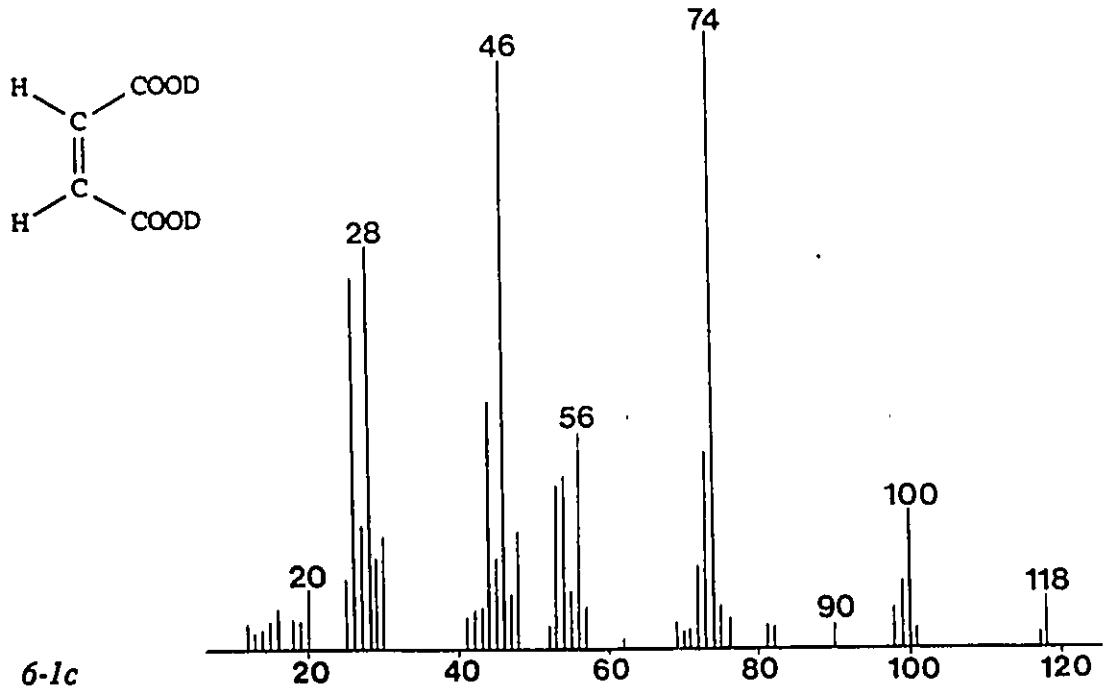

6-1c

Figure 6-1 *EI mass spectra of unlabelled maleic acid (6-1a), maleic acid-2,3-d_2 (6-1b) and maleic acid-carboxyl-d_2 (6-1c), probe heater temperature at 110 °C.*

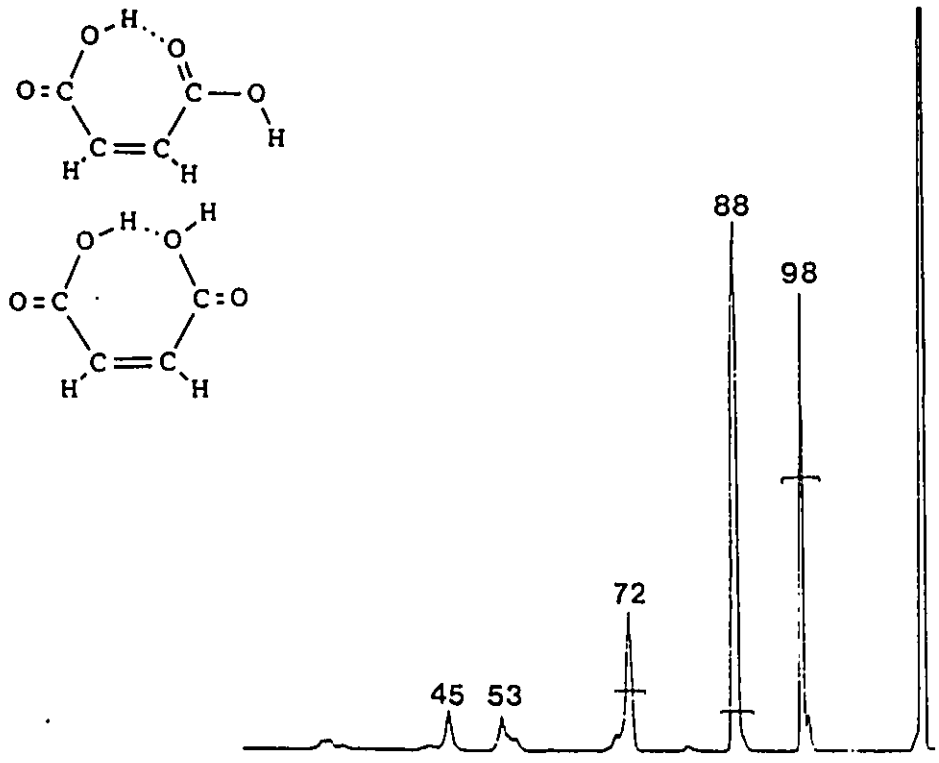

Figure 6-2 *He (90% T) CA mass spectrum of the m/z 116 ion from maleic acid. The signals above the bars are contributions due to metastable ions.*

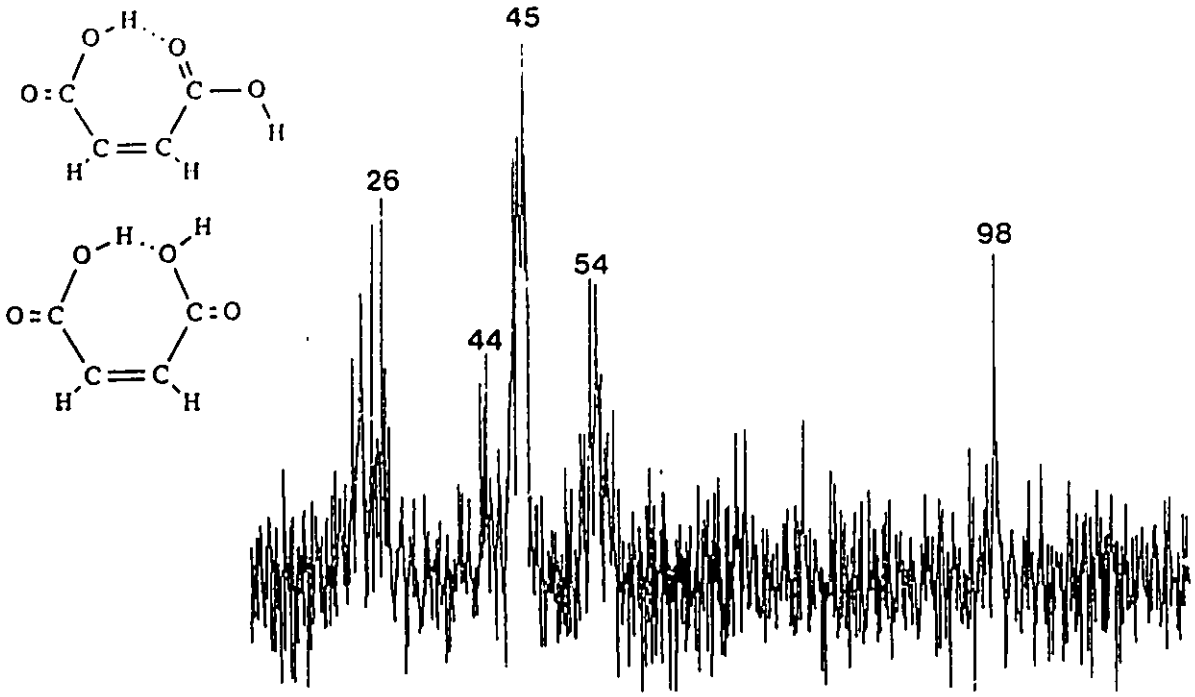

Figure 6-3 *NR mass spectrum of the m/z 116 ion from maleic acid. Xe (90% T) was the charge-exchange neutralization target and O_2 (90% T) the reionization target.*

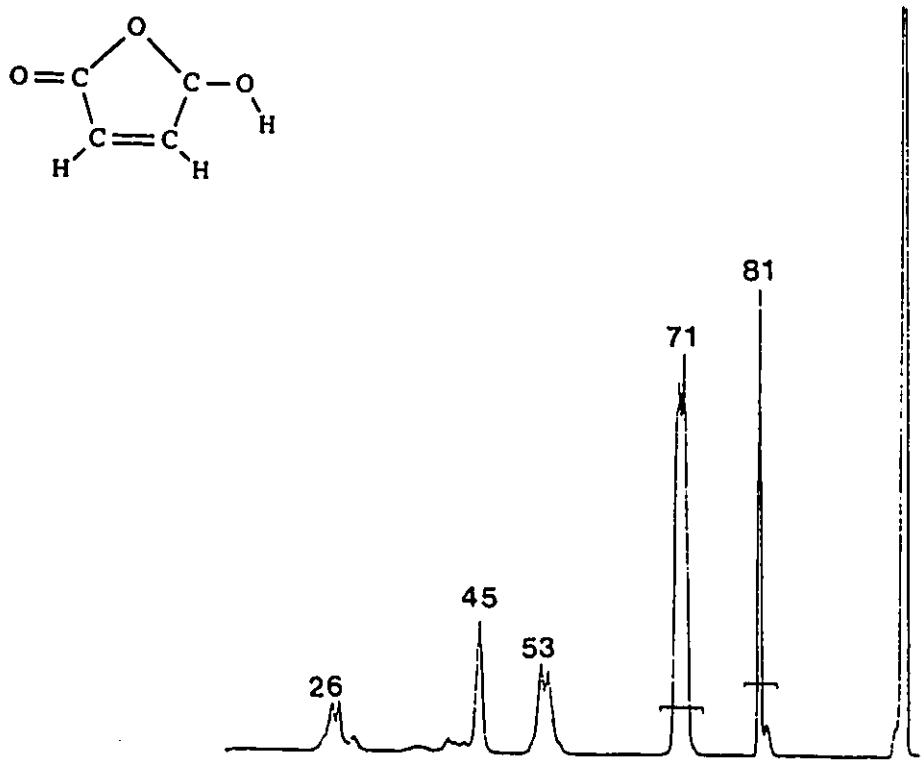

Figure 6-4 *He (90% T) CA mass spectrum of the m/z 99 ion from maleic acid. The signals above the bars are contributions due to metastable ions.*

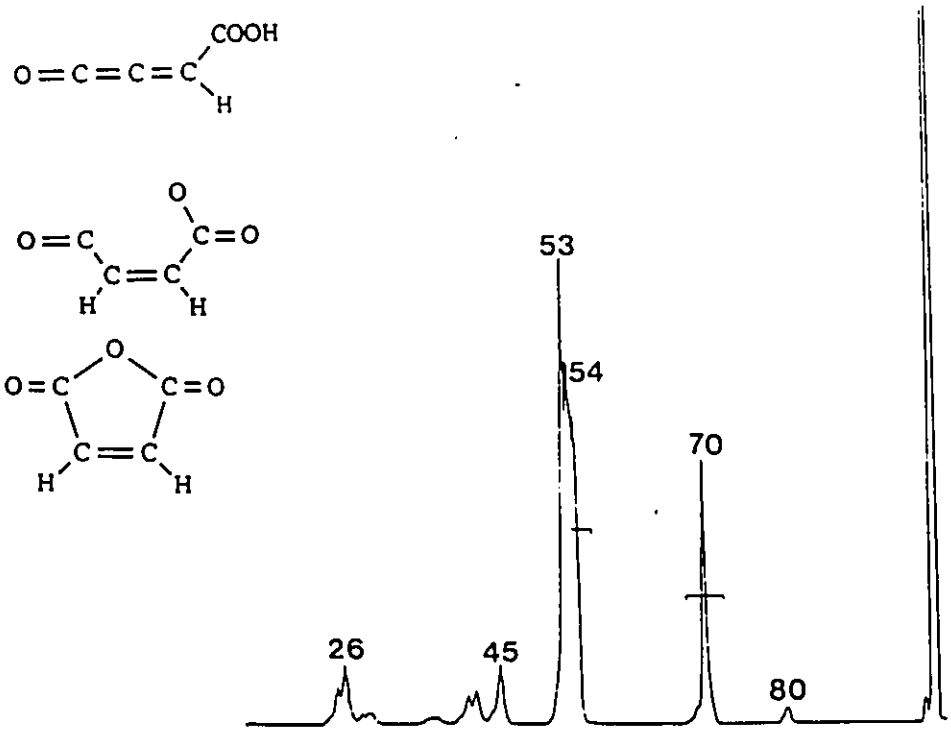

Figure 6-5 *He (90% T) CA mass spectrum of the m/z 98 ion from maleic acid. The signals above the bars are contributions due to metastable ions.*

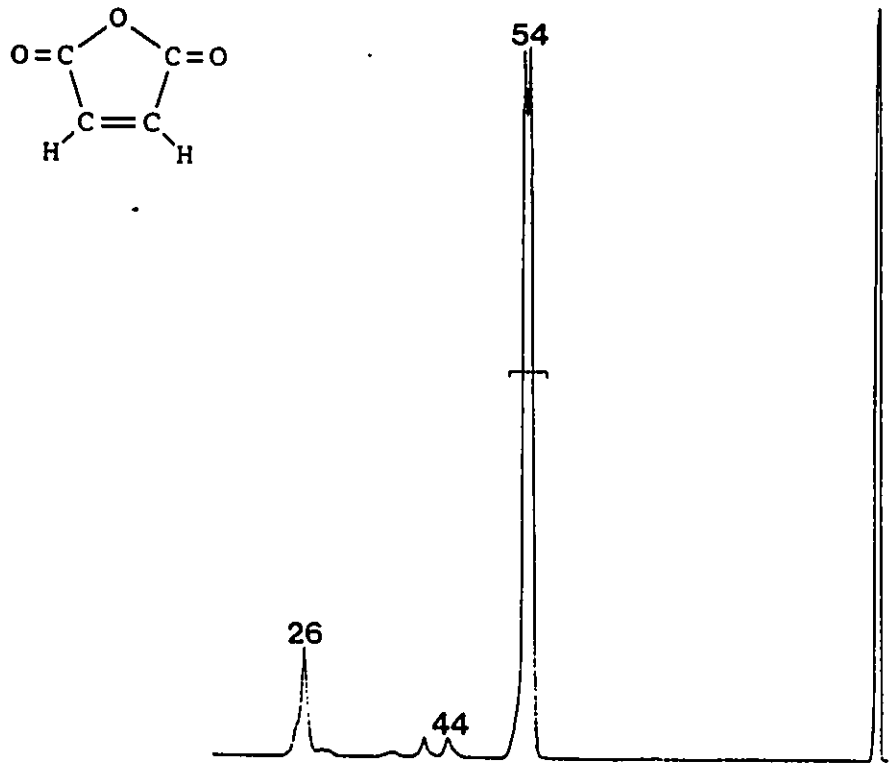

Figure 6-6 *He (90% T) CA mass spectrum of the m/z 98 ion from maleic anhydride. The signal above the bar is the contribution due to metastable ion.*

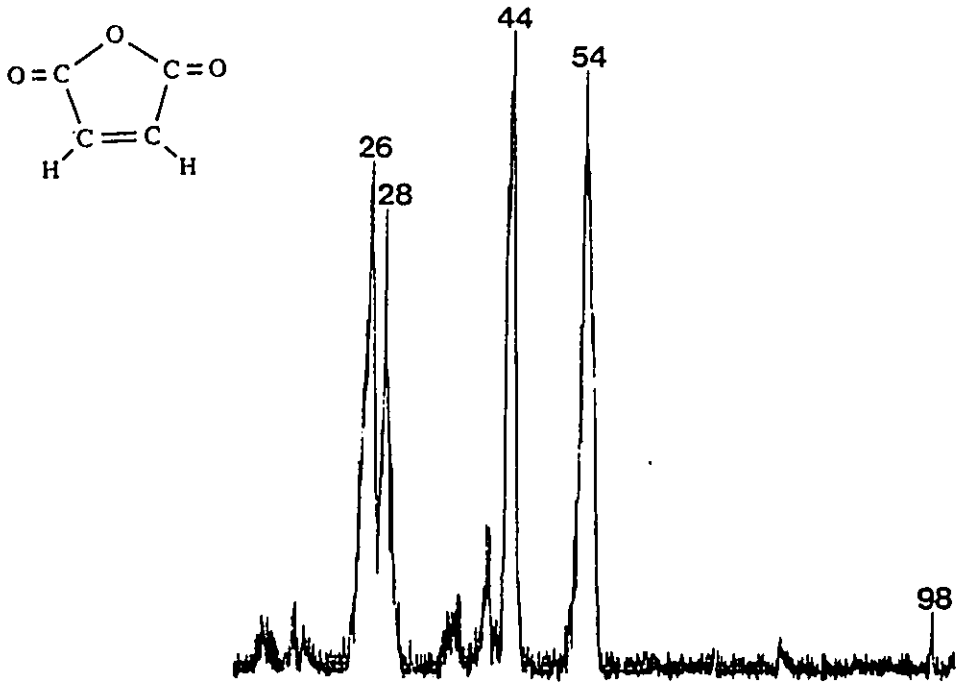

Figure 6-7 *NR mass spectrum of the m/z 98 ion from maleic anhydride. Xe (90% T) was the charge-exchange neutralization target and O_2 (90% T) the reionization target.*

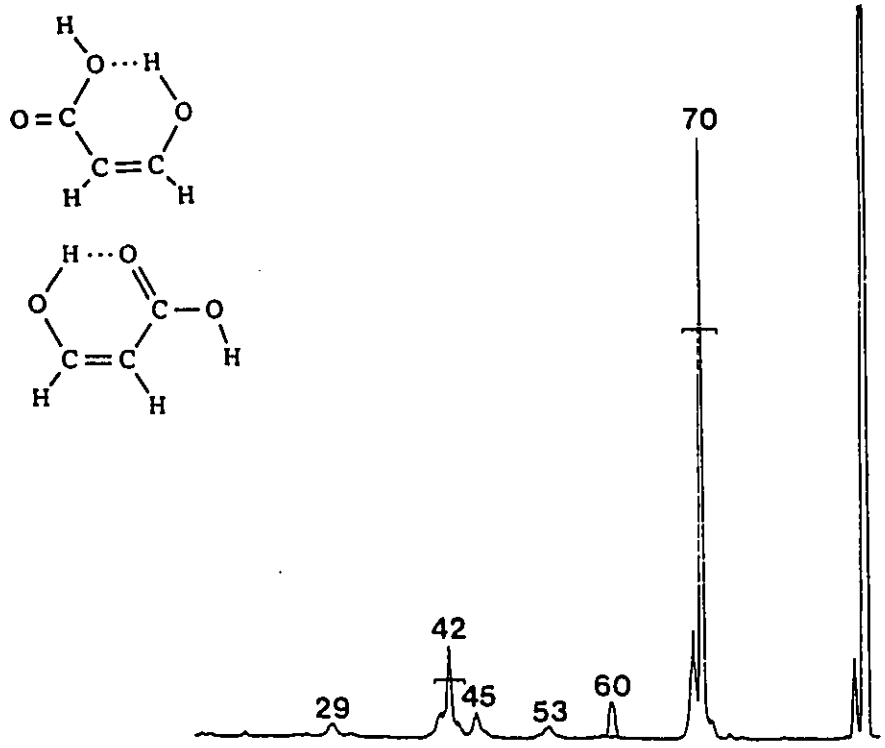

Figure 6-8 *He (90% T) CA mass spectrum of the m/z 88 ion from maleic acid. The signals the bars are contributions due to metastable ions. The signal at m/z 60 is totally contribution due to metastable ion.*

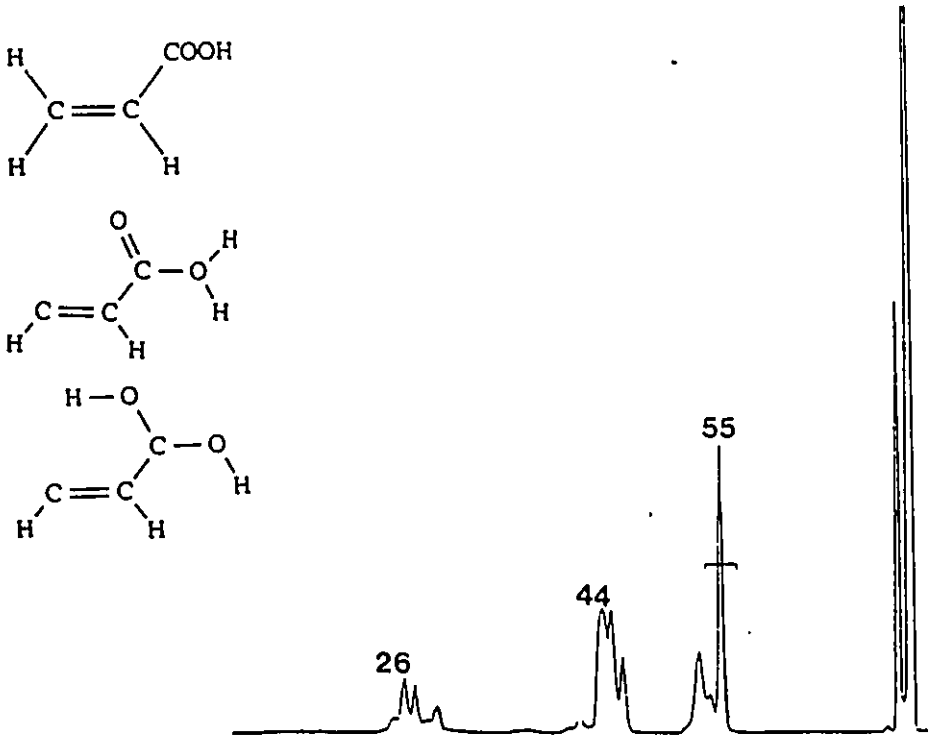

Figure 6-9 *He (90% T) CA mass spectrum of the m/z 72 ion from maleic acid. The signal above the bar is the contribution due to the metastable ion. The signals at m/z 71 and 44 are totally contributions due to metastable ions.*

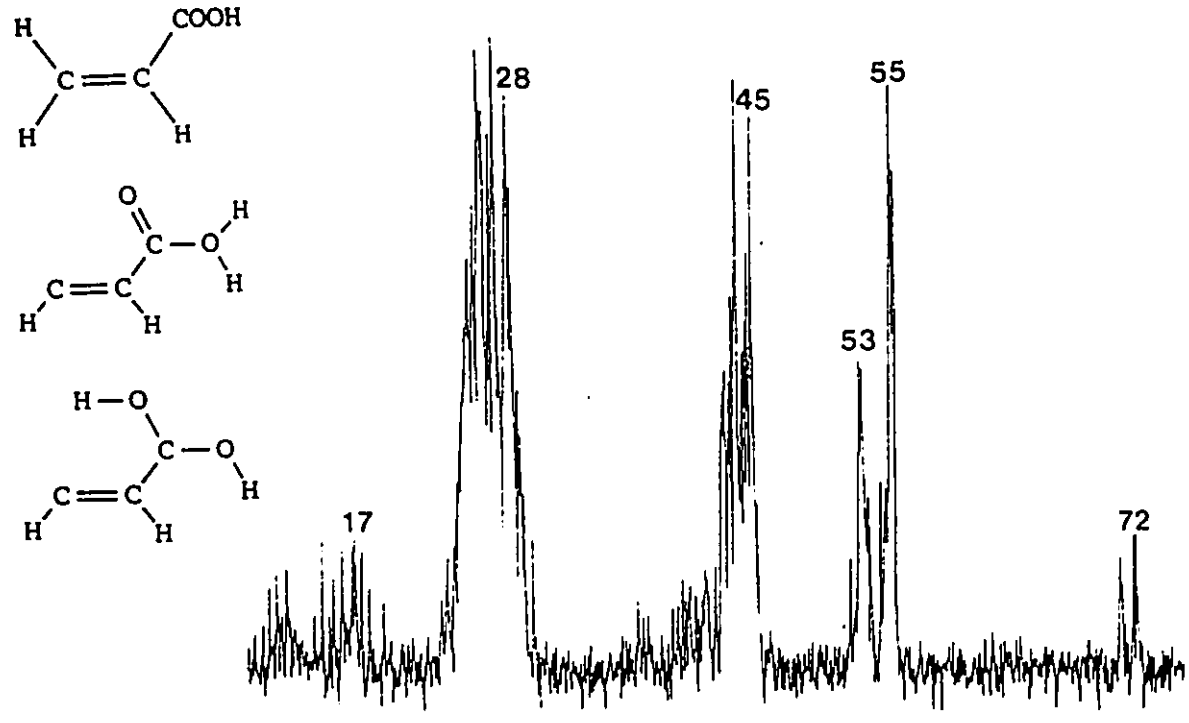

Figure 6-10 *NR mass spectrum of the m/z 72 ion from maleic acid. Xe (90% T) was the charge-exchange neutralization target and O_2 (90% T) the reionization target.*

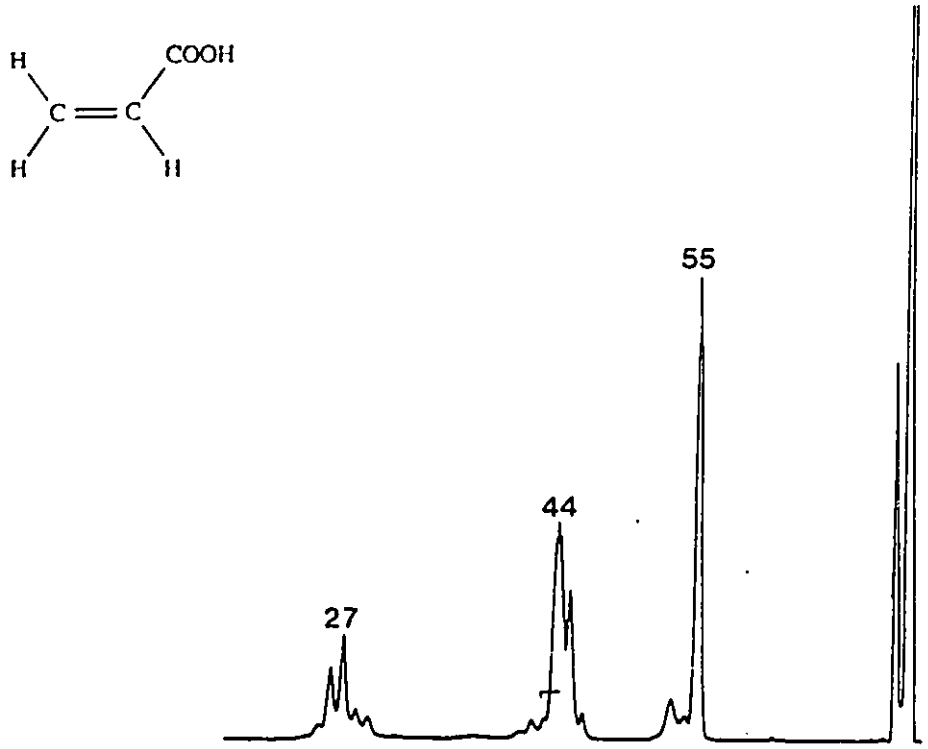

Figure 6-11 *He (90% T) CA mass spectrum of the m/z 72 ion from acrylic acid. The signal above the bar is the contribution due to the metastable ion. The signal at m/z 71 is totally the contribution due to the metastable ion.*

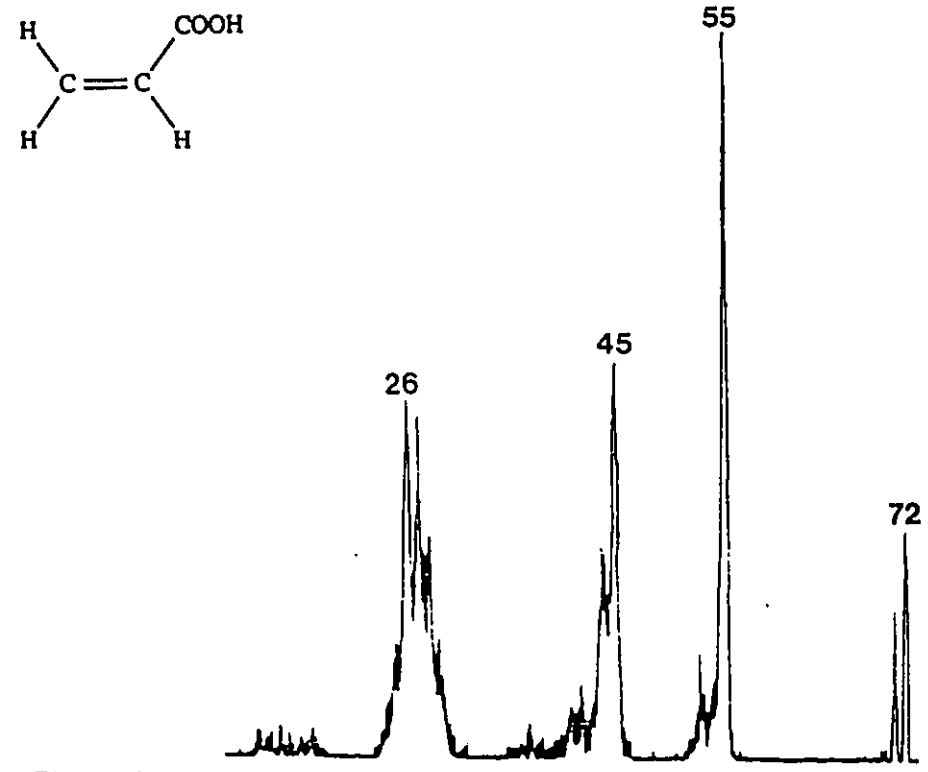

Figure 6-12 *NR mass spectrum of the m/z 72 ion from acrylic acid. Xe (90% T) was the charge-exchange neutralization target and O_2 (90% T) the reionization target.*

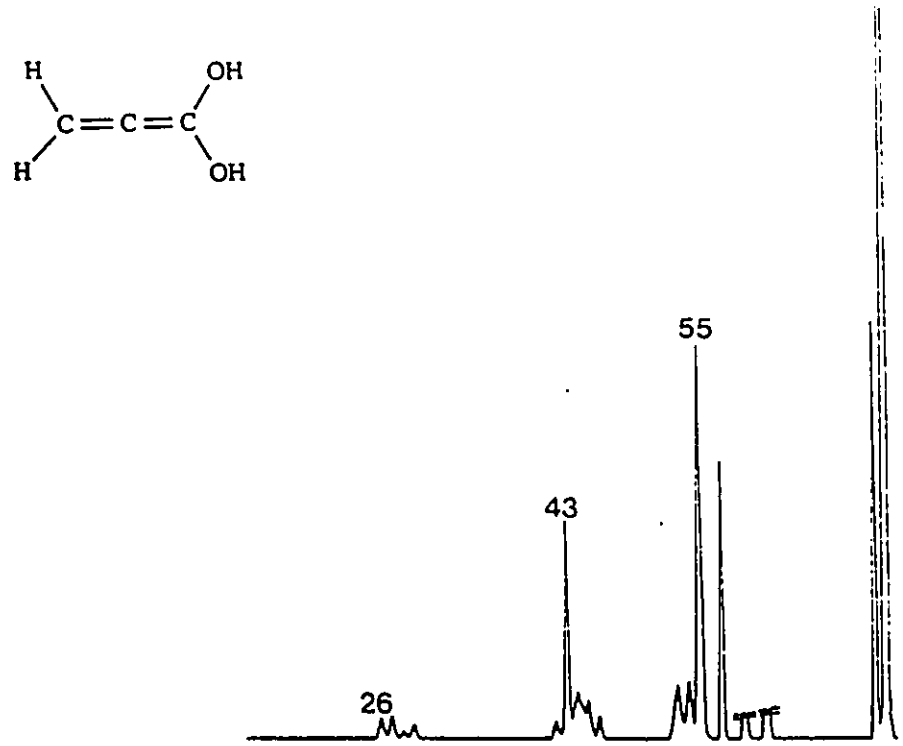

Figure 6-13 *He (90% T) CA mass spectrum of the m/z 72 ion from α-ethylacrylic acid. The signals are not corrected for contributions of metastable ions.*

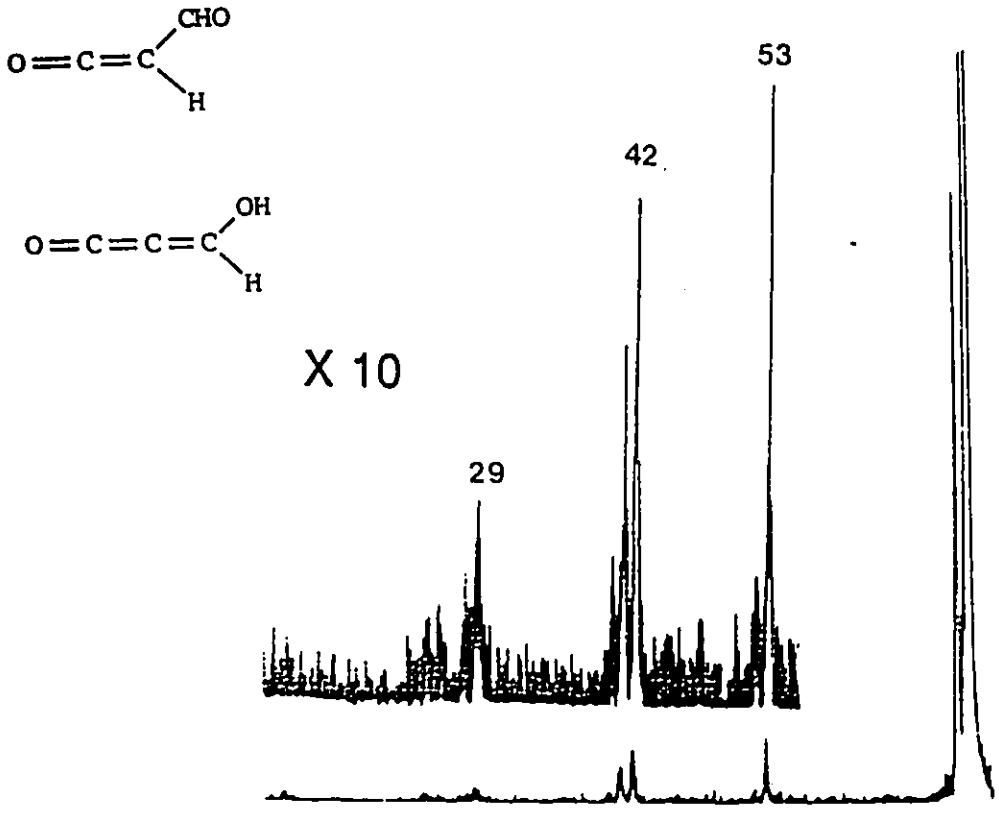

Figure 6-14 *He (90% T, collision cell 3) CA mass spectrum of the m/z 70 ion from maleic acid. The signals are not corrected for contributions of metastable ions.*

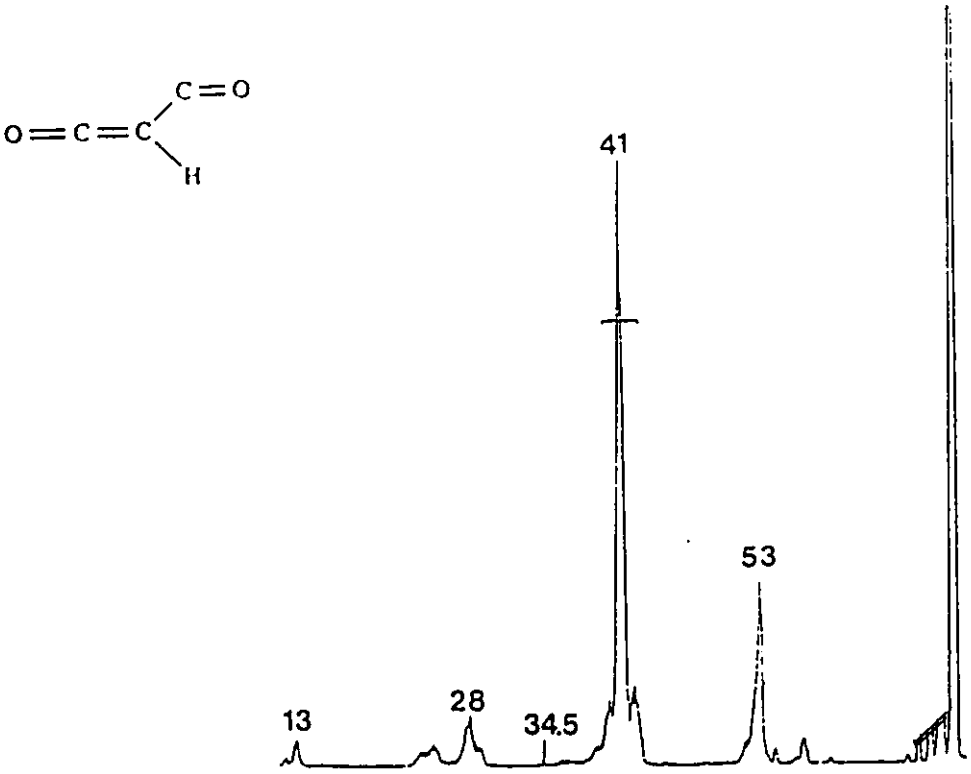

Figure 6-15 *He (90% T) CA mass spectrum of the m/z 69 ion from maleic acid. The signal above the bar is the contribution due to the metastable ion. The signals at m/z 68, 67 and 66 are totally artifacts.*

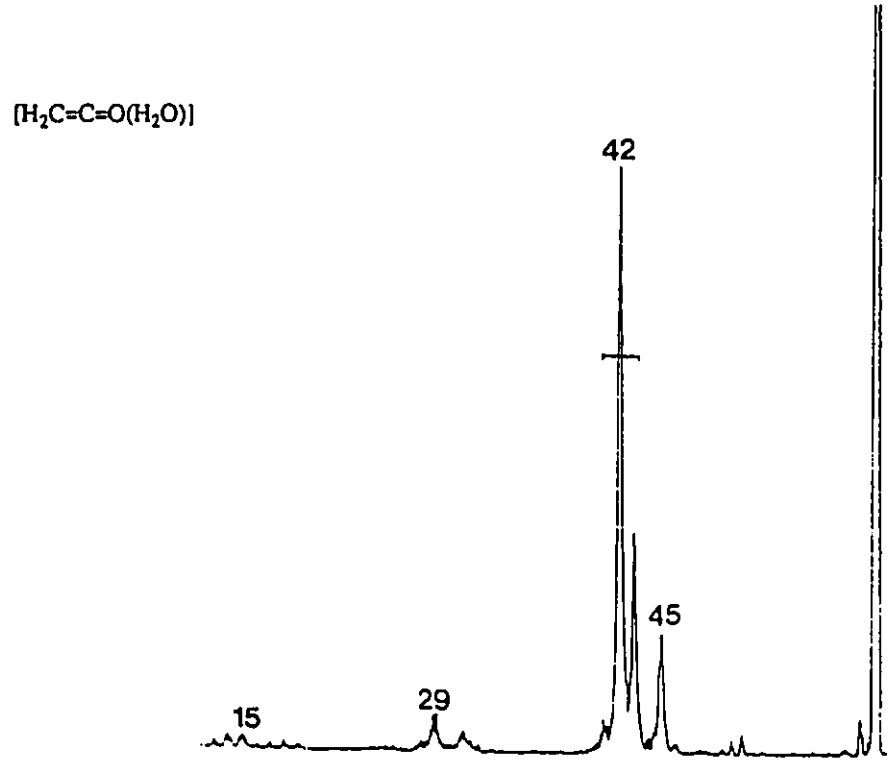

Figure 6-16 *He (90% T) CA mass spectrum of the m/z 60 ion from maleic acid. The signal above the bar is the contribution due to the metastable ion.*

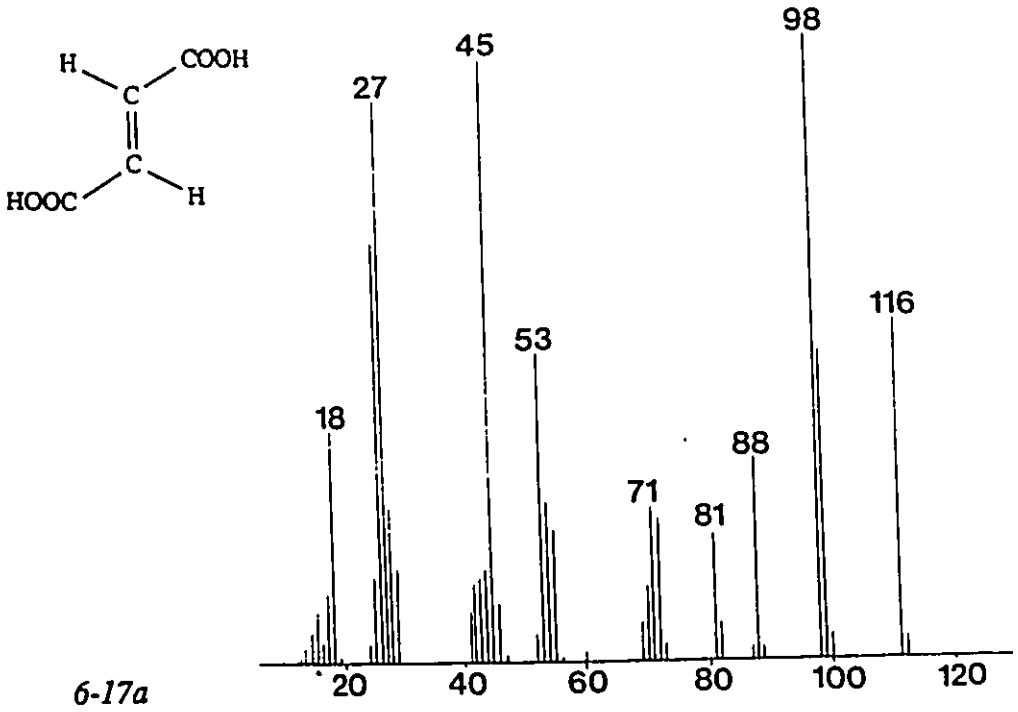
H
COOH
C
C
HOOC
H
98
45
27
116
53
18
88
71
81
20
40
60
80
100
120

6-17a

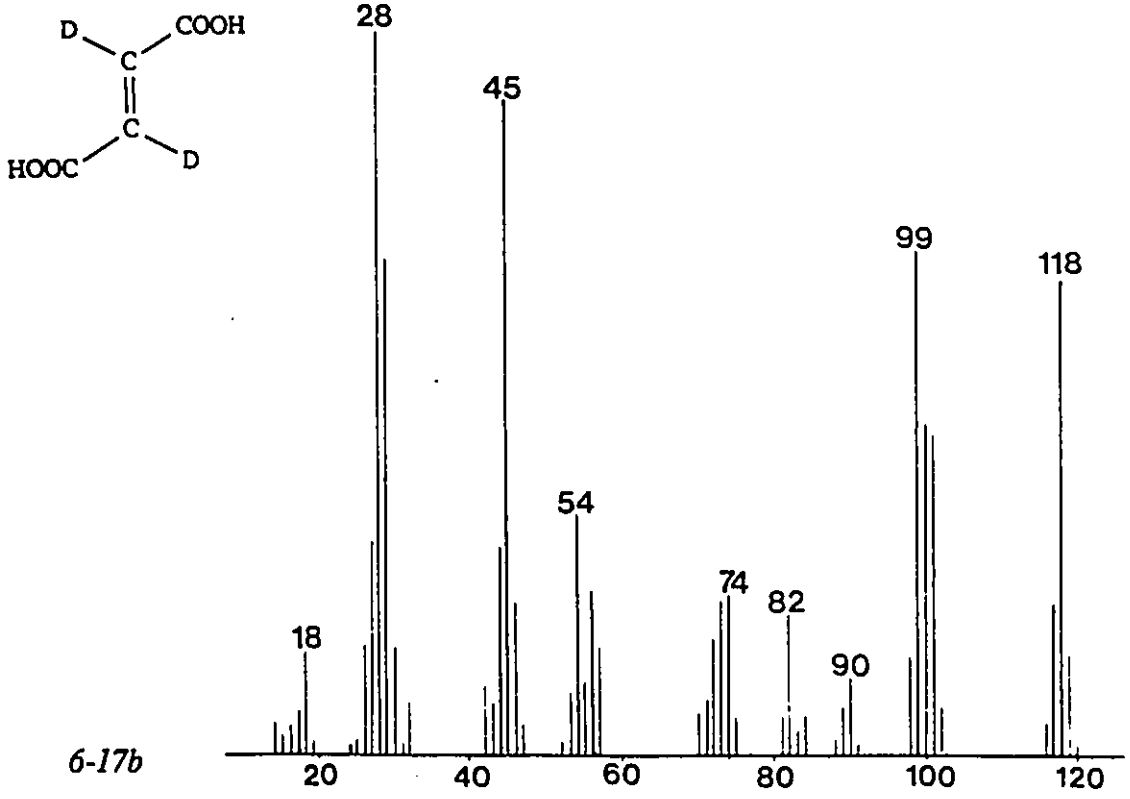
D
COOH
C
C
HOOC
D
28
45
99
118
54
74
82
18
90
20
40
60
80
100
120

6-17b

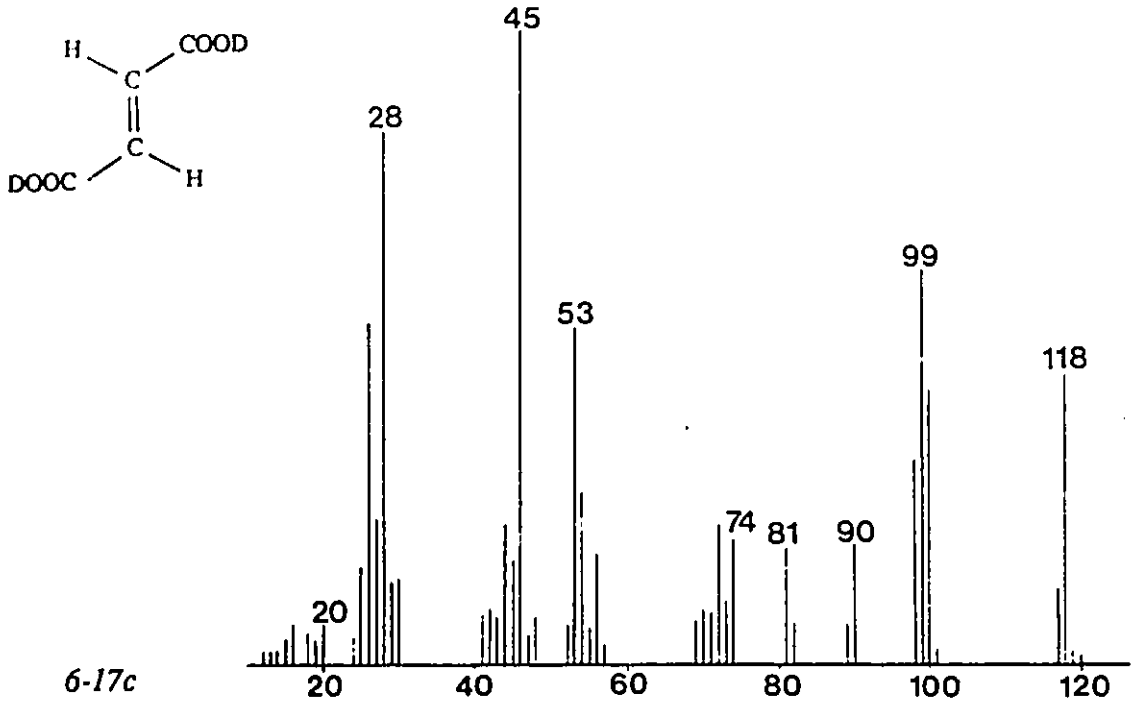

Figure 6-17 EI mass spectra of unlabelled fumaric acid (6-17a), fumaric acid-2,3-d_2 (6-17b) and fumaric acid-carboxyl-d_2 (6-17c), probe heater temperature at 170 °C.

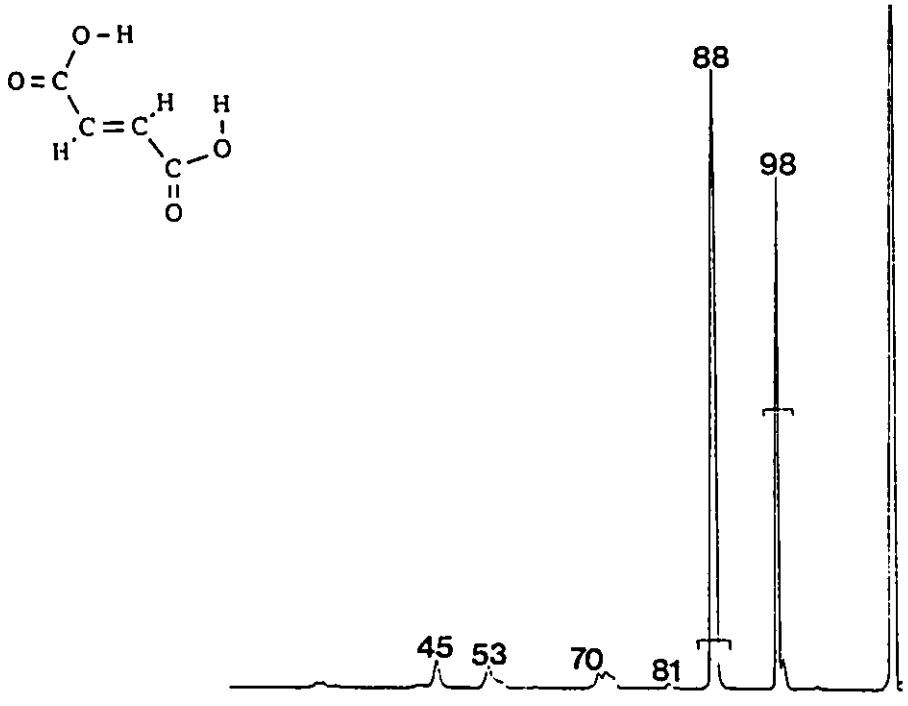

Figure 6-18 He (90% T) CA mass spectrum of the m/z 116 ion from fumaric acid. The signals above the bars are contributions due to metastable ions.

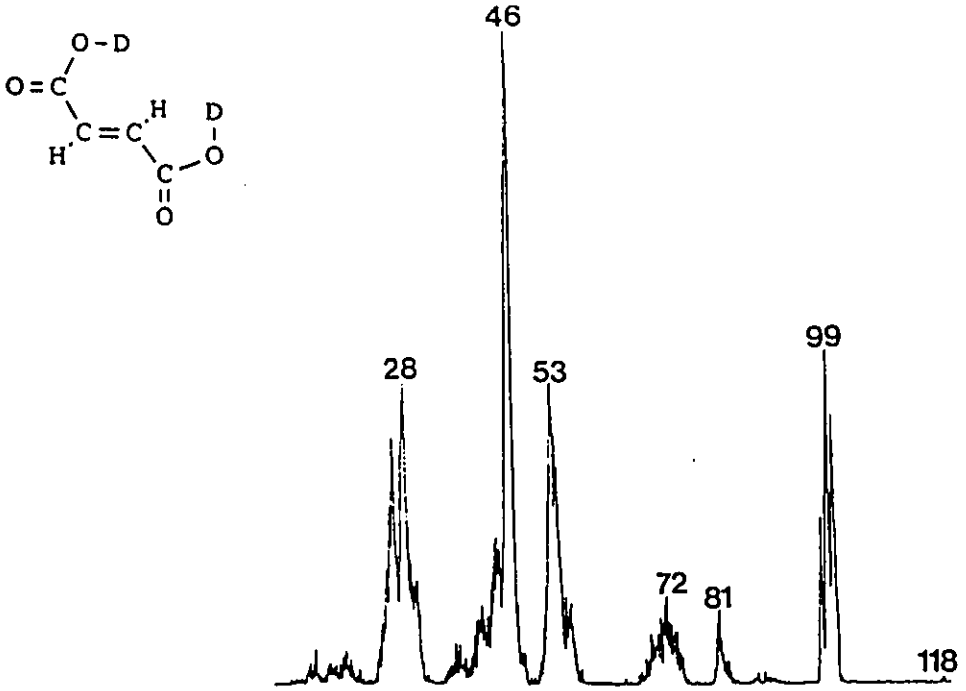

Figure 6-19 *NR mass spectrum of the deuterated m/z 116 (m/z 118) ion from fumaric acid-carboxyl-d_2. Xe (90% T) was the charge-exchange neutralization target and O_2 (90% T) the reionization target.*

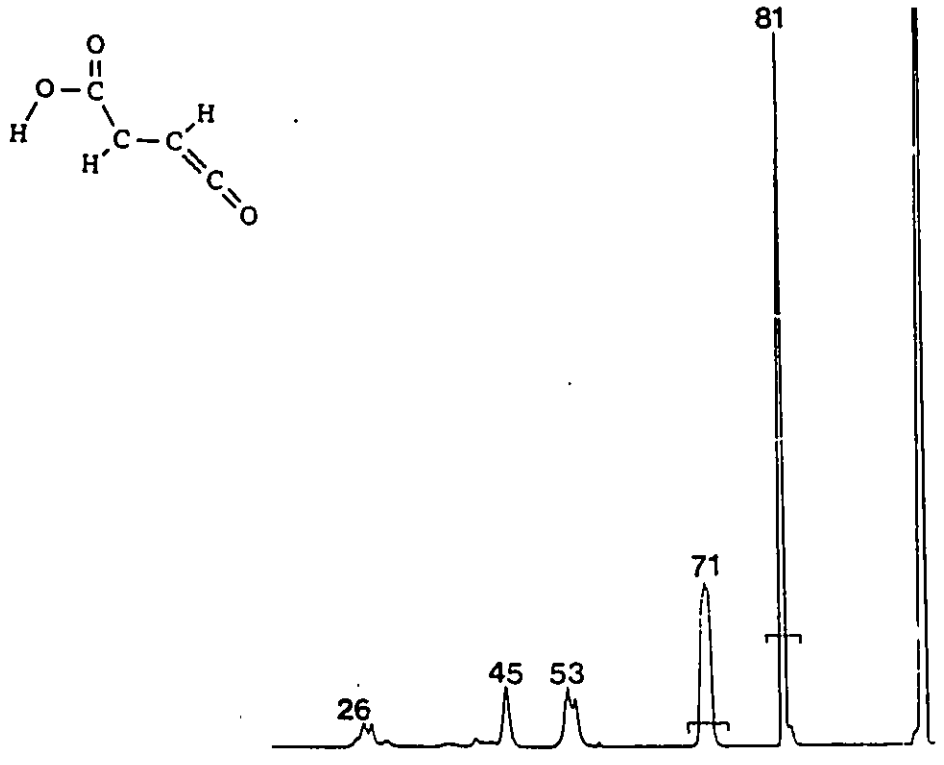

Figure 6-20 *He (90% T) CA mass spectrum of the m/z 99 ion from fumaric acid. The signals above the bars are contributions due to metastable ions.*

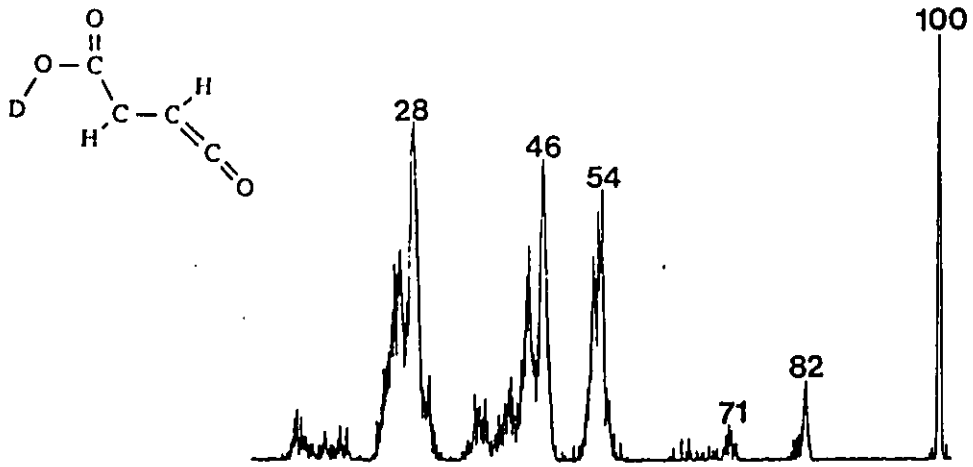

Figure 6-21 *NR mass spectrum of the deuterated m/z 99 (m/z 100) ion from fumaric acid-carboxyl-d_2. Xe (90% T) was the charge-exchange neutralization target and O_2 (90% T) the reionization target.*

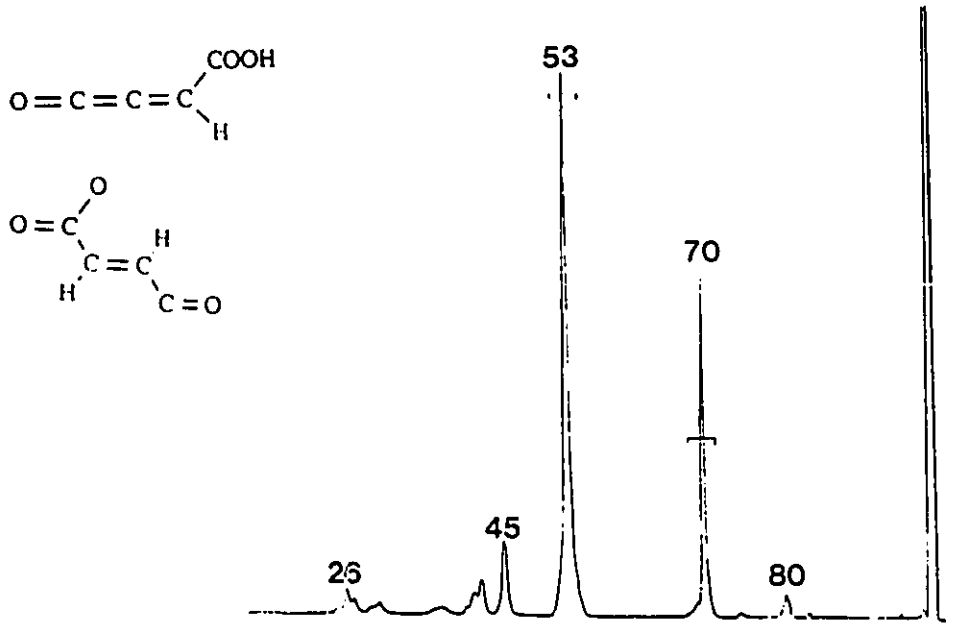

Figure 6-22 *He (90% T) CA mass spectrum of the m/z 98 ion from fumaric acid. The signals above the bars are contributions due to metastable ions.*

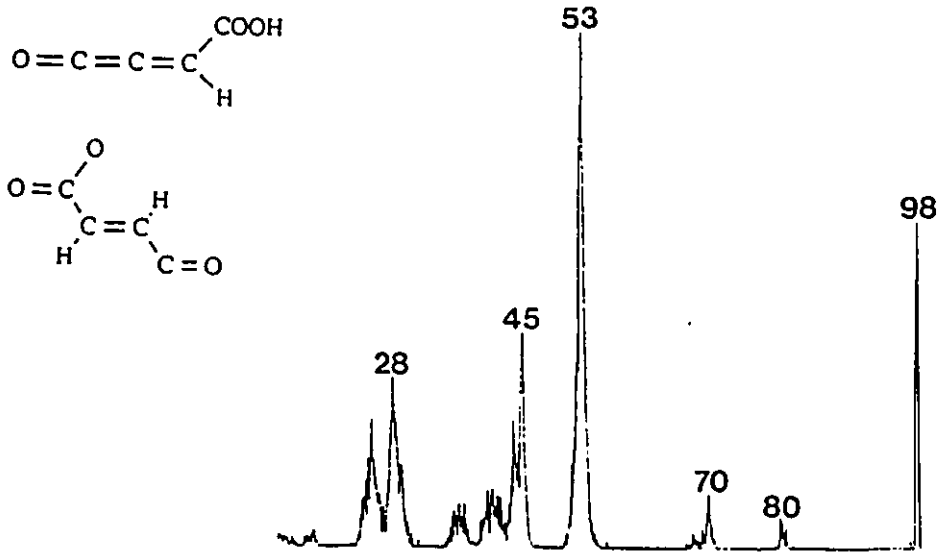

Figure 6-23 *NR mass spectrum of the m/z 98 ion from fumaric acid-carboxyl-d_2. Xe (90% T) was the charge-exchange neutralization target and O_2 (90% T) the reionization target.*

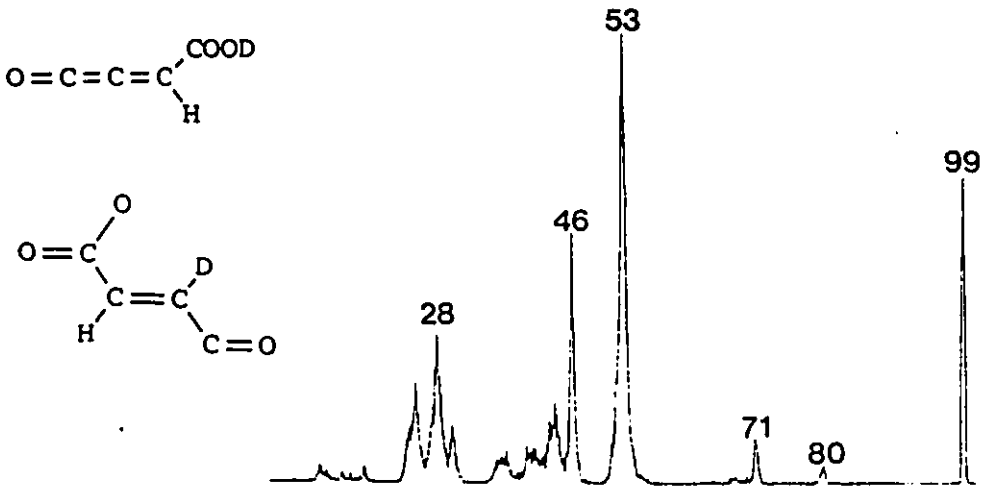

Figure 6-24 *NR mass spectrum of the deuterated m/z 98 (m/z 99) ion from fumaric acid-carboxyl-d_2. Xe (90% T) was the charge-exchange neutralization target and O_2 (90% T) the reionization target.*

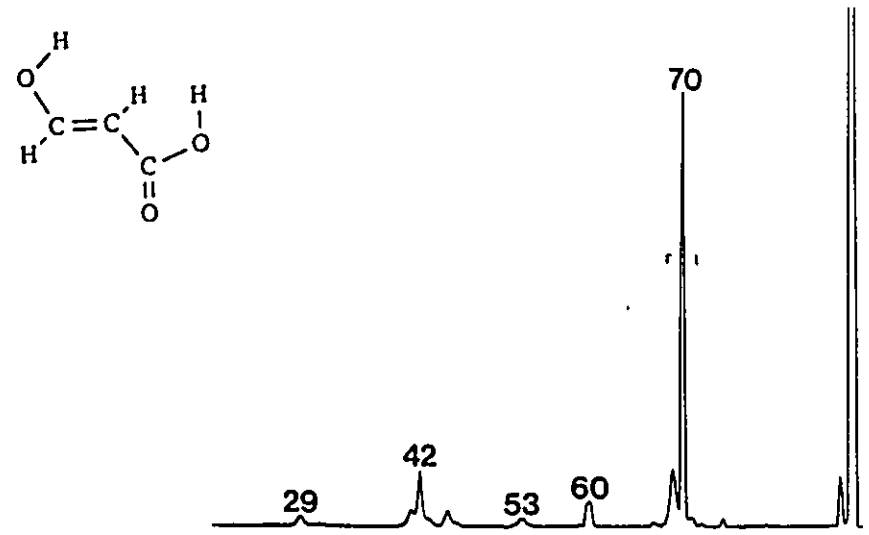

Figure 6-25 *He (90% T) CA mass spectrum of the m/z 88 ion from fumaric acid. The signal above the bar is contribution due to the metastable ion. The signals at m/z 60 and 42 are totally contributions due to metastable ions.*

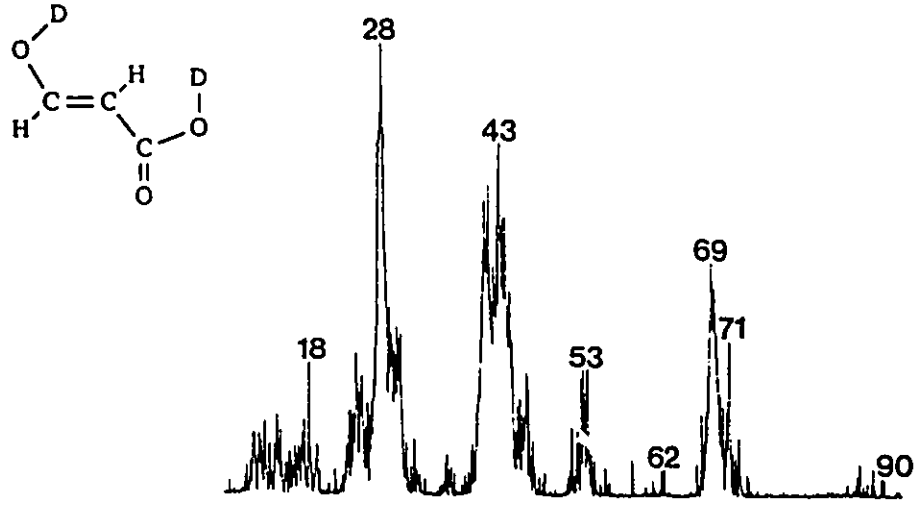

Figure 6-26 *NR mass spectrum of the deuterated m/z 88 (m/z 90) ion from fumaric acid-carboxyl-d_2. Xe (90% T) was the charge-exchange neutralization target and O_2 (90% T) the reionization target.*

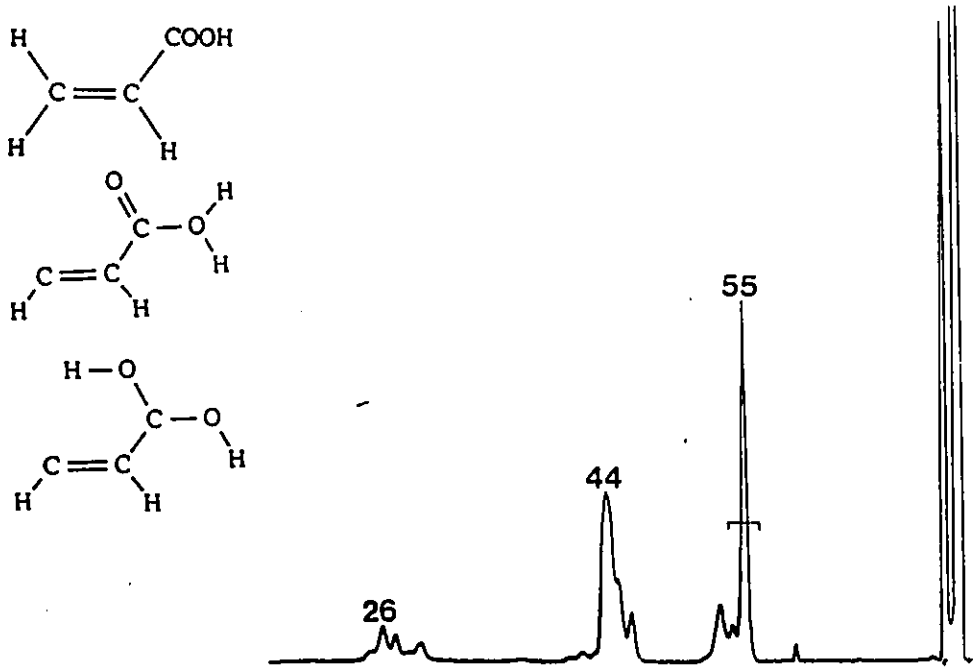

Figure 6-27 *He (90% T) CA mass spectrum of the m/z 72 ion from fumaric acid. The signal above the bar is contribution due to the metastable ion. The signals at m/z 71 and 44 are totally contributions due to metastable ions.*

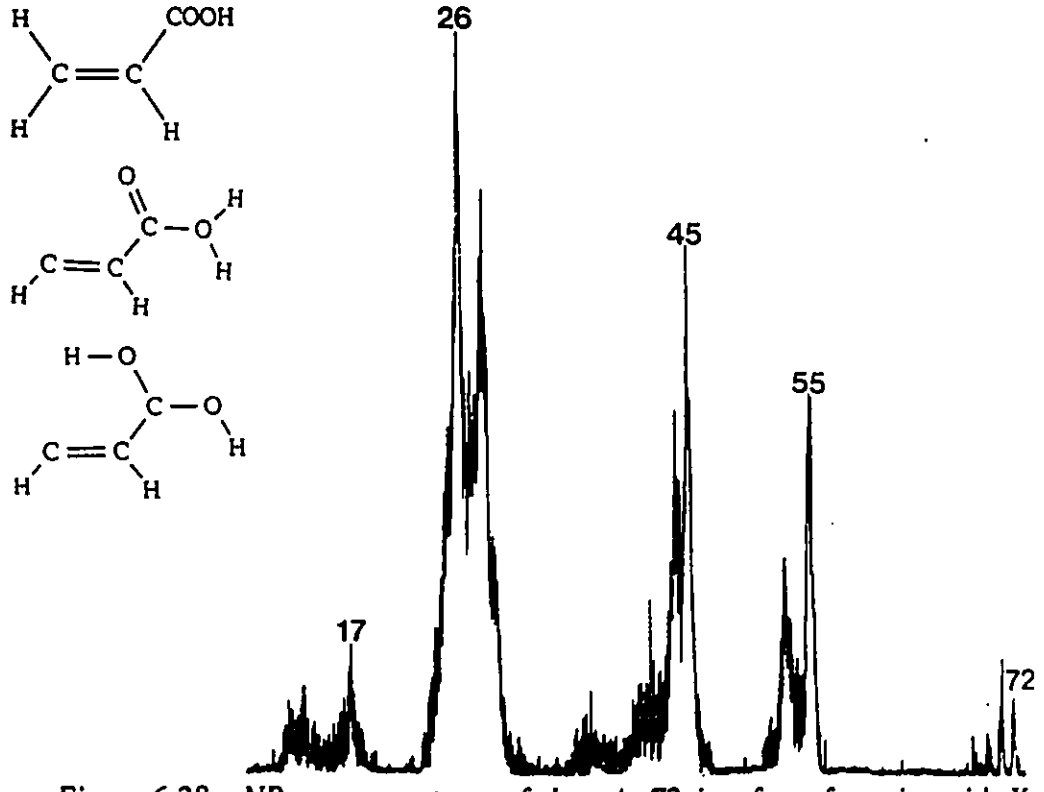

Figure 6-28 *NR mass spectrum of the m/z 72 ion from fumaric acid. Xe (90% T) was the charge-exchange neutralization target and O_2 (90% T) the reionization target.*

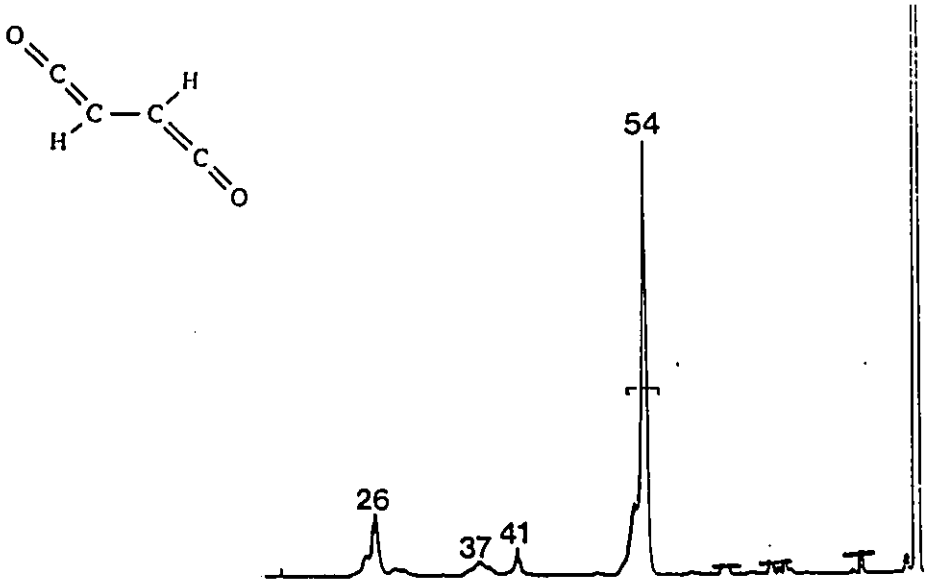

Figure 6-29 *He (90% T) CA mass spectrum of the m/z 82 ion from fumaric acid. The signal above the bar is contribution due to the metastable ion and C^{13} contribution from m/z 81.*

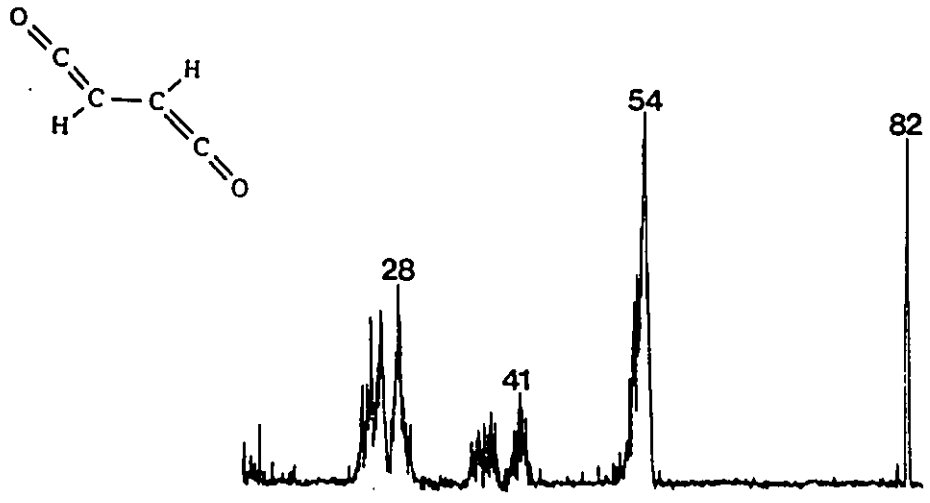

Figure 6-30 *NR mass spectrum of the m/z 82 ion from fumaric acid-carboxyl-d_2. Xe (90% T) was the charge-exchange neutralization target and O_2 (90% T) the reionization target.*

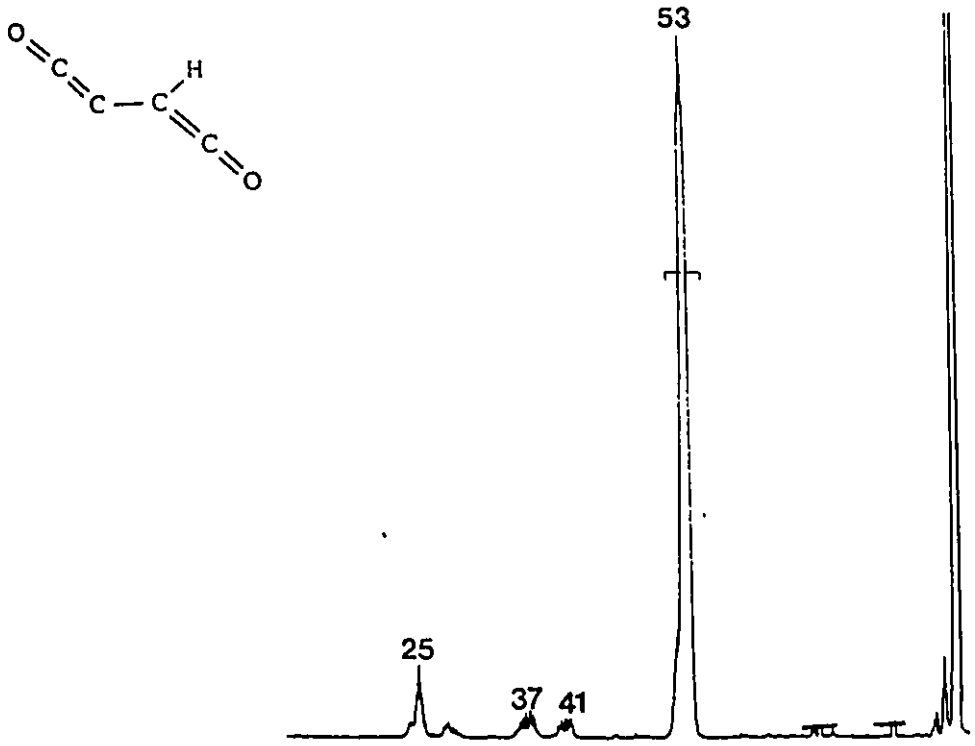

Figure 6-31 *He (90% T) CA mass spectrum of the m/z 81 ion from fumaric acid. The signal above the bar is the contribution due to the metastable ion.*

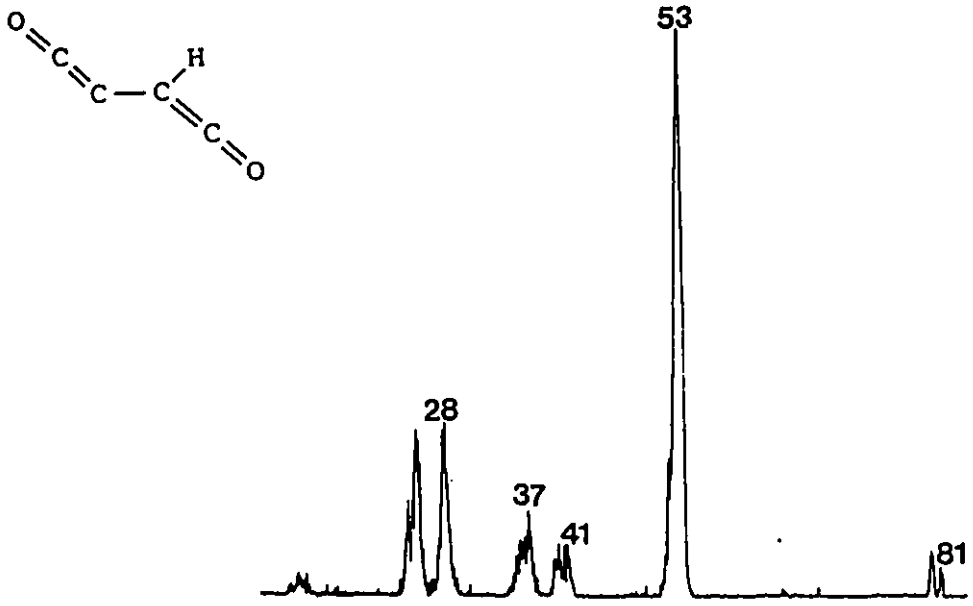

Figure 6-32 *NR mass spectrum of the m/z 81 ion from fumaric acid-carboxyl-d_2. Xe (90% T) was the charge-exchange neutralization target and O_2 (90% T) the reionization target.*

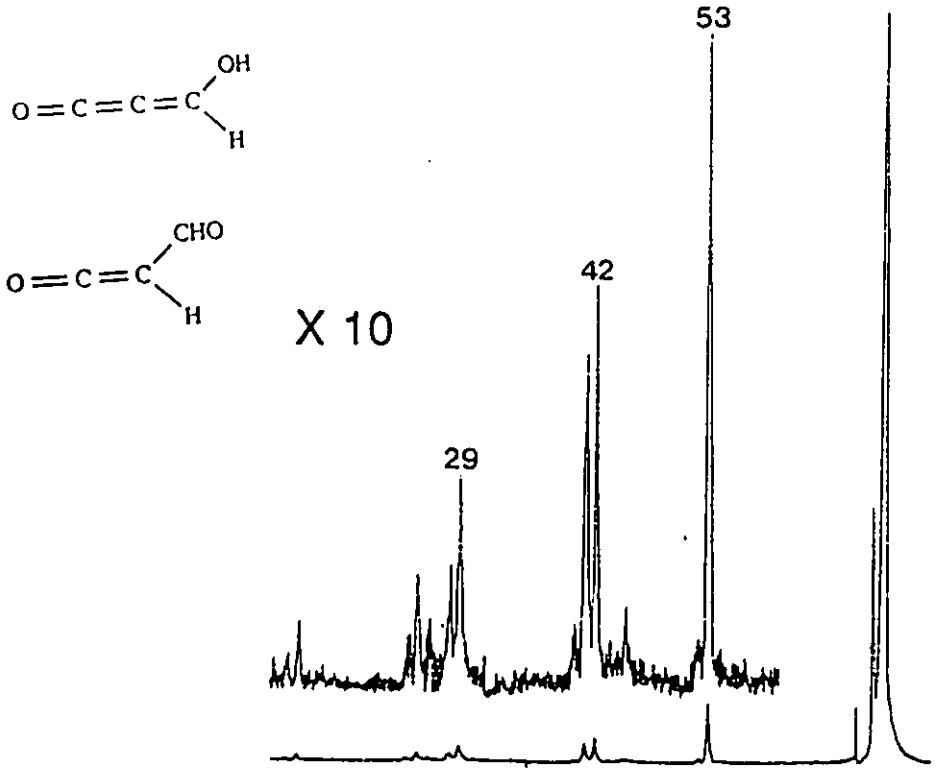

Figure 6-33 *He (90% T, collision cell 3) CA mass spectrum of the m/z 70 ion from fumaric acid. The signals are not corrected for contributions of metastable ions.*

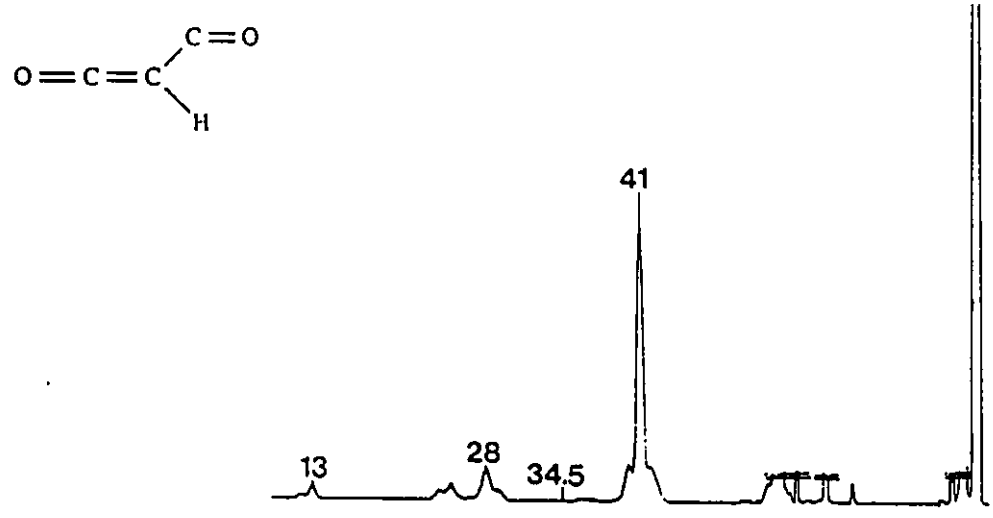

Figure 6-34 *He (90% T) CA mass spectrum of the m/z 69 ion from fumaric acid. The signals are not corrected for contributions of metastable ions.*

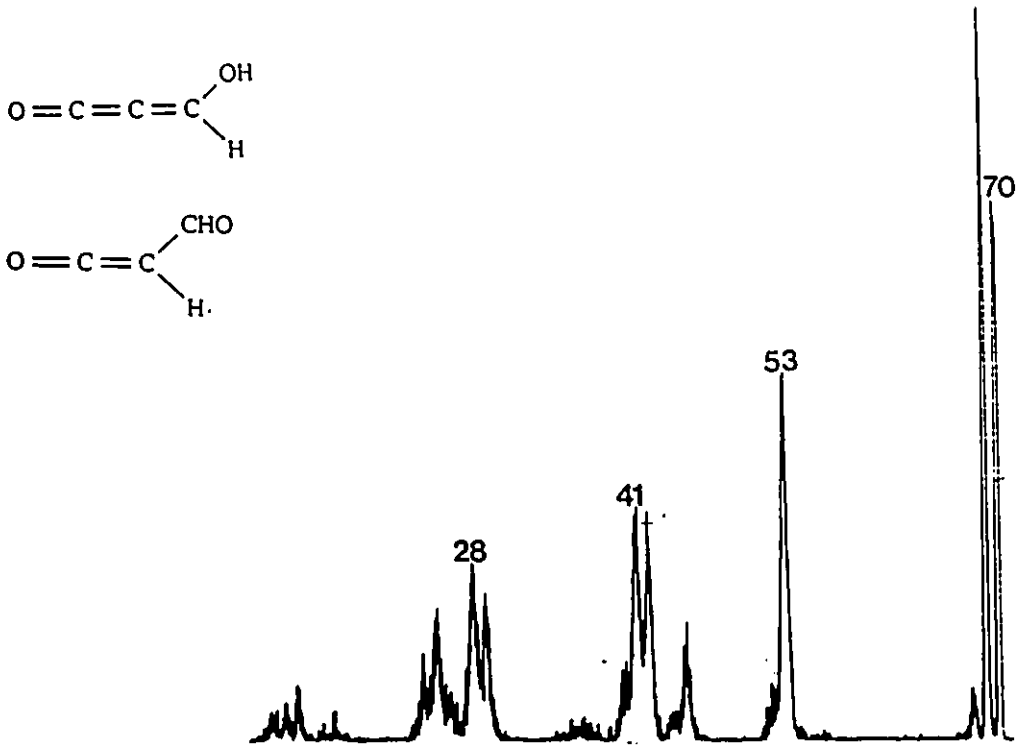

Figure 6-35 NR mass spectrum of the m/z 70 ion from fumaric acid. Xe (90% T) was the charge-exchange neutralization target and O_2 (90% T) the reionization target.

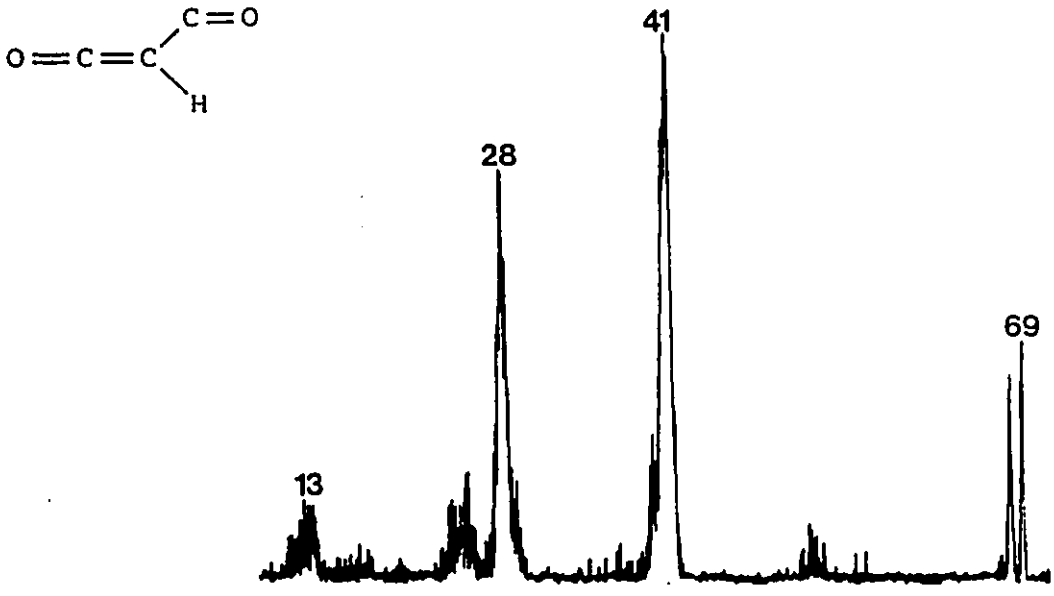

Figure 6-36 NR mass spectrum of the m/z 69 ion from fumaric acid. Xe (90% T) was the charge-exchange neutralization target and O_2 (90% T) the reionization target.

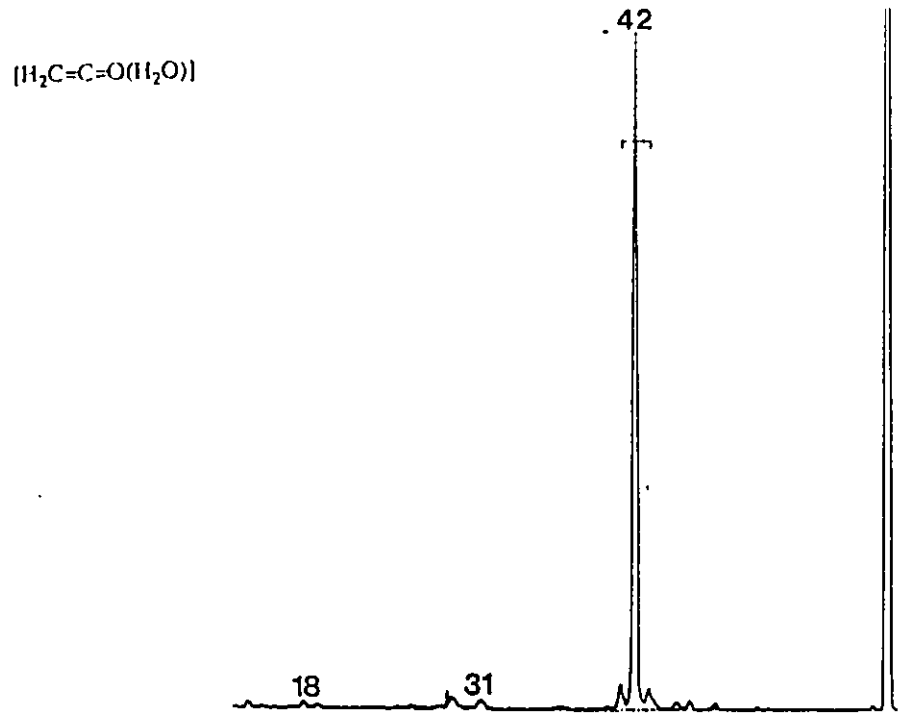

Figure 6-37 *He (90% T) CA mass spectrum of the m/z 60 ion from fumaric acid. The signal above the bar is the contribution due to the metastable ion.*

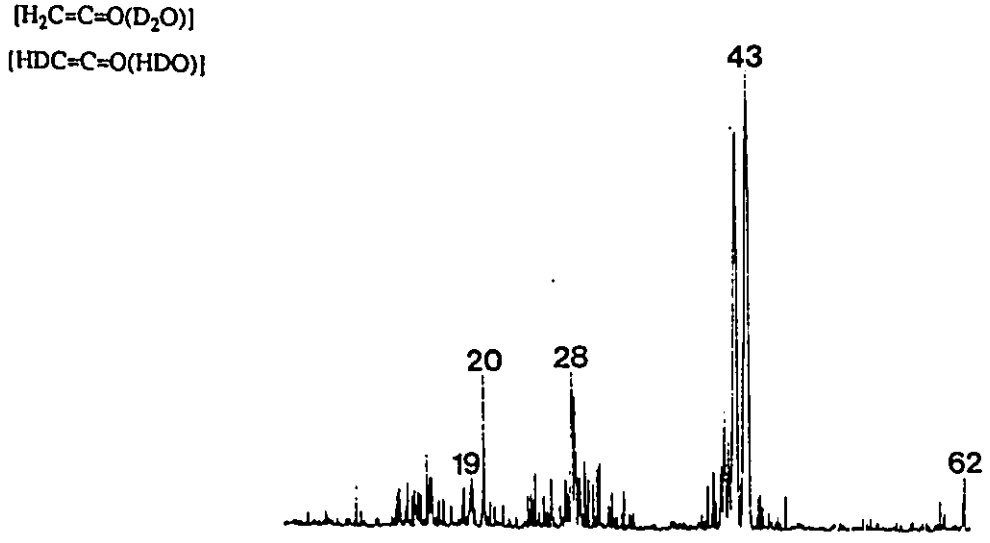

Figure 6-38 *NR mass spectrum of the deuterated m/z 60 (m/z 62) ion from fumaric acid-carboxyl-d_2. Xe (90% T) was the charge-exchange neutralization target and O_2 (90% T) the reionization target.*

$[H_2C=\dot{C}=O(H_2O)]^{+\bullet}$

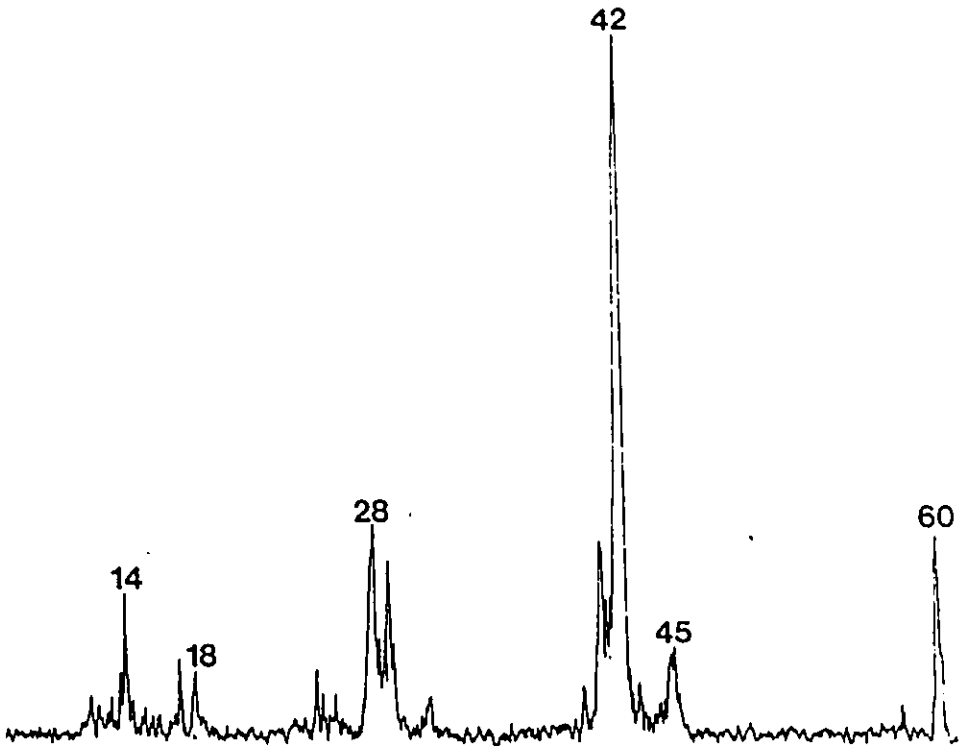

Figure 6-39 NR mass spectrum of the m/z 60 ion from dihydroxyacetone. Xe (90% T) was the charge-exchange neutralization target and O_2 (90% T) the reionization target.

References

Chapter 2

1. E. Goldstein, *Berl. Ber.* **39**, 691 (1886).
2. (a). W. Wien, *Wied. Ann.* **65**, 440 (1898); (b). W. Wien, *Ann. Physik Leipzig* **8**, 224 (1902).
3. (a). J.J. Thomson, *Rays of Positive Electricity and Their Application to Chmeical Analyses*, Longmans, Green and Co., London, (1913); (b). J.J. Thomson, *Phil. Mag.* **18**, 824 (1910).
4. F.A. Aston, *Phil. Mag.* **39**, 449 (1920).
5. A.J. Dempster, *J. Phys. Rev.* **20**, 631 (1922).
6. J.A. Hipple and E.U. Condon, *Phys. Rev.* **68**, 54 (1945).
7. M. Barber and R.M. Elliot, presented at ASTM E-14 Conference on Mass Spectrometry, Montreal, June 1964.
8. W.F. Haddon and F.W. McLafferty, *J. Am. Chem. Soc.* **90**, 4745 (1968).
9. K.R. Jennings, *Int. J. Mass Spectrom. Ion Phys.* **1**, 227 (1968).
10. R.G. Cooks, J.H. Beynon, R.M. Caprioli and R.R. Lester, *Metastable Ions*, Elsevier, Amsterdam, (1973).
11. P.M. Curtis, B.W. Williams and R.F. Porter, *Chem. Phys. Letters* **65**, 296 (1979).
12. (a). F.W. McLafferty, P.J. Todd, D.C. McGilvery and M.A. Baldwin, *J. Am. Chem. Soc.* **102**, 3360 (1980); (b). P.O. Danis, C. Wesdemiotis and F.W. McLafferty, *J. Am. Chem. Soc.* **105**, 7454 (1983).
13. C.F. Clark (ed.), *Encyclopedia of Spectroscopy*, pp. 628-647, Reinhold, New York (1960)
14. J.T. Watson, *Introduction to Mass Spectrometry* 2nd ed., Raven Press, New York (1985).
15. T.A. Lehman and M.M. Bursey, *Ion Cyclotron Resonance Spectrometry*, Wiley, New York (1976).
16. (a). K.P. Wanczek, *Int. J. Mass Spectrom. Ion Proc.* **60**, 11 (1984); (b). M.L. Gross and D.L. Rempel, *Science* **226**, 261 (1984).
17. P.H. Dawson (ed.), *Quadrupole Mass Spectrometry and Its Applications*, Elsevier, New York (1976).

18. R.E. March and R.J. Hughes, *Quadrupole Storage Mass Spectrometry*, Chemical Analysis Series, vol. 102, Wiley, New York (1989).

19. (a). K. Maeda, G.P. Semeluk and F.P. Lossing, *Int. J. Mass Spectrom. Ion Proc.* **1**, 395 (1968); (b). F.P. Lossing and J.C. Traeger, *Int. J. Mass Spectrom. Ion Phys.* **19**, 9 (1976).

20. H.M. Rosenstock, M.B. Wallenstein, A.L. Wahrhaftig and H. Eyring, *Proc. Nat. Acad. Sci. U. S.* **38**, 667 (1952).

21. (a). L.S. Kassel, *J. Phy. Chem.* **32**, 225 (1928); (b). R.A. Marcus, *J. Chem. Phy.* **20**, 359 (1952); (c). O.K. Rice and H.C. Ramsberger, *J. Am. Chem. Soc.* **49**, 1617 (1927).

22. P.C. Burgers and J.L. Holmes, *Int. J. Mass Spectrom. Ion Proc.* **58**, 15 (1984).

23. J.L. Holmes, *Org. Mass Spectrom.* **20**, 169 (1985).

24. J.L. Holmes and J.K. Terlouw, *Org. Mass Spectrom.* 15, 383 (1980).

25. (a). J. Franck, *Trans. Faraday Soc.* **21**, 536 (1926); (b). E.U. Condon, *Phys. Rev.* **32**, 858 (1928).

26. S.G. Lias, J.E. Bartmess, J.F. Liebman, J.L. Holmes, R.D. Levin and W.G. Mallard, *J. Phys. Chem. Ref. Data* **17**, Suppl. 1 (1988).

27. J.B. Pedley and J. Rylance, *Sussex-NPL Computer Analysed Thermochemical Data: Organic and Organometallic Compounds*, University of Sussex (1977).

28. S.W. Benson, *Thermochemical Kinetics, 2nd ed.*, Wiley-interscience, New York (1976).

29. (a). J.L. Holmes, M. Fingas and F.P. Lossing, *Can. J. Chem.* **59**, 80 (1981); (b). J.L. Holmes and F.P. Lossing, *Can. J. Chem.* **60**, 2365 (1982); (c). J.L. Holmes and F.P. Lossing, *Org. Mass Spectrom.* **26**, 537 (1991).

30. W.A. Chupka, *J. Chem. Phys.* **30**, 191 (1959).

31. K.C. Kim, J.H. Beynon and R.G. Cooks, *J. Chem. Phys.* **61**, 1305 (1974).

32. J.W. Warren, *Nature* **165**, 810 (1950).

33. P.C. Burgers and J.L. Holmes, *Org. Mass Spectrom.* **17**, 123 (1982).

34. F.P. Lossing, *J. Am. Chem. Soc.* **99**, 7526 (1977).

35. (a). J.L. Holmes, F.P. Lossing, J.K. Terlouw and P.C. Burgers, *J. Am. Chem. Soc.* **104**, 2931 (1982); (b). J.L. Holmes, F.P. Lossing, J.K. Terlouw and P.C. Burgers, *Can. J. Chem.* **61**, 2305 (1983).

36. T. Baer and T.E. Carney, *J. Chem. Phys.* **76**, 1304 (1982).

37. C. Lifshitz, P. Gotchiguian and R. Roller, *Chem. Phys. Lett.* **95**, 106 (1983).

38. P.C. Burgers, J.L. Holmes, A.A. Mommers, J.E. Szulejko and J.K. Terlouw, *Org. Mass Spectrom.* **19**, 442 (1984).

39. T.W. Shannon and F.W. McLafferty, *J. Am. Chem. Soc.* **88**, 5021 (1966).

40. H.M. Rosenstock, V.H. Dibeler and F.N. Harllee, *J. Chem. Phys.* **40**, 591 (1964).

41. (a). F.W. Aston, *Proc. Cambridge Philos. Soc.* **19**, 317 (1919); (b). H.D. Smyth, *Phys. Rev.* **25**, 452 (1925).

42. K.R. Jennings, *Int. J. Mass Spectrom. Ion Phys.* **1**, 227 (1968).

43. W.F. Haddon and F.W. McLafferty, *J. Am. Chem. Soc.* **90**, 4745 (1968).

44. (a). K. Levsen and H. Schwarz, *Mass Spectrom. Rev.* **2**,77 (1983); (b). F.W. McLafferty (ed.), *Tandem Mass Spectrometry*, Wiley-Interscience, New York, (1983).

45. F.W. McLafferty, P.F. Bente III, R. Kornfeld, S.-C. Tsai and I. Howe, *J. Am. Chem. Soc.* **95**, 2120 (1973).

46. (a). J.K. Terlouw, C.G. de Koster, W. Heerma, J.L. Holmes and P.C. Burgers, *Org. Mass Spectrom.* **18**, 222 (1983); (b). J.K. Terlouw, J. Wezenberg, P.C. Burgers and J.L. Holmes, *J. Chem. Soc., Chem. Commun.*, 1121 (1983).

47. (a). J.H. Beynon, *Anal. Chem.* **42**, 97A (1970); (b). R.G. Cooks, J.H. Beynon and T. Ast, *J. Am. Chem. Soc.* **94**, 1004 (1972); (c). T. Ast, J.H. Beynon and R.G. Cooks, *J. Am. Chem. Soc.* **94**, 6611 (1972); (d). R.G. Cooks, T. Ast and J.H. Beynon, *Int. J. Mass Spectrom. Ion Phys.* **11**, 490 (1972).

48. M.P. Barbalas, F. Turecek and F.W. McLafferty, *Org. Mass Spectrom.* **17**, 595 (1982).

49. T. Ast, *Adv. Mass Spectrom.* **10A**, 471 (1986).

50. D.L. Kemp, J.H. Beynon and R.G. Cooks, *Org. Mass Spectrom.* **11**, 857 (1976).

51. (a). R.D. Bowen, M.P. Barbalas, F.P. Pagan, P.J. Todd and F.W. McLafferty, *Org. Mass Spectrom.* **15**, 51 (1980); (b). J.L. Holmes, J.K. Terlouw, P.C. Burgers and R.T.B. Rye, *Org. Mass Spectrom.* **15**, 149 (1980).

52. D. Harnish, J.L. Holmes, F.P. Lossing, A.A. Mommers, A. Maccoll and M.N. Mruzek, *Org. Mass Spectrom.* **25**, 381 (1990).

53. G.I. Gellene and R.F. Porter, *Acc. Chem. Res.* **16**, 200 (1983).

54. C. Wesdemiotis and F.W. McLatterty, *Chem. Rev.* **87**, 405 (1987).

55. J.L. Holmes, *Mass Spectrom. Rev.* **8**, 513 (1989).

56. J.K. Terlouw and H. Schwarz, *Angew. Chem. Int. Ed. Engl.* **26**, 805 (1987).

57. J.A. Laramée, P. Cameron and R.G. Cooks, *J. Am. Chem. Soc.* **103**, 12 (1981).

58. C.E.C.A. Hop, *Mass Spectrometric Experiments with Beams of Fast Neutrals*, PhD Thesis, University of Utrecht, Utrecht (1988).

59. C.E.C.A. Hop, J.L. Holmes, F.P. Lossing and J.K. Terlouw, *Int. J. Mass Spectrom. Ion Processes* **83**, 285 (1988).

60. (a). G.I. Gellene and R.F. Porter, *Int. J. Mass Spectrom. Ion Processes* **64**, 55 (1985); (b). P.O. Danis, R. Feng and F.W. McLafferty, *Anal. Chem.* **58**, 355 (1986).

61. (a). J.L. Holmes, C.E.C.A. Hop and J.K. Terlouw, *Org. Mass Spectrom.* **21**, 776 (1986); (b). N. Heinrich, J.Schmidt, H. Schwarz and Y. Apeloig, *J. Am. Chem. Soc.* **109**, 1317 (1987).

62. J.L. Holmes and M. Sirois, *Org. Mass Spectrom.* **25**, 481 (1990).

63. J.L. Holmes, *Org. Mass Spectrom.* **20**, 169 (1985).

64. (a) C.E.C.A. Hop, J.L. Holmes, K.J. van den Berg and J.K. Terlouw, *Rapid Commun. Mass Spectrom.* **1**, 52 (1987); (b) C.E.C.A. Hop, K.J. van den Berg, J.L. Holmes and J.K. Terlouw, *J. Am. Chem. Soc.* **111**, 72 (1989).

65. C.E.C.A. Hop, J.L. Holmes, P.J.A. Ruttink, G. Schaftenaar and J.K. Terlouw, *Chem. Phys. Letters.* **156**, 251 (1989).

66. (a) C. Wesdemiotis and F.W. McLafferty, *Chem. Rev.* **87**, 405 (1987); (b) J.K. Terlouw and H. Schwarz, *Angew. Chem. Int. Ed. Engl.* **26**, 805 (1987); (c) C.E.C.A. Hop, *Mass Spectrometric Experiments with Beams of Fast Neutrals*, PhD Thesis, University of Utrecht, Utrecht (1988); (d) J.L. Holmes, *Mass Spectrom. Rev.* **8**, 513 (1989).

67. S.G. Lias, J.E. Bartmess, J.L. Liebman, J.L. Holmes, R.D. Levin and W.G. Mallard, *J. Phys. Chem. Ref. Data* **17**, Suppl. 1 (1988).

68. K. Kimura, S. Katsumata, Y. Achiba, T. Yamazaki and S. Iwata, *Handbook of Hel Photoelectron Spectra of Fundamental Organic Compounds*, Japan Scientific Soc. Press, Tokyo (1981) and Halsted Press, New York (1981).

69. H.B. Schlegel, P. Gund and E.M. Fluder, *J. Am. Chem. Soc.* **104**, 5347 (1982).

70. J.P. Kiplinger, A.T. Maynard and M.M. Bursey, *Org. Mass Spectrom.* **22**, 534 (1987).

71. (a) J.R. Bews and C. Glidewell, *J. Mol. Struct.* **67**, 141 (1980); (b) J.R. Bews and C. Glidewell, *J. Mol. Struct.* **67**, 151 (1980).

72. (a) E. Bamberger and R. Seligman, *Chem. Ber.* **36**, 685 (1903); (b) L. Batt and B.G. Gowenlock, *Trans. Faraday Soc.* **56**, 682 (1960).

73. P.D. Adeney, W.J. Bouma, L. Radom and W.R. Rodwell, *J. Am. Chem. Soc.* **102**, 4069 (1980).

74. (a) L. Batt, B.G. Gowenlock and J. Trotman, *J. Chem. Soc.* 2222 (1960); (b) L. Batt and R.T. Milne, *Int. J. Chem. Kinet.* **5**, 1067 (1973).

75. D.C. Frost, W.M. Lau, C.A. McDowell and N.P.C. Westwood, *J. Phys. Chem.* **86**, 3577 (1982).

76. D.P. Chong, D.C. Frost, W.M. Lau and C.A. McDowell, *Chem. Phys. Letters* **90**, 332 (1982).

77. A. Dargelos and C. Sandorfy, *J. Chem. Phys.* **67**, 3011 (1977).

78. J.P. Dognon, C. Pouchan, A. Dargelos and J.P. Flament, *Chem. Phys. Letters* **109**, 492 (1984).

79. J.B. Pedley, R.D. Naylor and S.P. Kirby, *Thermochemical Data of Organic Compounds*, 2nd edn, Chapman and Hall, London (1988).

80. S.W. Benson, *Thermochemical Kinetics*, 2nd edn., Wiley, New York (1976)

81. M.A. Robb and I.G. Csizmadia, *J. Chem. Phys.* **50**, 1819 (1969).

82. For a review of the chemistry of nitrones and oxaziridines see G.G. Spence, E.C. Taylor and O. Buchardt, *Chem. Rev.* **70**, 231 (1970).

83. (a) W.D. Emmons, *J. Am. Chem. Soc.* **78**, 6208 (1956); (b) W.D. Emmons, *J. Am. Chem. Soc.* **79**, 5739 (1957).

84. E. Oliveros, M. Riviere, J.P. Malrieu and Ch. Teichteil, *J. Am. Chem. Soc.* **101**, 318 (1979).

85. By Benson's additivity scheme [80] and assigning -132 kJ.mol^{-1} to the CO(N)(O) increment (obtained from $\Delta H_f(H_2NC(O)OCH_2CH_2CH_3)$ = -471 kJ.mol^{-1} [79] and using the known increments).

86. By Benson's additivity scheme [80] and assigning -29 kJ.mol^{-1} to the CO(CO)(N) increment. The latter was obtained by taking the average of the differences between the $CO(C)_2$ and CO(C)(CO) increments and the CO(C)(O) and CO(CO)(O) increments (17 kJ.mol^{-1}) and adding it to the CO(C)(N) increment.

87. It was assumed that the C-C bond strength in H_3C-C(O)NH_2 is equal to the average of the C-C bond strengths in H_3C-C(O)CH_3 and H_3C-C(O)OH [67], i.e. 363 kJ.mol^{-1}. $\Delta H_f(H_3CC(O)NH_2)$ = -238 kJ.mol^{-1} and $\Delta H_f(\cdot CH_3)$ = 146 kJ.mol^{-1} [67].

88. (a) M. Dupuis, D. Spangler and J. Wendolowski, *NRCC Software Catalog* **1**, Programme No QG01, GAMESS (1980); (b) M.F. Guest and J. Kendrick, *GAMESS User Manual, An Introductory Guide*, CCP/86/1, Daresbury Laboratory (1986).

89. B.G. Gowenlock and J. Trotman, *J. Chem. Soc.* 4190 (1955).

90. G.P. Raine, H.F. Schaefer III and R.C. Haddon, *J.Am. Chem. Soc.* **105**, 194 (1983).

91. L.D. Brown and W.N. Lipscomb, *J. Am. Chem. Soc.* **99**, 3968 (1977).

92. (a) C. Wesdemiotis and F.W. McLafferty, *Chem. Rev.* **87**, 405 (1987); (b) J.K. Terlouw and H. Schwarz, *Angew. Chem., Int. Ed. Engl.* **26**, 805 (1987); (c) J.L. Holmes, *Mass Spectrom. Rev.* **8**, 513 (1989).

93. D. Sülzle and H. Schwarz, *Angew. Chem., Int. Ed. Engl.* **27** 1337 (1988).

94. D. Sülzle and H. Schwarz, *Chem. Ber.* **122**, 1830 (1989).

95. D. Sülzle and H. Schwarz, *Angew. Chem., Int. Ed. Engl.* **29**, 908 (1990).

96. D. Sülzle, J.K. Terlouw and H. Schwarz, *J. Am. Chem. Soc.* **112**, 628 (1990).

97. H. Staudinger and E. Anthes, *Ber. Dtsch. Chem. Ges.* **46**, 1426 (1913).

98. J. Strating, B. Zwanenburg, A. Wagenaar and A.C. Udding, *Tetrahedron Lett.* 125 (1969).

99. D.L. Dean and H. Hart, *J. Am. Chem. Soc.* **94**, 687 (1972).

100. L.B. Knight Jr., J. Steadman, P.K. Miller, D.E. Bowman, E.R. Davidson and D. Feller, *J. Chem. Phys.* **80**, 4593 (1984).

101. S.H. Linn, Y. Ono and C.Y. Ng, *J. Chem. Phys.* **74**, 3342 (1981).

102. (a) M.S.B. Munson, F.H. Field and J.L. Franklin, *J. Chem. Phys.* **37**, 1790 (1962); (b) S.L. Chong and J.L. Franklin, *J. Chem. Phys.* **54**, 1487 (1971); (c) M. Meot-Ner and F.H. Field, *J. Chem. Phys.* **61**, 3742 (1974).

103. (a) R.N. Varney, *Phys. Rev.* **89**, 708 (1953); (b) M. Saporoschenko, *J. Chem. Phys.* **49**, 768 (1968).

104. R.C. Haddon, D. Poppinger and L. Radom, *J. Am. Chem. Soc.* **97**, 1645 (1975).

105. R.C. Haddon, *Tetrahedron Lett.* **37**, 3897 (1972).

106. P. Mathies, F.O. Sladky and B.M. Rode, *J. Mol. Struc.* **90**, 335 (1982).

107. N. Bodor, M.J.S. Dewar, A. Harget and E. Haselbach, *J. Am. Chem. Soc.* **92**, 3854 (1970).

108. S.G. Lias, J.E. Bartmess, J.F. Liebman, J.L. Holmes, R.D. Levin and W.G. Mallard, *J. Phys. Chem. Ref. Data* **17**, Suppl. 1 (1988).

109. P.C. Burgers, A.A. Mommers and J.L. Holmes, *J. Am. Chem. Soc.* **105**, 5976 (1983).

110. O. Diels and B. Wolf, *Ber.* **39**, 689 (1906).

111. L.H. Reyerson and K. Kobe, *Chem. Rev.* **7**, 479 (1930).

112. D.A. Long, F.S. Murfin and R.L. Williams, *Proc. Roy. Soc. (London)* **A223**, 251 (1954).

113. W.H. Smith and J.J. Barrett, *J. Chem. Phys.* **51**, 1475 (1969).

114. L.A. Carreira, R.O. Carter, J.R. Durig, R.C. Lord and C.C. Milionis, *J. Chem. Phys.* **59**, 1028 (1973).

115. A.W. Mantz, P. Connes, G. Guelachvili and C. Amiot, *J. Mol. Spectrosc.* **54**, 43 (1975).

116. C. Willis and K.D. Bayes, *J. Am. Chem. Soc.* **88**, 3203 (1966).

117. K.H. Becker and K.D. Bayes, *J. Chem.* Phys. **48**, 653 (1968).

118. E. Tschuikow-Roux and S.Kodama, *J. Chem. Phys.* **50**, 5297 (1969).

119. C.E.M. Strauss, S.H. Kable, G.K. Chawla, P.L. Houston and I.R. Burak, *J. Chem. Phys.* **94**, 1837 (1991).

120. A. Almenningen, S.P. Arnesen, O. Bastiansen, H.M. Seip and R. Seip, *Chem. Phys. Lett.* **1**, 569 (1968).

121. A. Clark and H.M. Seip, *Chem. Phys. Lett.* **6**, 452 (1970).

122. J.W.D. Connolly, H. Siegbahn, U. Gelius and C. Nordling, *J. Chem. Phys.* **58**, 4265 (1973).

123. I.H. Hillier and J. Kendrick, *J. Chem. Soc. Faraday Trans. II* **71**, 1369 (1975).

124. U. Gelius, C.J. Allan, D.A. Allison, H. Siegbahn and K. Siegbahn, *Chem. Phys. Lett.* **11**, 224 (1971).

125. H.W. Thompson and N. Healey, *Proc. Roy. Soc. (London),* **A157**, 331 (1936).

126. J.L. Roebber, J.C. Larrabee and R.E. Huffman, *J. Chem. Phys.* **46**, 4594 (1967).

127. J.L. Roebber, *J. Chem. Phys.* **54**, 4001 (1971).

128. E. A. Williams, J.D. Cargioli and A. Ewo, *J.C.S. Chem. Comm.*, 366 (1975).

129. S.M. Schildcrout and J.L. Franklin, *J. Am. Chem. Soc.* **92**, 251 (1970).

130. J.R. Sabin and H. Kim, *J. Chem. Phys.* **56**, 2195 (1972).

131. L.J. Weimann and R.E. Christoffersen, *J. Am. Chem. Soc.* **95**, 2074 (1973).

132. R.D. Bardo and K. Ruedenberg, *J. Chem. Phys.* **60**, 932 (1974).

133. P. Lindner, Y. Öhrn and J.R. Sabin, *Int. J. Quant. Chem. Symp.* **7**, 261 (1973).

134. H.H. Jensen, E.W. Nilssen and H.M. Seip, *Chem. Phys. Lett.* **27**, 338 (1974)/

135. J.F. Olsen and L. Burnelle, *J. Phys. Chem.* **73**, 2298 (1969).

136. M.E. Jacox, D.E. Milligan, N.G. Moll and W.E. Thompson, *J. Chem. Phys.* **43**, 3734 (1965).

137. R.L. DeKock and W. Weltner Jr., *J. Am. Chem. Soc.* **93**, 7106 (1971).

138. C. Devillers and D.A. Ramsay, *Can. J. Phys.* **49**, 2839 (1971).

139. T.R. Forbus, P.A. Birdsong and P.B. Shevlin, *J. Am. Chem. Soc.* **100**, 6425 (1978).

140. G.R. Smith and W. Weltner Jr., *J. Chem. Phys.* **62**, 4592 (1975).

141. R.J. Van Zee, R.F. Ferrante and W. Weltner Jr., *Chem. Phys. Lett.* **139**, 426 (1987).

142. M.T. Bowers, M. Chau and P.R. Kemper, *J. Chem. Phys.* **63**, 3656 (1975).

143. C. Thomson and B.J. Wishart, *Theor. Chim. Acta* **31**, 347 (1973).

144. S.P. Walch, *J. Chem. Phys.* **72**, 5679 (1980).

145. C.F. Chabalowski, R.J. Buenker and S.D. Peyerimhoff, *J. Chem. Phys.* **84**, 268 (1986).

146. R.L. DeKock, R.S. Grev and H.F. Schaefer III, *J. Chem. Phys.* **89**, 3016 (1988).

147. F. Benoit, J.L. Holmes and N.S. Isaacs, *Org. Mass Spectrom.* **2**, 591 (1969).

148. S.H. Heller and G.W.A. Milne, *EPA/NIH Mass Spectral Data Base, vol 1*, National Bureau of Standards, United States, 1978.

149. S.G. Lias, J.E. Bartmess, J.F. Liebman, J.L. Holmes, R.D. Levin and W.G. Mallard, *J. Phys. Ref. Data* **17**, Suppl. 1 (1988).

150. J.B. Pedley and J. Rylance, *Sussex-NPL Computer Analysed Thermochemical Data: Organic and Organometallic Compounds*, University of Sussex (1977).

151. J.L Holmes, J.K. Terlouw and P.C. Burgers, *Org. Mass Spectrom.* 15, 140 (1980).

152. J.L. Holmes, M. Fingas and F.P. Lossing, *Can. J. Chem.* **59**, 80 (1981).

153. (a). R. Postma, P.J.A. Ruttink, J.K. Terlouw and J.L. Holmes, *J. Chem. Soc., Chem. Commun.*, 683 (1986); (b). J. K. Terlouw, C.G. de Koster, W. Heerma, J.L. Holmes and P.C. Burgers, *Org. Mass Spectrom.* **18**, 222 (1983).

154. F.M. Benoit, A.G. Harrison and F.P. Lossing, *Org. Mass Spectrom.* **12**, 78 (1977).

155. J.G. Atkinson, J.J. Csakvary, G.R. Herbert and R.S Stuart, *J. Am. Chem. Soc.* **90**, 498 (1968).

156. E. Campaigne and W.M. LeSuer, *Org. Syn.* Coll. IV 919.